UNIVERSITY OF COPENHAGEN
FACULTY OF SCIENCE

Master Thesis

Incorporating a dynamical Greenland Ice Sheet into a Global Climate Model System

Laurent Lindpointner

Advisors: Marianne Sloth Madsen, Aslak Grinsted, Shuting Yang

Handed in: 01.09.2021

Thesis project in collaboration between NBI and DMI

Abstract

The Greenland ice sheet is projected to continually lose mass at an accelerating pace during the 21^{st} century. Being the second largest single ice mass on Earth and the largest in the Northern Hemisphere, this has implications both for future sea level rise and the surrounding climate system. In order to realistically represent the changing Greenland ice sheet in a global climate model system, two-way coupled climate model - ice sheet model systems are needed. In this project, a dynamical ice sheet model for the Greenland ice sheet was coupled to a global climate model and emerging consequences investigated.

The interface for coupling the climate model EC-Earth 3 and the ice sheet model PISM v1.2, which was developed in this project, is described in detail. The interface offers two different ways of forcing the PISM ice sheet model: one with surface forcing generated by EC-Earth 3 and another with surface forcing generated by the downscaled energy balance model CISSEMBEL, which itself uses atmospheric forcing data from EC-Earth 3.

CISSEMBEL experiments are performed and resulting surface mass and energy fluxes compared with stand-alone EC-Earth 3 model data. The experiments use atmospheric forcing from 29 year EC-Earth 3 experiments: two pre-industrial historical and two SSP5-8.5 scenario experiments. One of each uses a constant albedo over glaciated areas and one uses a variable albedo scheme, allowing albedo-melt feedback. Using the variable albedo scheme, CISSEMBEL generates 218% and 238% more melt than EC-Earth 3 in the pre-industrial and scenario experiments, respectively.

Ice sheet initial states for the coupled system experiments are generated with PISM initialization experiments under pre-industrial surface forcing. Separate initial state ice sheets are generated for the two different forcing methods in the coupled system. The resulting ice sheet based on surface forcing from EC-Earth 3 has 15.0% more mass and covers a 28.0% larger area than the observed present-day Greenland ice sheet. The ice sheet forced by CISSEMBEL data has 8.5% less mass but covers a 5.2% larger area than the observed present-day Greenland ice sheet. Spatial differences in surface mass balance forcing from the two models are the key factor in determining the resulting ice sheet geometries.

Finally, two 80 year abrupt-4xCO_2 scenario experiments for testing the fully coupled system are performed. In one, PISM is forced with surface forcing data from EC-Earth 3 and in the other with surface forcing data from CISSEMBEL.
The impact of the coupling on the two meter air temperature, surface mass and surface energy fluxes in EC-Earth 3 is assessed by comparison to a 50 year EC-Earth 3 stand-alone experiment of the same scenario.

The Greenland ice sheet has an increasingly negative mass balance throughout both coupled experiments. The EC-Earth 3 forced ice sheet has an average ice discharge contribution of 18.1% to the total mass balance while for the CISSEMBEL forced ice sheet this fraction is 4.7%. The EC-Earth 3 and CISSEMBEL forced ice sheets lose 5.7% and 6.1% of their mass, respectively. This equals respective cumulative contributions to global mean sea level rise of 473 mm and 406 mm.

Acknowledgements

This master project was carried out in collaboration between the Danish Meteorological Institute (DMI) and The University of Copenhagen, Department for Physics of Ice, Climate and Earth (PICE).

I would like to express my gratitude and appreciation to my supervisors, Marianne Sloth Madsen and Shuting Yang at DMI and Aslak Grinsted at PICE who, under the difficult conditions during the past year, were always available and happy to help me with my project, to provide guidance and new ideas.

I would also like to thank Christian Rodehacke who provided guidance and insights regarding the surface energy balance model CISSEMBEL.

I am thankful to my parents, Elisabeth and Rudolf, who through their support have helped making this possible.

Contents

1 Introduction

The present-day Greenland ice sheet is estimated to hold freshwater with the potential to raise the global mean sea level by 7.4 meters. [Morlighem et al., 2017] Since the late 1990s, it is losing mass at an accelerating pace due to increases in both melt water runoff and ice discharge. [Broeke et al., 2016] In its 6^{th} assessment report, the Intergovernmental Panel on Climate Change (IPCC) rates it as very likely, that human influence has contributed to surface melting over the Greenland ice sheet and as virtually certain, that it will continually lose mass during the 21^{st} century. [IPCC, 2021] The extent to which this will be the case and thus, how large the Greenland ice sheet's contribution will be to future sea level rise in a warming climate is of considerable interest and subject of numerous projection studies. [Goelzer et al., 2020], [Muntjewerf et al., 2020a]
A changing Greenland ice sheet has implications for not only the future sea level but the surrounding climate system, affecting the atmosphere through, among other things, its changing topography and surface albedo and the ocean through potentially increased freshwater fluxes. In order to capture the numerous complex interactions and feedback mechanisms between large ice sheets and the climate system (section 2), two-way coupled climate - ice sheet model systems are needed, which allow a dynamical ice sheet to be influenced by the climate state and vice versa.
Development of these model systems has been a growing area of research and recent progress is described in the following paragraphs.
One of the first two-way coupled general circulation - ice sheet models was presented by [Ridley et al., 2005]. The third Hadley Centre Coupled Ocean–Atmosphere general circulation model (HadCM3) with a horizontal resolution of 2.5° latitude by 3.75° longitude and 19 vertical levels in the atmospheric part as well as 1.25°x1.25° and 20 vertical levels in the ocean model is coupled to the three-dimensional Greenland ice sheet model (GISM, 20 km x 20 km resolution). HadCM3 is run for one year and provides monthly 1.5 meter air temperature anomalies and annual precipitation values to the ice sheet model, which then in turn runs for one year and uses a positive degree day model to calculate surface melt and the surface mass balance. The ice sheet model returns an updated orography and fluxes of ice surface runoff, basal ice melt, land surface runoff and iceberg calving. An ice sheet mask is defined based on the orography to determine the area over Greenland, where the land surface scheme is modified to represent ice sheet conditions.
This system contains many vital parts of any two-way coupled system. Over the years multiple improvements were made such as the inclusion of a vegetation and a thermodynamical ice sheet model into a coupled general circulation model - ice sheet model system ([Mikolajewicz et al., 2007]). [Vizcaíno et al., 2013]'s coupled system (Community Earth System Model 1.0 (CESM1.0) with Glimmer Community Ice Sheet Model (Glimmer-CISM)) features a significant increase in horizontal resolution (0.9°x1.25° in atmosphere model, 1°x1° in ocean model, 5 km x 5 km in ice sheet model) as well as calculation

of the surface mass balance in a dedicated land surface model by solving the surface energy balance, rather than relying on a positive degree day scheme. This system also includes downscaling of the surface mass balance to the ice sheet resolution by the use of fixed elevation classes in the land model, where each elevation class receives the same temperature, specific humidity, and downward radiative fluxes from the atmosphere, but calculates its own latent and sensible heat fluxes, upward radiative fluxes, subsurface temperature and water content.
DMI's first two-way coupled climate model - ice sheet model system couples the climate model EC-Earth version 2.3 (approximate horizontal resolution in atmosphere model 125 km, 1°x1° in ocean model), which includes models for atmospheric dynamics, surface processes, the ocean and sea ice, with the ice sheet model PISM (horizontal resolution 20 km x 20 km). It was developed by [Svendsen et al., 2015]. Surface melt is modeled in the coupled system by solving the surface energy balance. The model takes the ice sheet extent into account, allows calculation of melt over these areas and modifies soil properties, such as setting a constant 0.8 albedo, to reflect the presence of ice. Ice sheet surface forcing is provided as surface mass balance and below-firn temperature by EC-Earth 2.3, where the temperature is lapse rate corrected to account for topography differences between the climate and the ice sheet model. Surface mass balance forcing is not downscaled to the ice sheet topography.
One of the most recent additions to the list of coupled global climate - ice sheet models is the coupled CESM2.1-CISM2.1, developed by [Muntjewerf et al., 2021]. Its calculation of surface mass balance in the surface component is based on the surface energy balance and uses elevation classes to downscale the air temperature, upon which further elevation class specific climate variables are calculated, and downward long wave radiation. SMB is calculated for each elevation class and tri-linearly remapped to the finer ice sheet model topography while ensuring mass conservation. Albedo is calculated by a sophisticated model taking, among other things, snow grain size evolution and impurities into account. The land model distinguishes different surface types and has 15 layers for ice as well as up to 12 layers to represent snow and firn, depending on snow depth. Compaction of snow into firn is modeled as a result of overburden pressure, snow metamorphism and enhanced wind-driven surface compaction.

1.1 Overview

A coupled EC-Earth - PISM system was developed by [Svendsen et al., 2015]. It is based on EC-Earth version 2.3 and PISM version 0.5. In their report, the authors highlight several areas for possible improvement of the coupled system, among them an increase in resolution, use of an improved albedo scheme and use of a multi-layer snow or surface energy balance model. The release of EC-Earth 3, offered the opportunity for development of an updated coupling interface. Development of this updated coupling interface, the ISM-Mapper, was the primary goal of this project. The updated coupled system in its current state, features updated model versions (EC-Earth 3 and PISM version 1.2),

improvements the report's authors made to the land ice physics in EC-Earth 3 (including an albedo scheme enabling albedo-melt feedback, [Madsen et al., 2021a]) and a higher resolution in both EC-Earth 3 and PISM. The downscaled surface energy balance model CISSEMBEL can be used in the coupled setup for calculating surface forcing for PISM, instead of calculating it directly from EC-Earth 3 model variables. This addresses the lack of a downscaling option for calculating the surface mass balance and of a sophisticated multi-layer snow scheme in EC-Earth 3.
The second goal was to estimate the Greenland ice sheet's response to high greenhouse gas forcing in two coupled 4xCO_2 scenario experiments.

Section 2 gives an overview over interactions and feedback processes between the Greenland ice sheet and the surrounding climate system, followed by short descriptions of the concepts of ice sheet mass balance and surface energy balance.

Section 3 offers descriptions of the models which are used in this project. A high level overview over the developed EC-Earth 3 - PISM coupled system and its two different ways of forcing the ice sheet is given. The following subsection on the global climate model EC-Earth 3 describes its different components, relevant configurations and details on the calculation of the surface energy balance, runoff as well as albedo and ice discharge in the model. The subsection on the downscaled surface energy balance model CISSEMBEL provides details on the surface energy balance calculation and albedo schemes in the model. Additionally, the lapse-rate based downscaling feature is described. Theory on ice dynamics and thermodynamics in PISM along with modeling choices regarding surface forcing and ice discharge are addressed in the final subsection.

The coupled EC-Earth 3 - PISM system is described in detail in section 4.

Section 5 explores the differences in modeled surface mass balance and surface energy balance components from EC-Earth 3 (uncoupled) and CISSEMBEL in order to better understand their respective impact on later performed coupled experiments. A comparison to surface mass balance data from ERA5-Reanalysis is provided.

Section 6 addresses PISM ice sheet initialization experiments under surface forcing from EC-Earth 3 and CISSEMBEL. The resulting ice sheet states are used as initial states in the coupled experiments.

Section 7 describes the results of the first test runs of the coupled EC-Earth 3 - PISM systems. Results examine the Greenland ice sheet's response to a warming climate in an abrupt-4xCO_2 simulation. Effects on the local climate in EC-Earth 3 are explored as well.

Section 8 concludes the thesis, summarizes the key findings and provides an outlook on future work.

2 The Greenland Ice Sheet and its Environment

Ice sheets are important parts of the climate system. Both direct interactions with the climate and feedback processes shape the evolution of ice sheets. The atmosphere and ocean influence ice sheets through surface and sub-ice shelf mass and energy fluxes. Ice sheets influence the atmosphere through their changing topography, extent and surface type, and the ocean by being a source of freshwater influxes from runoff of surface and basal melt water and calving of icebergs.

The change in ice sheet mass is quantified via the ice sheet mass balance. Mass is gained through snow deposition on the surface while it is lost through runoff of melt water, calving and sublimation processes among others.

The surface mass balance is concerned with the balance of surface accumulation and ablation processes. Atmospheric forcing such as temperature and precipitation play an important role.

The surface energy balance is calculated from surface energy fluxes such as solar and thermal radiative fluxes and sensible and latent heat fluxes. The surface energy balance determines the presence and amount of melting.

Figure 1 gives an overview of ice sheet - climate system interactions which affect both the climate system and the ice sheet itself. Some of these interactions will be described in detail in this section.

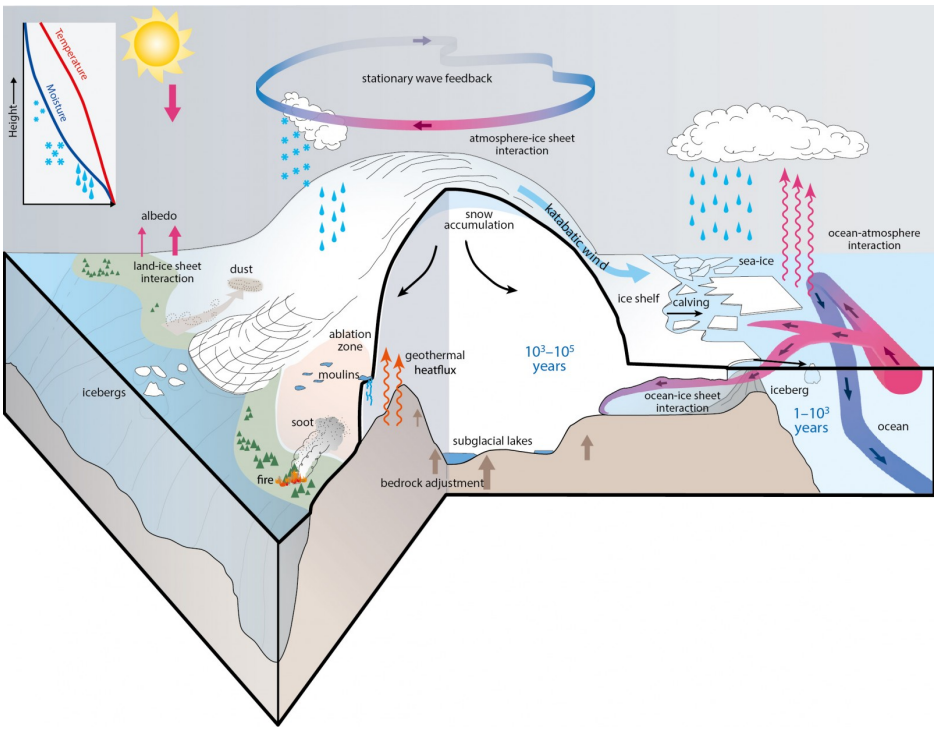

Figure 1: Overview of the interactions of an ice sheet with the climate system. Credit: Figure 1 in Box 5.2, IPCC AR5, [Pachauri et al., 2014].

2.1 Greenland Ice Sheet - Climate Interaction

Since the focus of this work is the Greenland ice sheet (GrIS), its interaction with its environment will be the primary focus of this section. Three categories of interactions are described:

1. the climate system's impact on the GrIS,
2. the Greenland ice sheet's impact on the climate system and
3. feedback mechanisms arising from this two way relationship.

2.1.1 The Climate System's Impact on the GrIS

The GrIS has multiple boundary surfaces, through which it interacts with its environment. Different components of the climate system exert forcing on it and change its mass. The top ice sheet surface acts as an interface to the atmosphere, submarine boundaries interact with the ocean while the ice sheet base interacts with the lithosphere-mantle.

Atmosphere

The atmosphere impacts the surface mass and energy balance of the ice sheet. At the surface, the GrIS gains mass through solid precipitation and loses mass through surface ice melt and turbulent moisture transport.

The seasonality and location of **precipitation** over Greenland is strongly influenced by cyclonic systems in the North Atlantic region. [Fyke et al., 2018] These systems form along the Eastern North American coast and follow a north-eastward path with the westerly winds towards the southern tip of Greenland. From there, they either travel along an eastward path into the Norwegian Sea or along a northward path along Greenland's coast. [Schwierz and Davies, 2002] The low pressure cyclonic systems advect moist air from the open North Atlantic to Greenland's southern coastal areas, where the topography changes rapidly. As the air gets lifted, it cools adiabatically and saturates, causing heavy precipitation over the ice sheet. [Schuenemann et al., 2009] Other varying regional climate patterns influencing precipitation over Greenland include the North Atlantic Oscillation (NAO), the Atlantic Multidecadal Oscillation (AMO), the northern polar jet stream and the Greenland Blocking Index (GBI). [Fyke et al., 2018] ERA5 data [Muñoz Sabater, 2019] shows a fraction of roughly 91% solid precipitation of the total precipitation over Greenland with the remaining part falling in liquid form, primarily in lower altitude areas along Greenland's south-western shores.
Figure 2 shows mean winter, summer and annual precipitation patterns over Greenland. In winter, precipitation is highest along the south-eastern shore of Greenland with less precipitation over the rest of the GrIS. During the summer months, a more even precipitation distribution over the ice sheet can be observed. A factor contributing to this is that a

high GBI, which is observed during the summer months, correlates with warmer, moister southerly winds being advected over the ice sheet. The southern part of Greenland shows a dry anomaly during this time which correlates with a northward migration and weakening of the northern polar jet stream during the spring months. [Hanna et al., 2016]

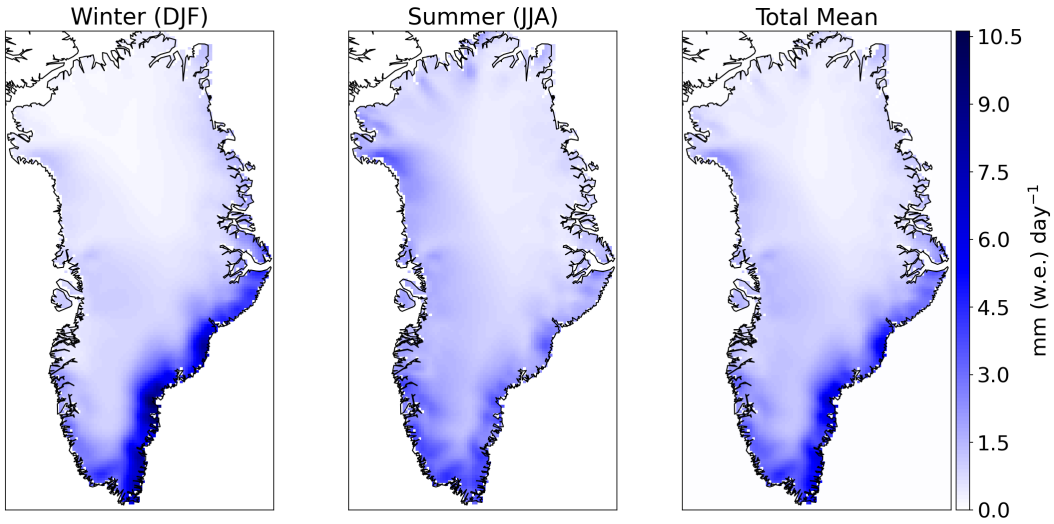

Figure 2: ERA5 [Muñoz Sabater, 2019] mean total precipitation over Greenland during the winter months December to February (left), the summer months June to August (middle) as well as over the whole time period (1981-2021, right). Data bilinearly interpolated to 15 km x 15 km grid.

Runoff off the Greenland ice sheet consists of fractions of melt and liquid precipitation. Melt affects the ice sheet's surface mass balance and it occurs, when the ice sheet's surface energy balance (SEB) is net positive. In that case, there is energy available for melting. The main components influencing the surface energy balance are the net shortwave and longwave radiation fluxes as well as turbulent fluxes and subsurface conductive heat fluxes. Not all melt and liquid precipitation, however, contribute to runoff. Retention and refreezing of melt water is an important process for the mass budget of the ice sheet. [Fausto et al., 2009]

The GrIS' **SEB** follows a seasonal cycle, which is strongly shaped by incoming shortwave radiation. Throughout the year, the ice sheet loses energy to the atmosphere by emitting longwave radiation. [Van den Broeke et al., 2011] During the summer months, the incoming shortwave radiation flux is highest and the ice sheet surface has a positive SEB during the day, causing melt. Many of the regional climate patters that influence precipitation, such as the NAO, AMO and GBI index, also affect the temperature and cloud patterns over Greenland during summertime. [Fyke et al., 2018]

Ocean

Submarine melting and iceberg calving are the two main ways, the Greenland ice sheet loses mass when interacting with the ocean. Submarine melting can be modeled taking ocean temperatures and currents close to the ice shelve base into account. [Jackson et al., 2014] Difficulties for modeling submarine melt are the required high resolution and model biases. Ice shelves, however, only account for less than 1% of the GrIS total area, which is why iceberg calving likely is the dominating force. [Fyke et al., 2018] While calving is mainly driven by the dynamics of the ice sheet, submarine melting and ocean conditions at the calving sites, such as the presence of ice shelves or an ice mélange, do play a role in the timing and frequencies of calving events. During winter time, growth of sea ice through freezing of the ice mélange inhibits calving and lets the ice shelf advance. During spring, as the formed sea ice retreats, calving is renewed. While the ice mélange influences the timing and frequency of calving events, it is unlikely to impact their magnitude. [Amundson et al., 2010]

Impact on Ice Dynamics

The discussed climate forcings on the Greenland ice sheet can be summarized as follows: mass is added over the high altitude interior, mostly through snow fall, and lost to running off melt water, submarine melting and iceberg calving at the low altitude ice sheet margin. The resulting positive surface gradient towards the interior of the ice sheet, causes a gravity-driven dynamical response by the ice sheet. Ice flows from higher altitude, thick ice regions in Greenland's interior, towards the lower altitude, thin ice regions on the margin of the ice sheet. [Fyke et al., 2018], [Rignot and Mouginot, 2012]

2.1.2 The Greenland Ice Sheet's impact on the Climate

While the GrIS' direct influence on large-scale **atmospheric** circulation is considered weak, it does affect the regional circulation. A damming of cold air over the ice sheet interior due to the ice sheet's high surface elevation and surface albedo influences cyclone development in the North Atlantic. Over Greenland, a quasi-permanent anticyclone can be observed. It is driven by topographic surface cooling over the ice sheet. [Fyke et al., 2018]

Ice sheet runoff, calving, submarine and basal melting represent freshwater influxes into the **ocean**. These fluxes directly affect the global sea level. With a coupled climate model - ice sheet model system, [Muntjewerf et al., 2020a] project increased ice loss from Greenland to cause a rise in global sea level of 10.9 cm until 2100 and under a high emission pathway. Depending on whether at a particular location the ice sheet is marine or land terminating, runoff enters the ocean at the surface or submarine at the grounding line, inducing very different fjord water circulations. Melt water entering at the depth of the grounding line, can induce turbulent mixing, driving warm and saline water upwards and

providing heat to the ice-ocean interface, a source for increased melt. In contrast, surface runoff which enters the sea at the surface from terrestrial points usually remains at the surface due to its comparatively low density. This means, that runoff from different parts of Greenland enters the open ocean in very different ways.
Depending on the conditions at the calving site, calved icebergs may enter the open ocean quickly or remain pinned in a fjord for some time. Generally they melt and decay slowly, so that freshwater from calving cannot be said to enter the ocean at a specific location but rather, is distributed over a larger area. Freshwater from runoff at the grounding line, as well as calved and melted icebergs typically enter the ocean as a vertically diffused signal, while surface runoff water stays at the surface for some time. This disparity has implications for the behaviour of the Atlantic meridional overturning circulation (AMOC). [Fyke et al., 2018] Considerations about other freshwater sources in the region, as well as recent modeling studies suggest however, that it is unlikely, that present day or future (up to 2100) enhanced Greenland freshwater supply has a significant impact on the AMOC. [Dahl-Jensen et al., 2009], [Devilliers et al., 2021], [Lenaerts et al., 2015]

Modeling results suggest that increased GrIS-melting related freshwater influx into the surrounding **marine ecosystem** will contribute to a decrease in net primary production (NPP) due to surface freshening and enhanced phytoplankton nutrient limitation, caused by a reduction in upwelling-favoring winds. [Kwiatkowski et al., 2019] A reduction in NPP will propagate through the Arctic marine food web to local populations of fish, birds and marine mammals. [Dahl-Jensen et al., 2009]

2.1.3 GrIS - Climate System Feedbacks

The GrIS and different parts of the climate system exert forcing on each other. A consequence of this two way relationship is the existence of feedbacks. Feedbacks are processes, that either dampen or amplify a given forcing. Positive feedbacks amplifies the initial forcing, while a negative feedbacks dampens the effect of the initial forcing on a system. Several ice sheet - atmosphere feedbacks are relatively well-known and studied while ice sheet - ocean feedbacks prove harder to detect and model. The latter are, as a result, not as well understood. In this section, three ice sheet - atmosphere feedbacks will be described.

Geometry - SMB Feedback: The interplay of geometry and surface mass balance gives rise to not one, but several important feedback mechanisms.
Ablation zones in Greenland are found at the margin in low elevation areas. The **positive elevation - SMB feedback** [Oerlemans, 1981] is based on temperatures generally rising with decreasing altitude. If there is initial melting at a given location, this will remove the and hence decrease the altitude at that point. It is now subject to increased temperatures, leading to more melt and ablation, amplifying the initial signal. Of course, this also works in reverse. Accumulation increases elevation, decreasing local tempera-

tures, leading to less melt (but not necessarily higher accumulation). [Fyke et al., 2018] The rate of change in surface mass balance with elevation is different for ablation and accumulation areas, however, which makes it difficult to capture this feedback, using only a temperature lapse rate. SMB-gradients have also been shown to vary spatially over the GrIS. [Helsen et al., 2012] [Vizcaino et al., 2015] estimate, that under different Representative Concentration Pathways, the elevation - SMB feedback contributes an additional 8-11% of GrIS mass loss until 2100 and an additional 24-31% until 2300, compared to fixed-elevation simulations.
Another important feedback is the **negative accumulation - ice sheet advance** feedback. Assuming an ice sheet in equilibrium with given climate forcing, if we were to observe additional accumulation over the interior, this would cause increased ice dynamic flow. Assuming enough persistent accumulation, an advance of the ice sheet on low elevation land until it meets the coast line would follow. This in turn means, that the ablation zone is increasing or that we observe increased iceberg calving, both of which have a negative impact on the ice sheet mass balance. This feedback counter-acts the initial positive mass balance contribution of increased accumulation and stabilizes the ice sheet. [Fyke et al., 2018]
Other ice sheet topography related feedbacks exist. As mentioned in section 2.1.1, the southern GrIS experiences orographic precipitation. Under warm conditions with increased ablation, the ice sheet would likely evolve to have a gentler slope along the southern perimeter, allowing warm, moist air masses to advect further inland over the interior of the ice sheet. Increased accumulation over the interior, would increase the elevation gradient towards the margin, leading to increased ice dynamic flow, yielding a negative feedback to the initial decreased precipitation along the margin of the ice sheet. [Fyke et al., 2018]

Albedo - Melt Feedback: Satellite-derived surface albedo time series show a connection between near-surface air temperature and albedo. As mentioned in section 2.1.1, the annual cycle of the surface energy balance of the GrIS is strongly shaped by the influx of shortwave radiation (SW). How much of the incoming SW is absorbed by the surface, depends on the surface albedo α:

$$\mathrm{SW}_{net} = \mathrm{SW}_{\downarrow}(1 - \alpha) \tag{1}$$

The surface albedo of ice sheets depends on factors such as snow grain size, impurity content, snow pack thickness and radiation incidence angle and wavelength. The first being considered the most important physical parameter regarding albedo. [Painter et al., 2009], [Adolph et al., 2017] Generally, albedo decreases with increasing snow grain size and increasing radiation wave length. Snow grain size increases as snow ages, especially under warm conditions and melt. As a result, broadband snow albedo is generally highest for pure, fresh snow at a value of about 0.84. [Konzelmann and Ohmura, 1995] Growing snow grain size leads to a higher absorption of solar radiation by the ice sheet, further warming the ice sheet surface and amplifying the initial warm signal, yielding a posi-

tive feedback. In the GrIS ablation areas, where during summer the accumulated winter snow cover melts completely, this feedback is even more pronounced. Bare ice is exposed, which is associated with albedo values below 0.6. [Wehrlé et al., 2021] As such, the strongest impact of the positive albedo - melt feedback is found in the ablation area, while the strongest impact temporally is during the high solar irradiance summer season. [Box et al., 2012]

SMB - Discharge Feedback: As the earlier described accumulation - ice sheet advance feedback, this mechanism negatively impacts an initial surface mass balance signal. Ablation at the ice sheet margin reduces the ice thickness. As ice flow is nonlinearly related to ice thickness, small changes in ice thickness have a strong impact on ice flow. With decreasing ice thickness, comes a decrease in ice flow over the grounding line of marine terminating outlet glaciers, leading to reduced ice discharge. The limit of this is a glacier retreating to terminate on land, reducing the discharge flux to zero. Increased accumulation, on the other hand, leads to higher ice thickness, increased ice flow and thus increased ice discharge. [Fyke et al., 2018]

2.2 Ice Sheet Mass Balance

The ice sheet mass balance governs its evolution and can be formulated like this:

$$\text{MB} = \text{SMB} - \text{ID} + \text{BM} \tag{2}$$

SMB, or surface mass balance, is the balance of atmospherically driven accumulation or ablation of mass at the surface. ID, or ice discharge, sums up ice sheet mass loss to the ocean and includes calving and submarine melting. BM denotes basal melting, which occurs at the base of the ice sheet due to a reduced melting point of water under the high pressure of the ice column and basal friction of a sliding ice sheet. As the sign implies, ice discharge loss can only be larger or equal to zero, while SMB and BM can be larger or smaller than zero. Common units for surface mass balance include mm water equivalent, if one is interested in the SMB at a specific location, or Gt year^{-1}, if the integrated GrIS SMB is considered. Ice discharge and basal melt are commonly quantified in Gt year^{-1}.
Ice discharge and SMB are not independent, as was described in section 2.1.3. [Box and Colgan, 2013] show that runoff controls much of the variability in ID. The relative contributions of SMB and ice discharge to the total ice sheet mass balance varies over time. [Rignot et al., 2008] estimate ice discharge to dominate GrIS mass loss between 1958 - 2007 with 60% $\pm$ 20%. [Enderlin et al., 2014] arrive at a similar estimate of 58% ice discharge contribution to total GrIS mass loss between 2000 - 2005 but estimate a dominance of mass loss due to runoff between 2009 - 2012 with ice discharge only contributing 32% in that time span. Basal melting is often one to several orders of magnitudes smaller than ice sheet integrated SMB and ID and thus has a weaker effect on the total ice sheet mass balance.

2.2.1 Surface Mass Balance

The surface mass balance can be defined as follows:

$$\text{SMB = Accumulation - Ablation = Snow + Rain - TMT - Runoff} \tag{3}$$

where Snow is snowfall, Rain is rainfall and TMT is turbulent moisture transport by evaporation, sublimation and deposition. Runoff in turn is composed of:

$$\text{Runoff = Melt + Rain - Refreeze} \tag{4}$$

where Refreeze is the sum of refrozen melt water as well as rain freezing on the ice sheet surface. The amount of occurring melt depends on the surface energy balance.

2.3 Surface Energy Balance

The surface energy balance (SEB) can be defined as:

$$\text{SEB = SW}_{\downarrow}(1-\alpha) + \text{LW}_{\downarrow} - \varepsilon\sigma\text{T}_s^4 + H_{sens} + H_{lat} + H_{sub} + H_{rain} \tag{5}$$

where $\text{SW}_{\downarrow}$ is downward surface shortwave radiation, α is the surface albedo, $\text{LW}_{\downarrow}$ is downward surface longwave radiation, ε is the surface emissivity, σ is the Stefan-Boltzmann constant, T_s is the surface temperature and the last four terms are sensible, latent, subsurface (towards the surface) heat flux and heat flux due to liquid rain on the surface, respectively.
If the temperature of the surface is below the freezing point, a positive energy balance acts to increase the surface temperature and thus the temperature of the snow pack. If the surface temperature reaches the melting point of water, additional surface energy surplus will go towards phase change, so melting of the surface layer. In models which cannot rely on observations to determine presence and magnitude of surface melt, modeling the surface energy balance realistically is the key to modeling surface melting and thus is integral to modeling ice sheet surface mass balance.

3 Models

This section offers an overview over the coupled system and brief descriptions of the involved models: EC-Earth 3 - Veg, CISSEMBEL and PISM. A selection of relevant physical processes is described for each model.

3.1 Overview of the Coupled Climate Model - GrIS Model System

Section 2 addressed the different ways, the Greenland ice sheet and the rest of the climate system interact with each other. The representation of these interactions can be improved by coupling the PISM ice sheet model to the EC-Earth 3 global climate model, rather than relying on simplified parameterizations within EC-Earth 3.
Figure 3 shows an overview of the two coupling approaches that were implemented and tested. The standard EC-Earth 3 atmosphere-ocean-sea ice-vegetation coupled system is depicted in the black box with blue connections between models denoting data exchanges between the components. EC-Earth 3 will be described in the following section. The newly added components are connected to the standard EC-Earth 3 coupled system with the green, newly implemented connections, in order to facilitate the coupling to PISM. These data exchanges allow the different models to know about and be influenced by the state of other parts of the climate system and can thus be considered the heart of the coupling. The components with red boxes were added to the coupled system. Of these, PISM and CISSEMBEL are existing models that were used as is. The ISM-Mapper is the coupling interface that was developed in this project.
PISM and EC-Earth 3 are run asynchronously each year. Each model is run for one year, generating forcing fields that are then used by the other model as it runs for one year. An example for this is PISM running for one year, generating a new ice sheet topography and geometry. EC-Earth 3 then runs for one year as well, incorporating the updated topography and geometry and generating the forcing fields for the next PISM run.

PISM results influence the atmospheric dynamics model component IFS by providing updated ice sheet topography and extent. The ocean model NEMO receives fresh water influxes due to basal melt and ice discharge from PISM. These exchanges are shown by solid green arrows in figure 3. They are done the same way, independently of whether the PISM surface forcing is provided by CISSEMBEL or by EC-Earth 3.
PISM itself receives atmospheric forcing, consisting of the surface mass balance and below-firn ice temperature. Two different approaches for modeling this atmospheric forcing were implemented and tested in this project.
The first approach uses IFS variables of precipitation, evaporation and runoff directly to calculate the resulting surface mass balance. The soil temperature from the land surface model HTESSEL is used as the below-firn temperature. Data exchanges facilitating this

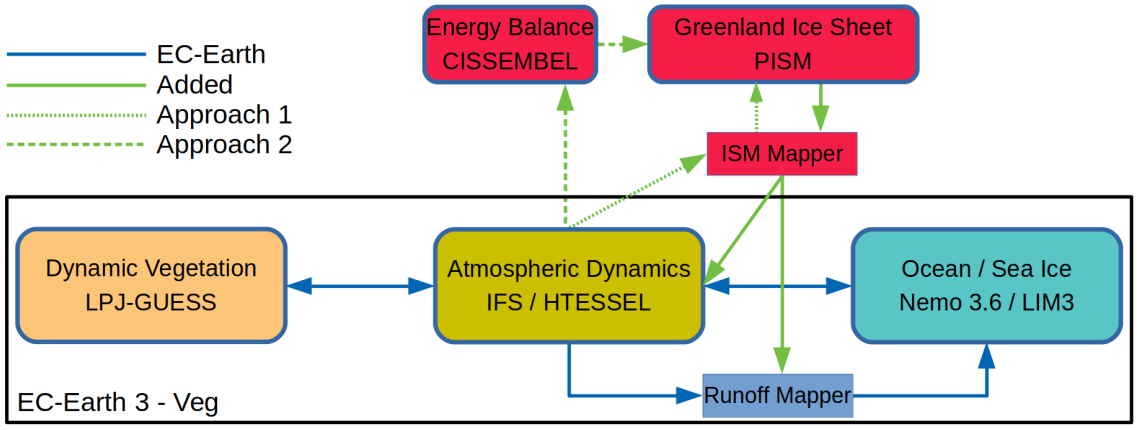

Figure 3: Illustration of EC-Earth 3 - PISM coupling. Model components within the black box are part of EC-Earth 3. Components that have a red box were added to the coupled system. PISM and CISSEMBEL are existing models which were coupled to EC-Earth 3. The ISM-Mapper is a coupling interface that was developed in this project. Green arrows show newly implemented connections to facilitate coupling between EC-Earth 3 and PISM in approach one (finely dashed green lines) and EC-Earth 3, PISM and CISSEMBEL in approach two (coarsely dashed lines). Solid green connections are used by both coupling approaches.

coupling approach are denoted by the finely dashed green arrows in figure 3.
In the second approach, the CISSEMBEL energy balance model, forced by atmospheric variables from IFS, is used to calculate the surface mass balance. The CISSEMBEL ice temperature at 10 m depth is used as the below-firn temperature when forcing PISM. Data exchanges facilitating this coupling approach are denoted by the more coarsely dashed arrows in figure 3.

When coupling different models, different timesteps, resolutions and domains have to be accounted for. This makes helper modules, such as the Runoff-Mapper and the ISM-Mapper necessary. The Runoff-Mapper is responsible for routing water that becomes available over land, such as runoff, to a set of pre-defined ocean points on the ocean model grid.
The ISM-Mapper prepares fields coming from PISM or IFS so that they can be used by the other models and thus functions as an interface between PISM and EC-Earth 3. Both of these components are described in more detail in section 4.

3.2 EC-Earth 3 - Global Climate Model

EC-Earth 3 is a full Earth system model, developed by the EC-Earth consortium, which counts 30 research institutes from 12 European countries. [EC-Earth-Consortium, 2021] Development was sparked in 2006 as an effort, to merge Earth system (ESM) and climate modeling, and numerical weather prediction (NWP) and thereby, allow each area to profit from advances in the others.
The most recent version of EC-Earth 3 is a full Earth system model which components for modeling atmospheric dynamics, land surface processes, the ocean, sea ice, dy-

namic vegetation, interactive aerosols and atmospheric chemistry and the carbon cycle. [Döscher et al., 2021] The configuration EC-Earth 3-Veg is used in this project with includes the components shown in figure 4 and table 3.2. Going forward, EC-Earth 3 refers to this configuration. The different components are coupled with the OASIS 3 coupler, which provides spatial and temporal interpolation routines. [Valcke et al., 2015] The table below, shows an overview of the active components, their versions and references.

	Model	Reference
Atmosphere	Integrated Forcasting System (IFS, cycle 36r4)	ECMWF
Land Surface	Hydrology Tiled ECMWF Scheme of Surface Exchanges over Land (HTESSEL)	[Balsamo et al., 2009]
Ocean	Nucleus for European Modelling of the Ocean (NEMO, Version 3.6)	[Madec et al., 2017]
Sea Ice	Louvain-la-Neuve Ice Model (LIM, Version 3.6)	[Vancoppenolle et al., 2009] [Rousset et al., 2015]
Dynamic Vegetation	LPJ-GUESS (Version 4.0)	[Smith et al., 2001]

Figure 4 shows a summary of the most important configurations of EC-Earth 3 - Veg in the present work. IFS, and with it also HTESSEL, is run with a T255 spectral resolution horizontally and 91 vertical levels on a linear N128 reduced Gaussian grid which corresponds to an approximate 80 km horizontal resolution globally. NEMO and LIM3 are run with resolution ORCA1L75, a 1° horizontal resolution with 75 vertical levels. Finally, LPJ-GUESS is also run with T255 spectral resolution.

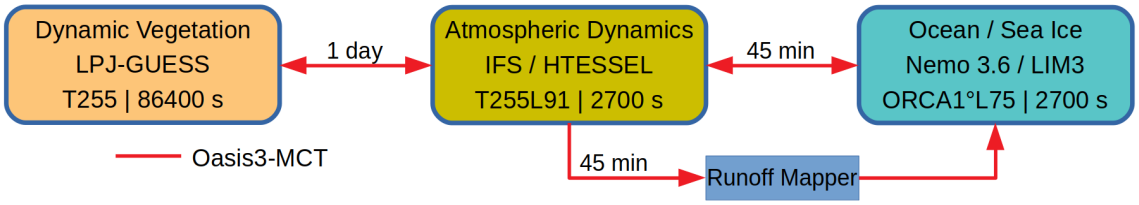

Figure 4: Coupling scheme and configurations of EC-Earth 3 - Veg. 3rd line of each component shows the resolution, followed by the model timestep. Coupling timesteps and connections are shown between the components. Red connections denote exchanges facilitated by Oasis3-MCT.

For simplicity, from here on, HTESSEL and LIM will be treated as sub-models of IFS and NEMO respectively. The components are coupled and fields are exchanged between IFS and LPJ-GUESS as well as between IFS and NEMO.
IFS provides soil and 2 meter air temperatures, precipitation, short-wave and long-wave radiation to LPJ-GUESS. LPJ-GUESS returns the dominant vegetation type, leaf area index and vegetation cover fraction for both high and low vegetation to IFS.

IFS exchanges momentum flux, solar and non solar heat flux, evaporation, solid and liquid precipitation and the sensitivity of non solar heat flux over ice with the ocean model NEMO, which in turn provides sea surface temperature, sea ice concentration, temperature, albedo and snow thickness on sea ice to IFS. Through the use of the so called Runoff-Mapper module, which distributes surface water fluxes to a pre-defined set of ocean points, IFS also sends runoff and calving fields to NEMO.

3.2.1 Surface Energy Balance and Runoff in EC-Earth 3-Veg

In this section, the calculation of surface energy balance and snow melt is described. First in words and then in more detail including equations. These calculations are handled by the land surface model HTESSEL.
This section largely follows the IFS documentation [ECMWF, 2010]. Other references are given where appropriate.

HTESSEL

HTESSEL is the land surface and soil hydrology model within IFS, handling the surface - atmosphere interactions including surface energy and mass fluxes and sub-surface quantities, such as the soil water budget. In HTESSEL, 8 different surface types, also called tiles, of surface are differentiated, each of which have different properties affecting surface energy and mass fluxes. The 8 surface tiles are open water, ice water, bare ground, interception reservoir, low vegetation, high vegetation, snow on low vegetation or bare ground and snow under high vegetation. A separate solution for the surface energy balance and skin temperature is found for each tile. These solutions are then combined in a weighted average of the values of each tile to obtain single values for each grid cell. Mixing of sea and land tiles is not allowed, so that a grid-cell is either 100% land or water, depending on which is dominant.
HTESSEL has a simple snow model which simulates an extra snow layer on top of the four soil layers for snow tiles. Snow can be added to the snow layer through snowfall and removed through snow melt, which in turn contributes to surface runoff, soil infiltration and evaporation. Snow melt occurs, if the calculated skin temperature of the snow tile is above the freezing point. Then, the temperature is set to the freezing point and the surplus heat is spent on melting snow. The snowpack is characterized by a single snow temperature T_{sn} and by snow mass per unit area S. The snowpack can hold liquid water which affects its heat capacity. How much it holds depends on snow mass, density and snowpack temperature.

Surface Energy Balance and Mass Balance of Snow Layer

Equation 6 shows the formulation of the skin energy balance in HTESSEL. The unit of mass fluxes and energy fluxes are kg m^{-2} s^{-1} and W m^{-2}, respectively. Constants which

are not given explicitly here, can be found in table 11 in the appendix. $T_f = 273.15$ is the freezing point temperature of water.

$$(\rho C)_{sn} D_{sn} \frac{\partial T_{sn}}{\partial t} = R^N_{sn} + L_s E_{sn} + H_{sn} - G^B_{sn} + L_f RF_{in} - L_f M_{sn} - Q^{INT}_{sn} \tag{6}$$

where

$(\rho C)_{sn} \approx \frac{(\rho C)_{ice}}{\rho_{ice}} \rho_{sn}$	volumetric heat capacity of snow
$D_{sn} = \frac{S}{\rho_{sn} c_{sn}} \in [0, 1]$ m	snow layer depth
$T_{sn} \leq T_f$	snow layer temperature
$R^N_{sn} = SW^N + LW^N$	net radiative flux
$H_{sens} = \rho_{air} C_{p,air} \lvert U_L \rvert C_{H,i} (T_L + g \frac{z_L}{C_{p,air}} - T_{sk,i})$	sensible heat flux
$L_s E_{sn} = L_s \rho_{air} \lvert U_L \rvert C_{H,i} [\, q_L - q_{sat}(T_{sk,i})]$	latent heat flux, sublimation
$G^B_{sn} = \frac{T_{sn} - T_{soil}}{r_{sn}}$	snow layer basal heat flux
$L_f RF_{in}$	latent heat flux, freezing of intercepted rain
$L_f M_{sn}$	latent heat flux, melting

The net short-wave radiation depends on the surface albedo α. In the EC-Earth 3 standard setup, it has a constant value of 0.8 over perennial ice sheets. If an ice sheet extent is provided, a variable surface albedo scheme allowing albedo-melt feedback can be used. (see sections 3.2.2, 4.3.1) $|U_L|$, T_L, z_L, q_L are the wind speed, temperature, height and humidity of the lowest atmospheric level. g is the gravitational acceleration, $C_{H,i}$ the tile specific turbulent exchange coefficient and $C_{p,air}$ the heat capacity of moist air. r_{sn} is the thermal resistance between the middle of the snow layer and the first soil layer. c_{sn} is the snow tile fraction of the whole grid-cell. $c_{sn} RF_{in}$ is the flux of rain that is intercepted in the snow pack. The temperature of rain falling on the snow layer is set as T_f.

The climatological snow depth in IFS is capped at 10 m. Only in the energy balance equation, the snow depth is limited to 1 m. Otherwise, over large ice sheets like the GrIS, where most grid-cells have a snow depth of 10 m, the thermal inertia of the snow layer would be very large, preventing the snow layer from reacting to climate forcing in reasonable time.

The last term in equation 6, Q^{INT}_{sn} captures the heat change due to snow layer internal phase changes and is calculated as:

$$Q^{INT}_{sn} = L_f M^{INT}_{sn} = L_f \frac{\partial S_l(T_{sn}, S)}{\partial t} \tag{7}$$

where S_l is the snow liquid water content in kg m^{-2}. Liquid water can exist in the snowpack if $T_{sn} > T_f - 2K$. Above this threshold, the snow liquid water content is a parameterized

function of the snow temperature and the snow liquid water capacity which increases with increasing temperature. Depending on the density of the snowpack, snow liquid water capacity reaches from 3% (at $\rho_{sn} < 200$ kg m^{-3}) to 10% (at $\rho_{sn} = 400$ kg m^{-3}) and more of the sum of snow and water in the snowpack. Q_{sn}^{INT} is strictly positive (but a negative contribution in 6) and acts as a heat capacity barrier close to T_f. In compacted snow, this term can increase the snow heat capacity by up to five fold.
The mass balance of the snowpack is:

$$\frac{\partial S}{\partial t} = SF + c_{sn}RF + c_{sn}E_{sn} - R_{sn} \tag{8}$$

where SF, RF, E_{sn} and R_{sn} are the mass fluxes due to snowfall, rainfall, sublimation and runoff.
Equation 6 can be solved numerically for an updated, preliminary snow temperature T_{sn}^{*}.
Two cases are considered:
1) No melt: In this case $T_{sn}^{*} < T_f$. The new snowpack temperature is $T_{sn}^{t+1} = T_{sn}^{*}$ and the snowpack thickness is updated using equation 8:

$$S^{t+1} = S^{t} + (SF + c_{sn}E_{sn})\Delta t \tag{9}$$

2) Melt: If $T_{sn}^{*} > T_f$, the timestep is split into two fractions: $\Delta t = \Delta_1 t + \Delta_2 t$.
In the first fraction, the snowpack temperature is reset to T_f, which will also be the new temperature: $T_{sn}^{t+1} = T_f$. The length of $\Delta_1 t$ is then calculated according to equation 6.
In the second fraction, the temperature is held constant and melting occurs. At constant temperature, equation 6 can be used to obtain the melt flux:

$$-c_{sn}M_{sn} = -\frac{c_{sn}}{L_f}[\,R_{SN}^{N} + L_s E_{sn} + H_{sn} + L_f RF_{in} - G_{sn}^{B}] \tag{10}$$

which can then be directly used to update the snow layer thickness:

$$S^{t+1} = S^{t} + (SF + c_{sn}E_{sn})\Delta t - c_{sn}M_{sn}\Delta_2 t \tag{11}$$

Depending on the whether there is snow left after a melt event, the basal heat flux is adjusted accordingly.
Finally, runoff is calculated as follows:

$$R = c_{sn}M_{sn} + \mathsf{max}\left(c_{sn}RF - \frac{S_l^{max}}{\Delta t}, 0\right) - I_{max} \tag{12}$$

where I_{max} is the maximum infiltration rate of the soil beneath the snow layer. Runoff is produced, once the melt and rainfall exceed the maximum infiltration rate. I_{max} depends on the standard deviation of orography in a given grid-cell, soil texture and soil water content of the first 50 cm of soil. In partially frozen soil, infiltration is inhibited, increasing the amount of runoff.

3.2.2 Albedo Scheme Copenhagen

In the EC-Earth 3 standard setup, the surface albedo over areas of perennial snow, and therefore ice sheets, is set to a constant value of 0.8. This fails to account for the important albedo - melt feedback.
Thus, a more sophisticated albedo scheme was integrated into EC-Earth 3 by [Madsen et al., 2021b], which was proposed and described as "Albedo Scheme Copenhagen" in [Helsen et al., 2017].
It is implemented in the HTESSEL code and applied over areas which are specified as ice sheet covered areas. In this scheme, the GrIS surface albedo can vary between 0.6 and 0.85. When snow falls, the albedo increases in proportion to the amount of snowfall, according to the equation:

$$\alpha^{t+1} = \alpha^t + \min\left(1, \frac{F\Delta t}{10}\right)(\alpha_{snow} - \alpha^t) \tag{13}$$

where $\alpha_{snow} = 0.85$ is the albedo of fresh snow, Δt is the model timestep in days and F is the snowfall rate. For the albedo to be set to the value for fresh snow, the snowfall rate has to exceed 10 kg m^{-2} day^{-1}.
In the absence of snowfall, three different scenarios are considered: melting, refreezing and snow ageing. In the case of melting conditions, which are defined in the albedo scheme at a snow temperature of $T_{sn} > -2^{\circ}$C, the albedo is instantly set to the minimum value of $\alpha_{min} = 0.6$. If melting occurred in the previous timestep and thus the albedo is below the albedo of refrozen snow $\alpha_{refrozen} = 0.65$, the albedo is instantly set to $\alpha_{refrozen}$.
Finally, in dry conditions, a slow exponential decay is applied to parameterize the effect of snow grain growth on albedo:

$$\alpha^{t+1} = \alpha_{firn} + \left[\max(\alpha^t, \alpha_{firn}) - \alpha_{firn}\right] \cdot \exp\left(-\frac{\Delta t}{\tau_{firn}}\right) \tag{14}$$

where $\alpha_{firn} = 0.75$ is the firn albedo and $\tau_{firn} = 30$ days is the e-folding timescale.

3.2.3 Ice Discharge

In EC-Earth 3 the maximum climatological snow depth is set at 10 m. Excess snow is routed to the ocean by the runoff mapper and regarded as calving. This is thus the ice discharge mechanism in EC-Earth 3.

3.3 CISSEMBEL - Energy Balance Model

CISSEMBEL is short for Copenhagen Ice Snow Surface Energy and Mass Balance modEL. It is mainly developed at the Danish Meteorological Institute (DMI) in the R&D department in collaboration with the Alfred Wegener Institute, Helmholtz Centre for Polar and Marine Research. [Rodehacke, 2020] It is based on research by [Langen et al., 2015] and [Langen et al., 2017].
Figure 5 shows a scheme of the CISSEMBEL model, taken from [Rodehacke, 2020]. The model takes climate forcing fields as input and solves the energy balance equation using

the Newton Method for the new surface temperature. CISSEMBEL can be run with different numbers of layers. In the standard setup, the model has 5 layers with thicknesses of 0.33, 1.0, 3.0, 6.0 and 9.0 meters. If snow is added or removed at the top due to accumulation or melt, the layer profile gets shifted, rather than the thickness of the top layer increased or decreased. The top layer is in contact with the atmosphere. Temperature and density are advected between the layers. Several different albedo schemes are implemented. Additionally, the model offers the possibility of downscaling atmospheric forcing from a more coarse topography to a finer topography field through lapse rate correction.

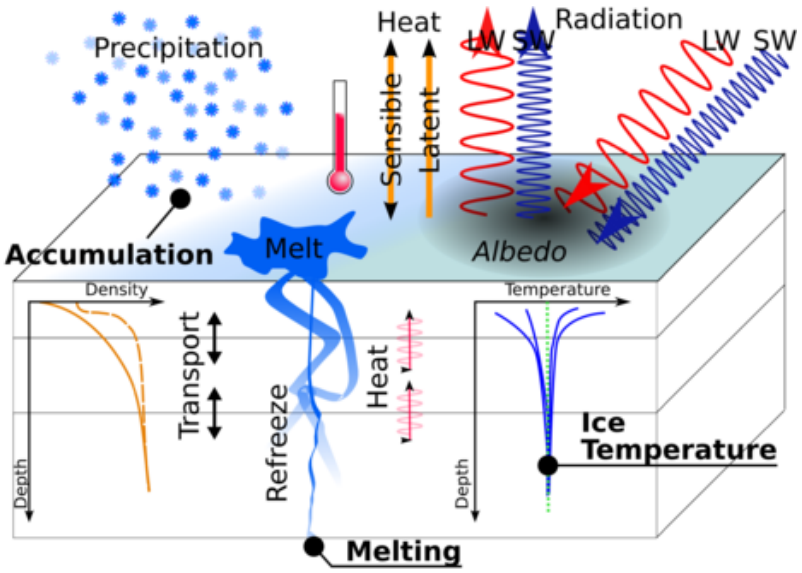

Figure 5: CISSEMBEL model scheme showing surface energy exchanges, as well as sub-surface processes. Taken from [Rodehacke, 2020]

.

CISSEMBEL is forced with atmospheric data. Here, this forcing data are fields, generated with EC-Earth 3 and include: climate model topography (m), surface pressure (Pa), 2 meter air and dew point temperature (K), 10 meter wind (m s^{-1}), total precipitation (convective + large-scale precipitation, kg m^{-2} s^{-1}) and downward surface solar and thermal radiation fluxes (W m^{-2}).

CISSEMBEL writes out a number of fields such as accumulation and ablation fluxes, albedo values and snow properties.

The model is initialized with a density and temperature profile in the snow layers. These quantities are then advected between the layers, depending on surface forcing and resulting new profiles in the sub-surface layers. Therefore, it is important, that the model is brought to equilibrium with surface conditions at the beginning of a simulations, in order to avoid unexpected behavior during the run. This is done by running the model with the provided surface forcing once, using the final state of this initialization as the initial state for the actual run.

3.3.1 Surface Energy and Mass Balance

Equation 15 shows the formulation of the surface energy balance, or surface heat flux, in CISSEMBEL. All heat fluxes are positive towards the surface. Before the equation is solved numerically for the new top layer temperature, relevant quantities are calculated according to the atmospheric forcing at a particular timestep. These quantities include the air density, vapor pressure and surface albedo. Quantities with subscript 'sn' belong to the surface layer. Constants can be found in table 12.

$$\Phi_q = (1-\alpha)SW_{\downarrow} + LW_{\downarrow} - \sigma T_{sn}^4 + H_{lat} + H_{sens} + G_{sn}^B + H_{pp} + H_{rain} \tag{15}$$

where

$(1-\alpha)SW_{\downarrow}$	net surface solar radiation flux
$LW_{\downarrow} - \sigma T_{sn}^4$	net surface thermal radiation flux
$H_{lat} = A\lvert U_L\rvert(e_L(T_{air}) - e_{sn}(T_{sn}))$	surface latent heat flux
$H_{sens} = c_d \rho_{air} \lvert U_L\rvert (T_{air} - T_{sn})$	surface sensible heat flux
$G_{sn}^B = (T_{sn-1} - T_{sn}) * C_{sn-1} * 2/(\Delta z_{sn} + \Delta z_{sn-1})$	snow layer basal heat flux
$H_{pp} \overset{<T_f}{=} SF\rho_{water}C_{p,snow}(T_{air} - T_{sn})$	precip. on snow, phase change
$\overset{>T_f}{=} RF\rho_{water}[C_{p,water}(T_{air} - T_f) + C_{p,snow}(T_f - T_{sn})]$	
$H_{rain} = RF\rho_{water}C_{p,water}(T_{air} - T_{sn})$	rain falling on surface

RF and SF denote rain- and snowfall flux, $C_{p,snow}$ and $C_{p,water}$ the specific heat capacities of snow and water in J kg^{-1} K^{-1}. $c_d = 1.515$ is the dimensionless surface drag coefficient. $A = 3.3 \cdot 10^{-2}$ is a constant, e_L and e_{sn} are the vapor pressure at the atmospheric dew point temperature and the surface temperature, respectively. They are calculated following [Buck, 1981]. The heat flux at the base of the surface layer G_{sn}^B is calculated from quantities of the surface layer and the layer below, which is denoted by $sn-1$. Thus, C_{sn-1} is the thermal conductivity of the layer below the surface layer. It depends on the density of that layer. Δz are the respective layer thicknesses.
The new surface layer temperature T_{sn}^* is found iteratively using the Newton Method, as the root of the function defined in equation 16. $T_{sn,prev}$ is the temperature at the previous timestep and ρ_{sn} is the density of the surface layer.

$$F(T) = -T + T_{sn,prev} + \Phi_q(T)\frac{\Delta t}{\rho_{sn}C_{p,snow}\Delta z_{sn}} \quad \text{with} \quad F(T_{sn}^*) = 0 \tag{16}$$

1) No Melt: $T_{sn}^* < T_f$. The surface layer temperature is updated as $T_{sn} = T_{sn}^*$.

2) Melt: $T_{sn}^* >= T_f$. the surface layer temperature is reset to $T_{sn} = T_f$ and the snow

albedo is updated to reflect melting conditions. With these updated values and the condition $F(T_f) = 0$, the excess temperature T_{excess} is calculated.

$$T_{excess} = T_{sn,prev} + \Phi_q(T_f)\frac{\Delta t}{\rho C_{p,snow}\Delta z_{sn}} - T_f \tag{17}$$

With the excess temperature, the surface melt flux is obtained.

$$S_{melt} = \max(T_{excess}, 0)\frac{\rho_{sn} C_{p,snow}\Delta z_{sn}}{L_f \rho_{ice}} \tag{18}$$

CISSEMBEL explicitly models refreezing. Melt water originates from the surface layer and can penetrate the layers beneath, as long as their density is below the pure close-off density of $\rho_{close} = 830$ kg m^{-3}. At each layer with a density below the close-off density, a potential refreezing flux is calculated, depending on the layer temperature. The actual refrozen melt water is then subtracted from the surface melt flux according to a prescribed profile. This is done as long as the refreezing flux is not larger than the surface melt flux. Depending on how much surface melt water refroze in a specific layer, the layer's temperature and density are adjusted.
In the absence of melt, deposition or sublimation mass fluxes are calculated from the latent heat and added to accumulation. Here, it is important to note, that accumulation in CISSEMBEL is net transport, so a sublimation flux that is larger than snowfall flux can lead to negative accumulation.
Finally, the density profile of all layers is adjusted to the net transport at the surface. Advection velocities are calculated, depending on the density of the layer above and the one below, for each layer. Figure 6 shows schematically the process as well as the equation for layer two. The density below the lowest layer is the density of ice ρ_{ice}. The densities of the layers are controlled by a reference density profile, depending on depth d, given in equation 19. $C_d = -0.024$ is a chosen constant.

$$\rho_{ref}(d) = \rho_{ice} - (\rho_{ice} - \rho_{snow})exp(C_d d) \tag{19}$$

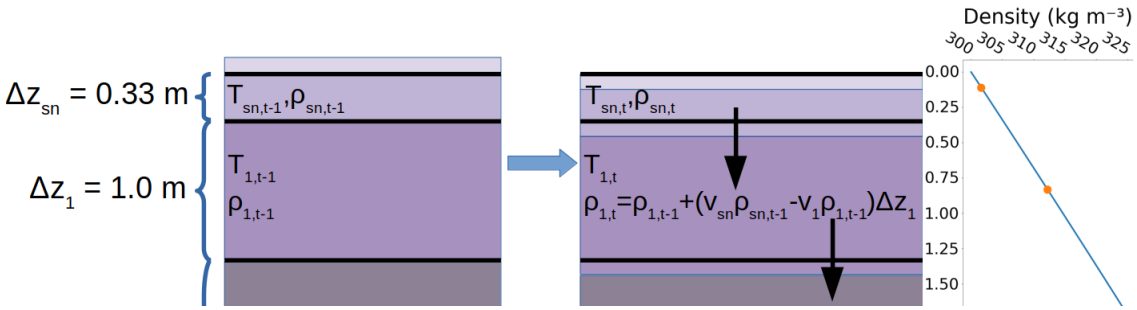

Figure 6: Illustration of density profile shifting in an accumulation scenario.

3.3.2 Albedo Schemes

CISSEMBEL offers different albedo schemes and also allows the user to define albedo schemes. Three different schemes are applied in this project.
The "**Albedo Scheme Copenhagen**" (Cph), described in section 3.2.2, is implemented in the same way. Albedo scheme Cph is used for producing results in section 5.
Additionally, the "**Albedo Scheme Copenhagen Modified**" (Cph-mod), features small differences to the original Cph scheme. In dry conditions, the decay towards the firn albedo is much faster, following equation:

$$\alpha^{t+1} = \alpha_{firn} + \left[\mathsf{max}(\alpha^t, \alpha_{firn}) - \alpha_{firn}\right] \cdot \mathsf{exp}\left(-\frac{age_{snow}}{\tau_{firn}}\right) \tag{20}$$

where age_{snow} is the age of the snow layer, defined as the time since the last snowfall in days. Contrary to value Δt, the model timestep in days, in equation 14, this value grows between dry condition timesteps, leading to a much faster decay.
Furthermore, the albedo in melting conditions is set to 0.55, instead of 0.6, the value in albedo scheme Cph.
Albedo scheme Cph-mod is used for producing surface forcing with CISSEMBEL in section 6 and in the coupled experiments in section 7.

3.3.3 Lapse Rate Downscaling

CISSEMBEL offers the possibility of downscaling incoming climate forcing variables with lapse rates. This requires that a topography is provided, that is different from the topography in the climate model that was used to generate the forcing data. Knowing both the climate model topography and an additional topography, CISSEMBEL then uses lapse rate correction in order to downscale the climate forcing to the additionally provided topography. This is especially useful, when aside from the coarse resolution climate model topography, a finer resolution topography is available - such as an ice sheet topography.
For pressure, a parameterization of the barometric formula is used. For temperature, a standard lapse rate of $\Gamma_T = -6.5$ K km^{-1}. Downward long-wave radiation is downscaled with a constant lapse rate of $\Gamma_{LW} = -\frac{75.0}{2600.0}$ W m^{-2}. Vapor pressure is implicitly downscaled through the downscaling of dew temperature and pressure.

This feature is not used in all CISSEMBEL simulations. For the results from experiments that are presented in section 5, it is not active. In the coupled setup, where the PISM ice sheet topography is available, it is used (results in section 7).

3.4 PISM - Ice Sheet Model

The Parallel Ice Sheet Model (PISM, version 1.2) is an open source model for glacier and ice sheet dynamics. It is developed at the University of Alaska. PISM implements a strict separation of ice dynamics and climate forcing and allows the interaction of the ice sheet with its surroundings through interfaces.

A large number of configurations and modeling choices are available, the presentation of which would vastly exceed the scope of this section. What is presented here, is the subset of modeling choices that are used for producing results in this project.
This section largely follows the PISM documentation [PISM-Authors, 2020]. Other references are given where applicable.
A summary of PISM parameter choices and constants can be found in 13.

3.4.1 Ice Dynamics and Thermodynamics

The evolution of a PISM ice sheet is governed by the mass continuity, energy conservation and stress balance equations.
The velocity of flowing ice is determined by the stress balance, which in turn is calculated as a function of geometry, temperature and basal strength. PISM approximates the non-Newtonian Stokes model for ice flow with a hybrid of the shallow ice approximation (SIA) and the shallow shelf approximation (SSA). Both the SIA and the SSA velocities are calculated over the entire ice sheet and then added. The SIA dominates in regions of non-sliding grounded ice which is present over the ice sheet interior. With the SSA, membrane stress is calculated for ice shelves and for grounded ice in areas of small basal resistance, such as ice streams and outlet glaciers. In the latter case, it effectively acts as a sliding law for grounded ice.
Figure 7 shows an illustration of the hybrid SIA-SSA flow modeling scheme.
In both approximations, hydrostatic pressure as well as a small thickness-to-width ratio for the ice sheet and ice shelves are assumed.
PISM also includes the Lingle-Clarke model for bed deformation, an improved generalization of the flat earth Elastic Lithosphere Relaxing Asthenosphere (ELRA) model.

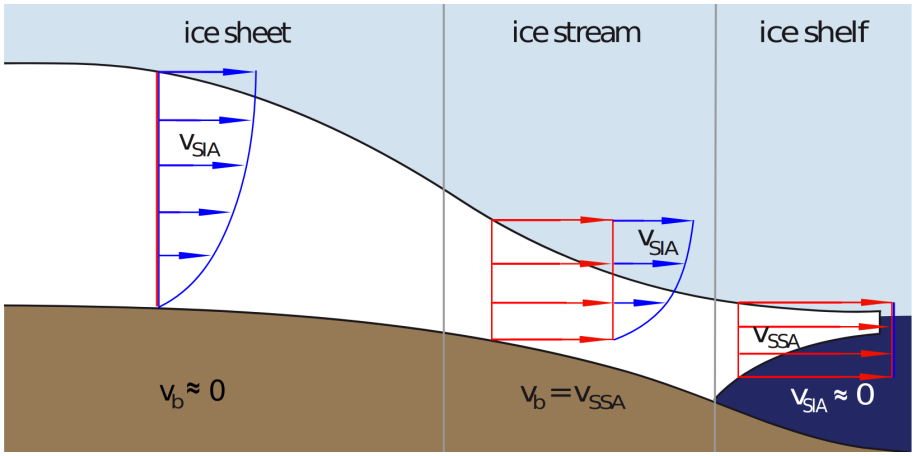

Figure 7: Illustration of hybrid SIA-SSA flow scheme in PISM. In the left column, the velocity of non-sliding grounded ice is is modeled with the SIA. In the middle, the velocity of an ice stream is modeled as a weighted average of the SIA and SSA solutions. On the right side, the velocity of an ice shelf is modeled with the the SSA alone. Credit: [Winkelmann et al., 2011].

Thermodynamics: Conservation of energy is solved for ice and a thin subglacial layer

with an enthalpy based scheme and for a bedrock layer. Ice can be polythermal. Latent heat of water is incorporated both for the liquid water in temperate ice and for the liquid water under the ice sheet. Since ice flow is considered slow (does not build inertia), heat is dissipated into the ice as a result of ice deformation through the gravitational driving stress. Frictional heating occurs at the base of the ice sheet as a result of sliding. This heat either goes toward changing the temperature, and thereby softness of the ice or toward producing melt water at the base. Basal melt water production is controlled by conservation of energy across the ice-bedrock interface and is stored locally in the till under the ice column. There, it can build up to an effective thickness of 2 meters and decay at a given rate. Basal melt water exceeding 2 meters is lost permanently, which means that the model in this configuration does not conserve mass.

Shallow Ice Approximation: The SIA considers local shear stress as a function of driving stress with zero basal sliding, meaning that only shear stress balances the gravitational driving stress. The flow law takes the Arrhenius-Glen-Nye form:

$$D_{ij} = E_{sia} A(T) \tau^2 \tau_{ij} \qquad \text{with} \qquad \tau^2 = \frac{1}{2} \tau_{ij} \tau_{ij} \tag{21}$$

where D_{ij} is the strain rate tensor, $E_{sia} = 3.0$ the flow enhancement factor (modeling choice), $A(T)$ is the temperature dependent ice softness, or flow factor. τ denotes the deviatoric stress tensor and i and j the two horizontal components. Together with the Stokes flow momentum balance equations and integration from the base to a height $\tilde{z}$ in the ice of the vertical derivatives of horizontal velocities, the ice velocities in the SIA are obtained:

$$(v_x, v_y)_{SIA} = -2(\rho_i g)^3 |\nabla h|^2 \left[\int_b^{\tilde{z}} E_{sia} A(T) (h - z)^3 dz \right] \nabla h \tag{22}$$

where v_x and v_y are the horizontal ice velocities, ρ_i is the ice density, g the gravitational acceleration and h the surface height.

Shallow Shelf Approximation: A sliding base introduces stresses that are fully or partially balanced by membrane stresses, depending on the basal strength. These are, contrary to shear stresses, independent of depth and nonlocal [Bueler and Brown, 2009]. The stress balance for the SSA is as follows:

$$\begin{aligned} \frac{\partial}{\partial x} \left[2\bar{\nu} H \left(2\frac{\partial v_x}{\partial x} + \frac{\partial v_y}{\partial y} \right) \right] + \frac{\partial}{\partial y} \left[\bar{\nu} H \left(\frac{\partial v_x}{\partial y} + \frac{\partial v_y}{\partial x} \right) \right] + \tau_{b_x} &= \rho_i g H \frac{\partial h}{\partial x} \\ \frac{\partial}{\partial x} \left[\bar{\nu} H \left(\frac{\partial v_x}{\partial y} + \frac{\partial v_y}{\partial x} \right) \right] + \frac{\partial}{\partial y} \left[2\bar{\nu} H \left(\frac{\partial v_x}{\partial x} + 2\frac{\partial v_y}{\partial y} \right) \right] + \tau_{b_y} &= \rho_i g H \frac{\partial h}{\partial y} \end{aligned} \tag{23}$$

where $\tau_\mathsf{b} = (\tau_{b_x}, \tau_{b_y})$ is the basal shear stress, $\bar{\nu}$ is the vertically averaged effective viscosity and H the ice thickness.
In ice shelves, the basal stress is zero. Whether grounded ice is sliding depends on the basal conditions. The basal shear stress is model by a pseudo plastic power law:

$$\tau_{\mathsf{b}} = -\tau_c \frac{\mathsf{v}}{v_{max}^q |\mathsf{v}|^{1-q}} \tag{24}$$

where τ_c is the yield stress, v_{max}^q is the threshold velocity and $q = 0.25$ is a modeling choice. The yield stress, in turn, is obtained through the Mohr-Coulomb law:

$$\tau_c = c_0 + (\tan\Phi) N_{till} \tag{25}$$

where c_0 is called "till cohesion" and set to 0 as a modeling choice, Φ is called "till friction angle" and a material property of the basal till, parameterized by chosen constants. Finally, N_{till} denotes the effective pore water pressure of the till. It is a function of the till water content. The more water the till holds, the smaller N_{till}, reducing the yield stress. The maximum value is $N_{till,max} = P_0 = \rho_i g H$, the overburden pressure, while the minimum effective pore water pressure is a modeling choice and set at $0.02 P_0$. Sliding can only occur if the basal shear stress reaches the value of the yield stress.

Hybrid SIA-SSA solution: The ice velocities $\mathbf{v}_{SIA}$ and $\mathbf{v}_{SSA}$, obtained from solving equations 22 and 23 respectively, are simply added to obtain the total ice velocity:

$$\mathbf{v} = \mathbf{v}_{SIA} + \mathbf{v}_{SSA} \tag{26}$$

3.4.2 Surface Forcing in PISM

The PISM ice dynamics core interacts with the atmosphere and ocean via interfaces. Figure 8 illustrates these interfaces.

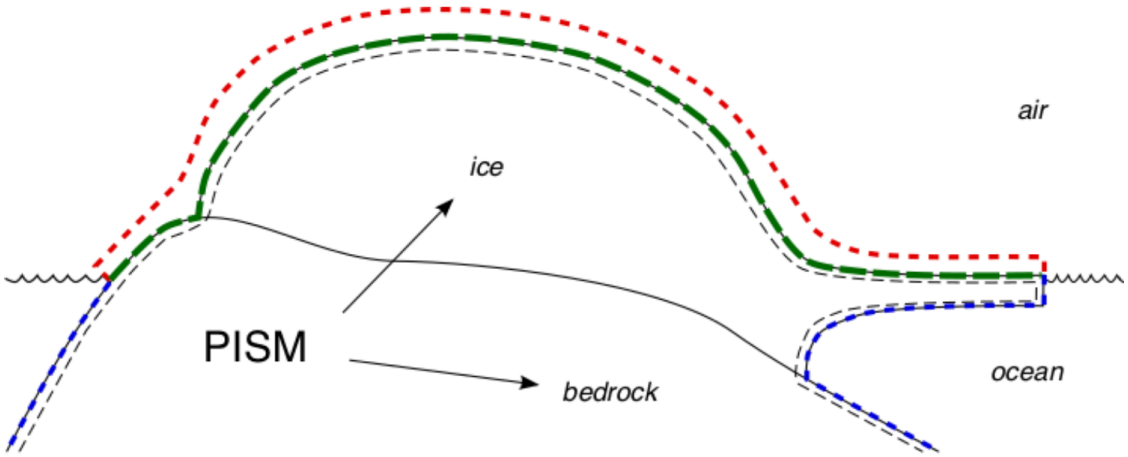

Figure 8: Illustration of the ice dynamics-environment interfaces in PISM. Atmosphere-ice sheet (grey), surface-ice sheet (green), ocean-ice sheet (blue). Taken from [PISM-Authors, 2020].

Different options for forcing the ice sheet at these interfaces exist. In this project, the ice sheet is forced at the surface through providing the surface mass balance (in kg m^{-2} s^{-1}) and below-firn temperature. If the below-firn temperature has not previously been downscaled (such as by the CISSEMBEL model in section 7), it is corrected by a constant

lapse rate of -5.4 K km^{-1}. This lapse rate was found from the EC-Earth 3 below-firn temperature forcing which is used in the initialization experiment (section 6).
At the ocean interface, the sub-shelf ice temperature is set to pressure-melting-point and a spatially and temporally constant sub-shelf melt rate of 0.051914 m yr^{-1} is set.

3.4.3 Ice Discharge

PISM comes with multiple different calving options. The most important discharge mechanism in this project is a constant retreat mask, which covers the entire Greenland land area and present-day ice shelve extent [Morlighem et al., 2017]. Ice that advances beyond the retreat mask, is immediately discharged.
Thickness calving is also used, where ice shelves with a thickness below 125 m automatically get calved. This calving only contributes little to the observed discharge fluxes.

4 The Climate - Greenland Ice Sheet Coupled System in Detail

This section describes details of the coupling of EC-Earth 3 and PISM, with the optional use of CISSEMBEL. First, the resolutions and domains are briefly described for the involved models. Following are details on the individual fields that are exchanged between component models.
The coupling interface Oasis3-MCT, or Oasis in short, is used for handling field exchanges between different component models. It handling interpolations between different resolutions and domains. For this, it requires the following files:

- grid definition file: contains grid point longitudes and latitudes of source and target grid
- domain definition file: specifies relevant grid points on the source and target grid via masks
- area definition file: contains the grid cell areas of the source and target grid

The ISM-Mapper was developed in this project as an interface between EC-Earth 3 and PISM. EC-Earth 3 is not coupled to PISM directly, but rather with the ISM-Mapper coupling interface ”in between”. The ISM-Mapper runs synchronously with other EC-Earth 3 model components. It receives and sends fields from and to EC-Earth 3 via Oasis. It also performs temporal interpolations and keeps track of the model date in order to account for leap years. PISM runs after one year of EC-Earth 3 simulation, taking surface forcing from EC-Earth 3 or CISSEMBEL into account and producing forcing fields for EC-Earth 3.
Surface forcing is provided to the PISM ice sheet via the respective forcing interface. In EC-Earth 3 modifications to the source code and run-script are required.

4.1 Resolutions and Domains

PISM is run with a 15 km x 15 km resolution. Figure 9 shows the PISM domain and the way it is split into land and ocean points. This distinction is necessary because PISM forcing requires a temperature greater than 0 K over the whole domain but the IFS soil temperature is only defined over land.
In EC-Earth 3, the resolutions of IFS, NEMO and the Runoff-Mapper are relevant.
IFS physics uses a linear reduced Gaussian grid and is run with a horizontal global resolution of approximately 80 km. Since all relevant fields concern surface quantities, the number of vertical levels does not need to be taken into account in the coupling explicitly.
NEMO is run at a resolution of 1°x1° with a refinement to about 1/3° near the equator on the so-called ORCA1 grid, a tri-polar ocean grid, for all ocean points.

The Runoff-Mapper is used on a regular grid with a resolution of approximately 0.7°x0.7°. Spatial interpolations between different grids are offered in Oasis through the SCRIPR library. N nearest-neighbor interpolation, weighted by the distance of the source and target grid points and a Gaussian function, is used for all scalar fields in this setup with $N = 9$. The distance weights are given by:

$$\exp\left(-\frac{d^2}{2\sigma^2}\right) \qquad \text{where} \qquad \sigma^2 = 2.0 \cdot \overline{d} \tag{27}$$

where d is the distance between target and source grid point and $\overline{d}$ the average distance between two source grid points. Masked target grid values are assigned a value of zero. If any of the target grid's nearest neighbors on the source grid are masked, the target grid value is calculated from the remaining, unmasked neighbors. [Valcke et al., 2015]
In the case of conservative remapping, the residual of the field between the target and source grid is distributed proportionally to the value of the field on the source grid.

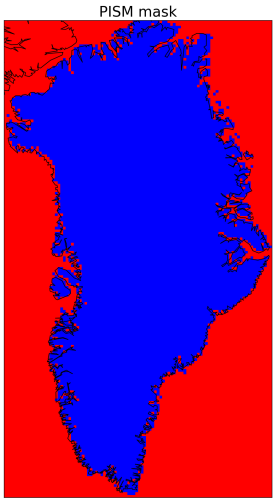

Figure 9: Distinction between masked (red) and unmasked (blue) points in Oasis. This mask is used in Oasis for interpolating to PISM land points.

4.2 Accounting for the Climate System's Impact on the Greenland Ice Sheet

PISM is forced at the atmosphere boundary with monthly-mean fields of surface mass balance (kg m^{-2} s^{-1}) and below-firn temperature (K). These forcing fields are generated either with IFS variables directly (approach 1) or with CISSEMBEL (approach 2).
At the ocean boundary, PISM is forced with a constant frontal melt rate and is therefore not interactive with EC-Earth 3.

4.2.1 Approach 1: Forcing from Global Climate Model EC-Earth 3

In order to calculate the surface mass balance from EC-Earth 3 variables, according to equation 3, four different fields are required: solid and liquid precipitation, runoff and evap-

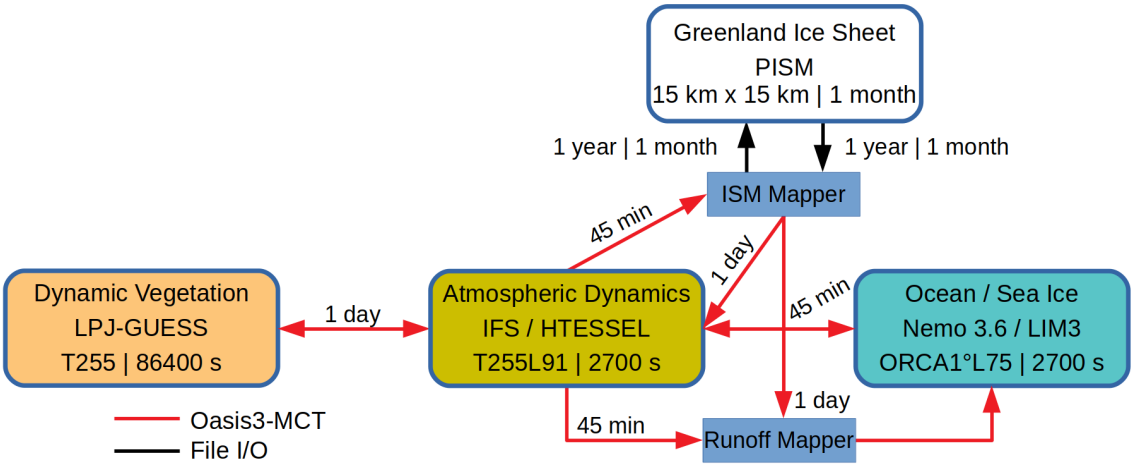

Figure 10: Illustration of coupling setup where surface forcing for PISM is generated from EC-Earth 3 data. Boxes with round edges show component models and their respective domains, names, resolutions and timesteps. Connections between component models denote data exchanges, the notes next to them frequency and, if different, the timestep of exchanged data. Red arrows show data exchanges facilitated by Oasis, black arrows show exchanges through NetCDF files. The ISM-Mapper helper module facilitates temporal integration and interpolation and reading and writing of NetCDF files, the Runoff-Mapper remaps runoff from land to a pre-defined set of coastal ocean points.

oration. Additionally, the soil layer four temperature and sea surface temperature are combined for land and ocean points, to generate a below-firn temperature forcing field.
The runoff and evaporation fluxes are calculated in IFS by HTESSEL, while liquid and solid precipitation fluxes (sum of convective and large-scale precipitation) are calculated by IFS' convection and cloud schemes. At each 45-minute timestep these four fields, available as timestep-average fluxes in kg m^{-2} s^{-1}, are sent to the ISM-Mapper. In the process, they are conservatively remapped from IFS' linear reduced Gaussian grid, with a mask excluding all points outside of Greenland land points, to the PISM regional grid's land points. In the ISM-Mapper, the fluxes are accumulated. It also keeps track of the current date in the model and at the end of each month, the ISM-Mapper calculates the monthly average fluxes and writes them to a NetCDF file.
The same procedure is followed for the temperature forcing fields. Over land, the HTESSEL soil layer 4 temperature, which covers a soil depth of 100-289 cm, is used. Since the PISM temperature forcing field cannot be 0 K anywhere on the domain, the sea surface temperature is used for ocean points on the PISM grid. The mask for ocean points is the inverse of the mask shown in figure 9. Monthly average temperatures are calculated by the ISM-Mapper and written to the same file as the surface fluxes above.

These exchanges are symbolised by the connection from IFS toward the ISM-Mapper in figure 10. At the end of one simulation year, a bash script is run which combines the surface flux and temperature fields so that the resulting forcing file contains one year of monthly surface mass balance and temperature forcing data. The bash script also sets up the PISM run script and submits it to run.

4.2.2 Forcing from Downscaled Energy Balance Model

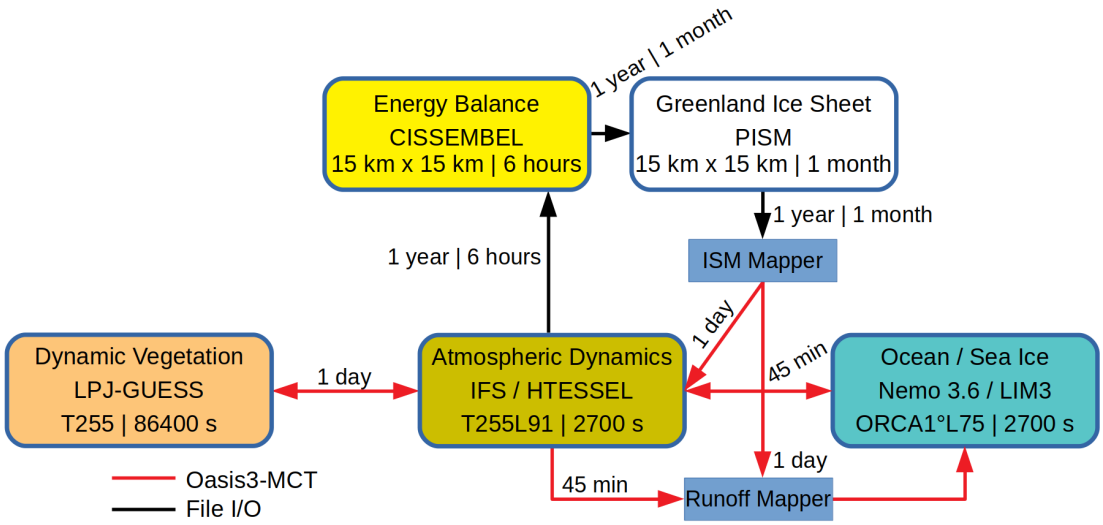

Figure 11: Illustration of coupling setup where surface forcing for PISM is generated from CISSEMBEL data. Boxes with round edges show component models and their respective domains, names, resolutions and timesteps. Connections between component models denote data exchanges, the notes next to them frequency and, if different, the timestep of exchanged data. Red arrows show data exchanges facilitated by Oasis, black arrows show exchanges through GRIB or NetCDF files. The ISM-Mapper helper module facilitates temporal integration and interpolation and reading and writing of NetCDF files, the Runoff-Mapper remaps runoff from land to a pre-defined set of coastal ocean points.

When CISSEMBEL calculates the surface forcing, climate forcing fields are required from IFS. After each year of EC-Earth 3 simulation, a bash script, hereafter referred to as coupling script, is run, which reads 6 hourly forcing fields from the IFS standard output GRIB files, converts them to NetCDF files and remaps them bilinearly to the PISM grid using CDO. The precipitation and radiation fields are written as timestep-accumulated fluxes in m (water equivalent) 6hr^{-1} and J m^{-2} 6hr^{-1} by IFS and converted to mean fluxes in kg m^{-2} s^{-1} and W m^{-2}. The PISM surface elevation from the end of the previous year is used as the reference topography for downscaling some forcing variables using lapse rates as described in section 3.3.3.

It is important to note, that this coupling approach is still under development. Since CISSEMBEL does not calculate the runoff but rather the ablation flux, this quantity cannot replace the IFS runoff directly. Therefore, the IFS runoff is routed to the surrounding ocean points instead of the CISSEMBEL ablation flux. Thus, this approach does not conserve mass and a synchronous coupling of CISSEMBEL with IFS is required in order to facilitate mass conserving couping in the future.

The CISSEMBEL simulation is restarted from the previous year's final state and run for one year to generate average monthly accumulation and ablation flux fields. These are combined to produce the monthly surface mass balance forcing fields. The average monthly "temperature below seasonal influence layer" variable, which is the temperature of a CISSEMBEL layer covering a depth of 10.33-19.33 meters, is used as the below-firn

temperature forcing field. The coupling script generates the NetCDF forcing file for PISM, sets up the PISM run script and submits it to run.

4.3 Accounting for the Greenland Ice Sheet's Impact on the Climate System

4.3.1 Providing Ice Sheet Topography and Extent to the Global Climate Model

In order to facilitate the realistic calculation of surface mass balance in EC-Earth 3, the climate model needs to know both the current ice sheet topography, as well as the extent of the ice sheet on Greenland. The ISM-Mapper coupling interface provides these from PISM fields. The coupling script extracts relevant fields from the PISM output.
The new ice sheet topography is given by the last timestep of the PISM "ice top surface elevation" variable. It is bilinearly remapped to the linear reduced Gaussian IFS grid. Additionally, the Greenland land mask on the IFS grid is applied to make sure, that the standard IFS topography is only updated over Greenland.
In IFS, the topography is set once at the beginning of each year and then kept constant throughout the rest of the year. Therefore, the topography update has to be handled via reading the updated Greenland topography from a NetCDF file. The IFS code, specifically the module responsible for initializing the grid-point orography fields of the model, was altered to take the new topography over Greenland into account. The module reads the Greenland topography file and converts surface elevation (m) to geopotential height (m^2 s^2) by multiplying by the IFS standard gravitational acceleration value of 9.80665 m s^{-2}. Over Greenland, where this field has values larger than zero, the standard IFS orography is replaced. In order to incorporate the updated orography on the model's spherical harmonics grid, the grid-point orography is transformed to the spherical harmonics grid and back.

While IFS has a snow scheme, the area where it is applied does not necessarily match with the area the ice sheet covers in PISM. In order to properly reflect the presence of the ice sheet in IFS, the ice sheet extent is needed.
In areas where the ice sheet extent demands it, changes are made to the calculation of the surface energy and mass balance. Albedo Scheme Copenhagen is applied in all grid cells covered by the ice sheet. Since IFS only produces a snow melt flux if there actually is snow, the ice sheet extent also specifies areas where snow melt is then also calculated for non-snow tiles in IFS. This additional snow melt flux is added to the runoff to facilitate the calculation of a realistic surface mass balance over the whole PISM ice sheet, and the resulting latent heat of fusion is subtracted from the surface energy balance. Furthermore, soil properties are changed for all four soil layers in HTESSEL to reflect the presence of the ice sheet such as a constant soil heat conductivity and capacity of 2.2 W m^{-1} K^{-1} and $2.05 \cdot 10^6$ J K^{-1} m^{-3}. Evaporation is treated as sublimation by changing the specific heat and the longwave emissivity is changed to 0.98.
The ice sheet extent is generated from the PISM land ice thickness variable. Every grid cell where the land ice thickness has a value greater than 10 meters is considered part

of the ice sheet extent. This results in a monthly binary field which is written to a NetCDF file. The ISM-Mapper reads this file and exchanges the monthly field via Oasis with IFS. On the IFS grid, the extent field has values between 0 and 1, depending on how many neighbors on the PISM grid have a value of 1. In order to avoid conflicts with the run length due to leap years and variable month lengths, the extent field is exchanged daily but is only updated once per month.

4.3.2 Providing Fresh Water Fluxes to the NEMO Ocean Model

The discharge flux from PISM consists of solid contributions from ice sheet advance beyond the retreat mask, calving and frontal melt. The liquid basal melting flux of grounded and floating ice is considered separately. These fluxes are sent to the ocean model via the Runoff-Mapper.
The coupling script writes these to a NetCDF file after the PISM run, which is then read by the ISM-Mapper and conservatively remapped to the Runoff-Mapper grid via Oasis. The general idea of the Runoff-Mapper is to pool water fluxes over land into drainage basins and remap the total flux over a set of pre-defined coastal ocean points, called arrival points. Greenland, together with Ellesmere Island, forms one of such basins. The Runoff-Mapper considers the basal melt flux as part of the runoff and adds it to the runoff flux coming from IFS. The runoff flux represents an influx of liquid freshwater into the ocean. The discharge flux around Greenland replaces the calving mechanism over Greenland in IFS. Calving is routed to the NEMO grid as a solid freshwater flux.

5 GrIS SMB-Modeling with Global Climate and Energy Balance Model

This section explores and compares surface mass balance results from EC-Earth 3, CISSEMBEL and ERA5-reanalysis data.
Section 5.1 deals with EC-Earth 3 and CISSEMBEL surface mass balance data from different experiments. The most important information on the EC-Earth 3 experiments, which both provide runoff, evaporation and precipitation for direct calculation of the GrIS SMB in EC-Earth 3 and climate forcing for the CISSEMBEL simulations, is summarized in table 1. All EC-Earth 3 experiments were performed by Marianne Sloth Madsen, the corresponding CISSEMBEL experiments by the author.

Experiment	Period	Type	AS EC-Earth 3	AS CISSEMBEL
HSTA	1850 - 1878	Historical	STA - 0.8	STA - 0.8
HCPH	1850 - 1878	Historical	CPH	CPH
SSTA	2015 - 2041	SSP5-8.5 Scenario	STA - 0.8	STA - 0.8
SCPH	2015 - 2043	SSP5-8.5 Scenario	CPH	CPH
20ST	1950 - 2014	Historical	STA - 0.8	CPH

Table 1: Properties of EC-Earth 3 experiments. The acronym AS is short for albedo scheme.

Albedo scheme STA - 0.8 denotes the standard EC-Earth 3 albedo scheme which has albedo 0.8 over areas of perennial snow in IFS. Albedo scheme CPH is Albedo Scheme Copenhagen (section 3.2.2).
All EC-Earth 3 experiments are run in the EC-Earth 3-Veg configuration, using IFS, NEMO with LIM3 and LPJ-Guess (figure 4). EC-Earth 3 data, both forcing and results, is bilinearly interpolated to the PISM grid for analysis.
Three hourly ERA5-Reanalysis data on single levels is used for the time periods 1950-1978 (preliminary back-extension) and 1979-2014, both for obtaining surface mass balance variables and climate forcing variables for CISSEMBEL. ERA5 snow melt, snowfall, snow evaporation as well as precipitation, runoff and evaporation variables are conservatively remapped to the PISM grid while forcing data for CISSEMBEL is bilinearly remapped to the PISM grid.
Ablation in CISSEMBEL is melt water that is generated when the surface layer has a positive temperature as calculated by the surface energy balance, minus refreezing. It does not, however, include contributions from rain and so is not directly comparable to the runoff variable in EC-Earth 3 or ERA5, which does include liquid precipitation that is not retained by the soil. Therefore, the surface mass balance is calculated in different ways from CISSEMBEL and EC-Earth 3 model variables. From EC-Earth 3 and ERA5 data, the SMB is calculated according to equation 3. From CISSEMBEL data, the SMB is calculated as accumulation (minus sublimation) minus ablation.
Comparisons of melt in this section refer to the net melting rate. In EC-Earth 3 and ERA5,

this variable is given as snow melt. In CISSEMBEL, it is the ablation plus the refreeze flux.
Accumulation rates are rates of solid precipitation minus sublimation (called snow evaporation in EC-Earth 3 and ERA5).
All integrated values are **calculated over the extent of the initialized ice sheet under CISSEMBEL surface forcing**, which is described in section 6. Going forward, "Greenland ice sheet" will refer to this initialized state. Spatial plots are shown for surface mass and energy balance fluxes over the same area. Still, the topography in EC-Earth 3 is the standard topography.

5.1 SMB in a Global Climate and an Energy Balance Model

5.1.1 Results

Figure 12 presents time series of SMB and the net melt rate, integrated over the GrIS. EC-Earth 3 and CISSEMBEL use the same albedo schemes, according to the respective experiments (table 1).

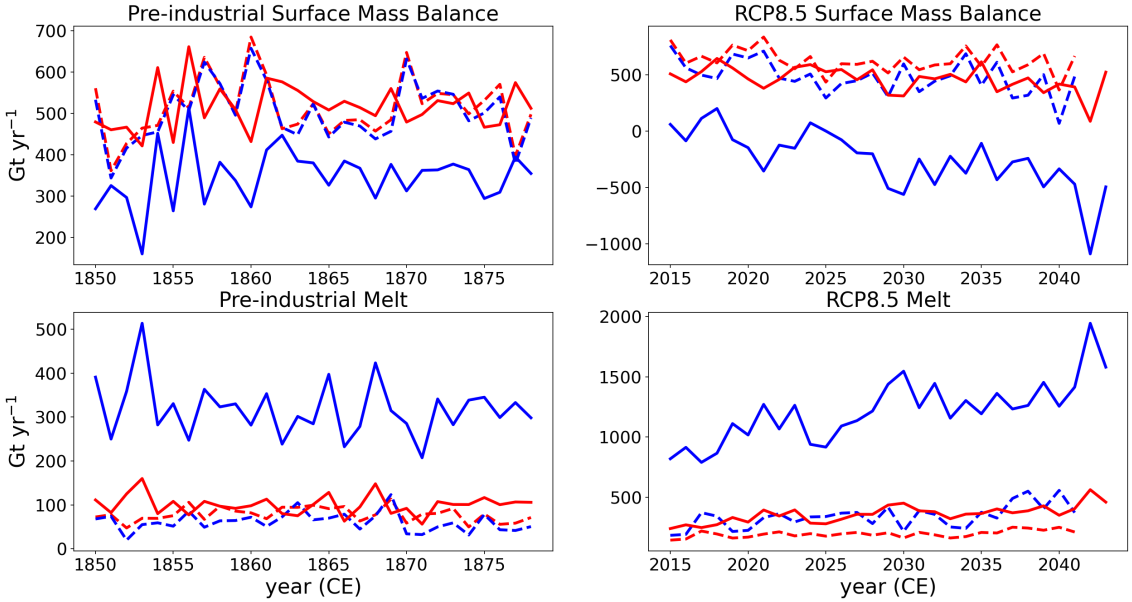

Figure 12: Surface mass balance and net melt rates as modeled by EC-Earth 3 (red lines) and CISSEMBEL (blue lines), integrated over the GrIS. Experiments HSTA and SSTA, using the EC-Earth 3 standard albedo of 0.8 over the ice sheet, are denoted by dashed lines. Solid lines signify experiments HCPH and SCPH which use Albedo Scheme Copenhagen, both in EC-Earth 3 and CISSEMBEL.

CISSEMBEL delivers lower accumulation rates than EC-Earth 3. Since the EC-Earth 3 two meter air temperature is the deciding factor for precipitation falling in solid or liquid form in both models, this is caused by differences in sublimation. The magnitude of the effect depends on the albedo scheme. The average difference between EC-Earth 3 and CISSEMBEL in integrated accumulation in the standard albedo scheme is (10.2 ± 1.0)% (of CISSEMBEL values). In Albedo Scheme Copenhagen it is (16.9 ± 0.9)%.

The differences in modeled melt strongly depend on the albedo scheme. In experiments where the standard albedo scheme is used, the differences are smaller than with albedo scheme Cph. For three out of four experiments, CISSEMBEL generates a higher average melt rate than EC-Earth 3, the HSTA experiment being the sole exception. Higher melt rates, combined with lower accumulation rates, lead to lower SMB rates in CISSEMBEL than EC-Earth 3 in all experiments.
Table 2 shows the net melt and surface mass balance rates, averaged over the whole experiment for both models. Uncertainties are given as the linearly detrended time series' standard deviations, which can be interpreted as the data's interannual variability.

	SMB (Gt yr^{-1})		Melt (Gt yr^{-1})	
Experiment	EC-Earth 3	CISSEMBEL	EC-Earth 3	CISSEMBEL
HSTA	(514 ± 70)	(502 ± 71)	(78 ± 16)	(61 ± 21)
HCPH	(507 ± 54)	(347 ± 67)	(100 ± 21)	(318 ± 61)
SSTA	(592 ± 96)	(482 ± 132)	(195 ± 23)	(339 ± 76)
SCPH	(419 ± 99)	(-250 ± 176)	(360 ± 47)	(1216 ± 159)

Table 2: Surface mass balance and net melt rates in Gt yr^{-1}, integrated over the GrIS.

Figure 13 shows a spatial comparison between the time-averaged EC-Earth 3 and CISSEMBEL generated SMB rate for the SCPH experiment, which displays the strongest differences in modeled surface mass balance and melt rates.

5.1.2 Analysis & Discussion

Surface mass balance and melt rates from EC-Earth 3 and CISSEMBEL show the same trends, albeit amplified in CISSEMBEL. This is true both for long term trends as well as year to year variability, where spikes in figure 12 match up.
Spatially, EC-Earth 3 and CISSEMBEL show very similar behavior as well. The highest melt rates occur in low elevation areas along Greenland's west coast, followed by the south eastern and northern coastal areas. CISSEMBEL calculates greater than zero melt rates further inland than EC-Earth 3, which leads to a more gradual decrease with rising elevation than in EC-Earth 3. This is also evident in the resulting SCPH surface mass balance, where EC-Earth 3 shows positive values right above 1500 m in the north and 2000 m along the western coast, while in CISSEMBEL, the SMB in these regions hovers around zero for several hundreds of meters of elevation more. (figure 13)
This results in significantly different average ablation areas in the two models. In CISSEMBEL it is (34.5 ± 7.2)% with a maximum value of almost 61% during the high ablation year of 2042. In EC-Earth 3 it is (15.9 ± 6.8)% with a maximum value of almost 42% during the same year. In the historical experiment HCPH, both CISSEMBEL ((9.3 ± 3.6)%) and EC-Earth 3 ((2.2 ± 2.0)%) model significantly smaller ablation zones.

In contrast to CISSEMBEL, the standard EC-Earth 3-Veg configuration calculates snow melt only where snow is present in IFS. This snow covered area is potentially smaller

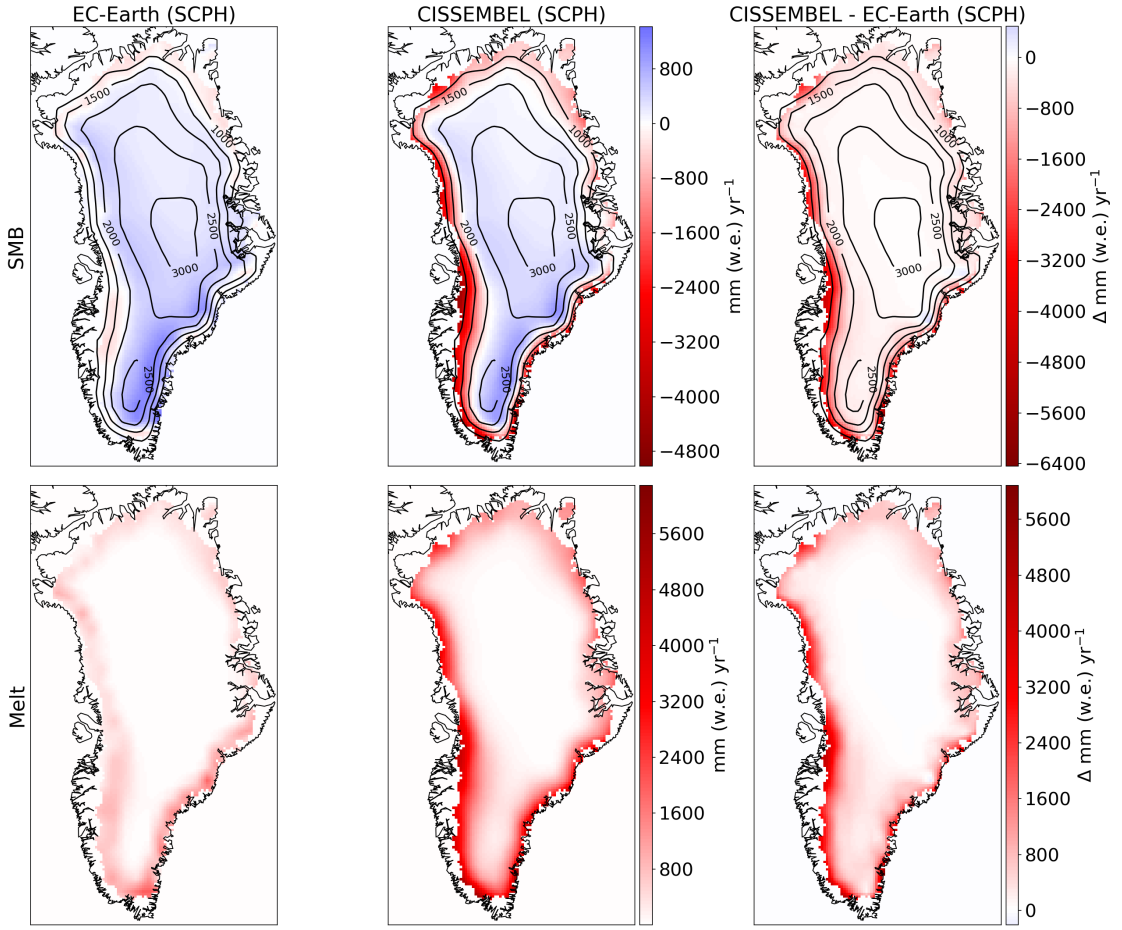

Figure 13: Average SMB (top) and snow melt (bottom) rates for SCPH experiment (Cph, 2015-2043). The left column shows EC-Earth 3, the middle CISSEMBEL values, the right the CISSEMBEL minus EC-Earth 3 difference.

than the ice sheet extent used here to produce ice sheet integrated surface mass balance rates. In order to find areas, that have the potential for underestimating snow melt, the minimum summer (June-July-August) snow depth is compared for each grid cell with the maximum summer 3-hourly snow melt rate. Figure 14 shows areas within the extent of the ice sheet, that have potential for underestimating snow melt in red, while areas that don't are shown in blue. On average, only 3 grid cells on the PISM grid show potential for underestimating melt in the historical experiments each year. In SSTA (64) and SCPH (244) this number is higher. To accurately determine the impact of underestimated snow melt on the results presented in this section, an EC-Earth 3 experiment with an artificially thick snow layer would have to be done, which covers the GrIS area sufficiently during the entire experiment. However, under the conditions in these experiments, the possible effect can be considered small. In SCPH, where out of all experiments the most grid cells are affected, these account for about 4% of ice sheet covered grid cells that show snow melt in IFS at any point during the entire experiment. Furthermore, since the lowest snow depth might be recorded in July and the highest melt rate in August, not all of these grid

cells necessarily experience underestimation of the snow melt rate.
In the SCPH experiment, the area where the snow layer in IFS has a thickness of more than 1 meter decreases by 14% during the 29-year experiment. This quick retreat shows a likely inability of the standard EC-Earth 3-Veg configuration to model realistic freshwater fluxes from the Greenland ice sheet under sustained warm conditions.

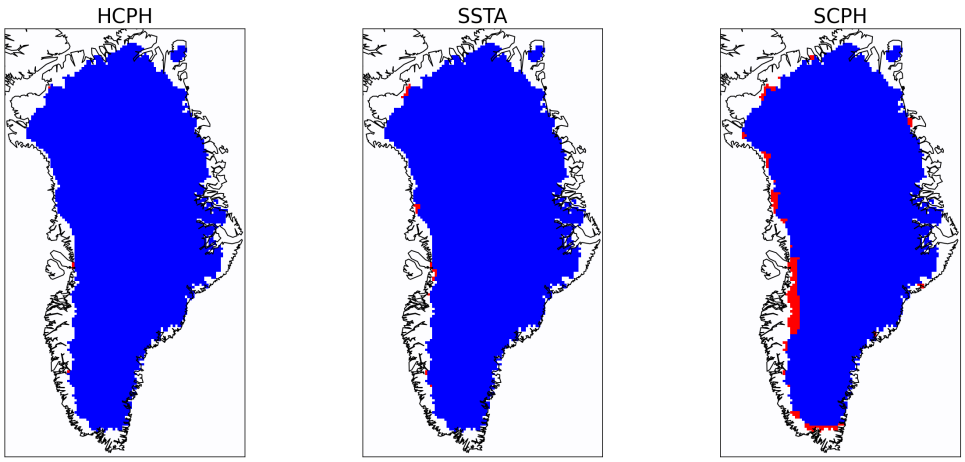

Figure 14: In red areas, the summer (JJA) minimum snow depth is smaller than the summer maximum 3-hourly snow melt rate in any year during the experiment. Affected grid cells have a potential for underestimating snow melt due to a smaller snow covered area in IFS than the ice sheet area that results here are integrated over. The left plot shows these areas for the HCPH experiment (comparable with HSTA), the middle for the SSTA experiment and the right for the SCPH experiment.

Albedo Scheme Copenhagen leads to higher melt rates in both models. While it allows for higher maximum albedo values than the standard scheme, the average annual albedo over the whole ice sheet is lower than 0.8 in all experiments. Since the variable albedo scheme has the highest impact in areas with greater than zero melt rates, a weighted average of the albedo by melt rates gives a better picture of the impact of Albedo Scheme Copenhagen. Table 3 summarizes average albedo values over the entire ice sheet.

	EC-Earth 3	CISSEMBEL	EC-Earth 3, weighted	CISSEMBEL, weighted
HCPH	(0.798 ± 0.003)	(0.792 ± 0.003)	(0.768 ± 0.003)	(0.761 ± 0.004)
SCPH	(0.790 ± 0.003)	(0.776 ± 0.004)	(0.764 ± 0.003)	(0.741 ± 0.005)

Table 3: Ice sheet average albedo for the HCPH and SCPH experiments in EC-Earth 3 and CISSEMBEL. The two right columns, show values weighted by normalized melt rates.

In the historical run HCPH, the average albedo values in EC-Earth 3 and CISSEMBEL are rather similar. Despite this, CISSEMBEL produces more than three times as high of an average annual melt flux as EC-Earth 3. In the scenario run SCPH, more frequent melting events and a significantly larger albation zone in CISSEMBEL lead to a lower average albedo than in EC-Earth 3.
Higher modeled melt rates in CISSEMBEL, under comparable albedo conditions (HCPH) call for a comparison of surface energy balance components between the two models.

	HCPH		SCPH	
all in W m^{-2}	EC-Earth 3	CISSEMBEL	EC-Earth 3	CISSEMBEL
Net solar RF	(23.8 ± 0.8)	(31.0 ± 0.7)	(26.8 ± 0.8)	(34.3 ± 0.8)
Net thermal RF	(-43.5 ± 0.9)	(-46.3 ± 0.9)	(-42.3 ± 0.7)	(-44.0 ± 0.6)
Sensible HF	(20.9 ± 0.6)	(22.6 ± 0.7)	(19.2 ± 0.4)	(22.4 ± 0.5)
Latent HF	(-0.8 ± 0.2)	(-6.2 ± 0.3)	(-1.9 ± 0.2)	(-7.1 ± 0.4)
Sum HF	(0.5 ± 0.3)	(1.1 ± 0.4)	(1.7 ± 0.4)	(5.7 ± 0.9)

Table 4: Average surface energy balance components in EC-Earth 3 and CISSEMBEL in the HCPH and SCPH experiments.

Figure 15 shows timeseries of net solar and thermal surface radiation fluxes as well as sensible and latent heat fluxes.

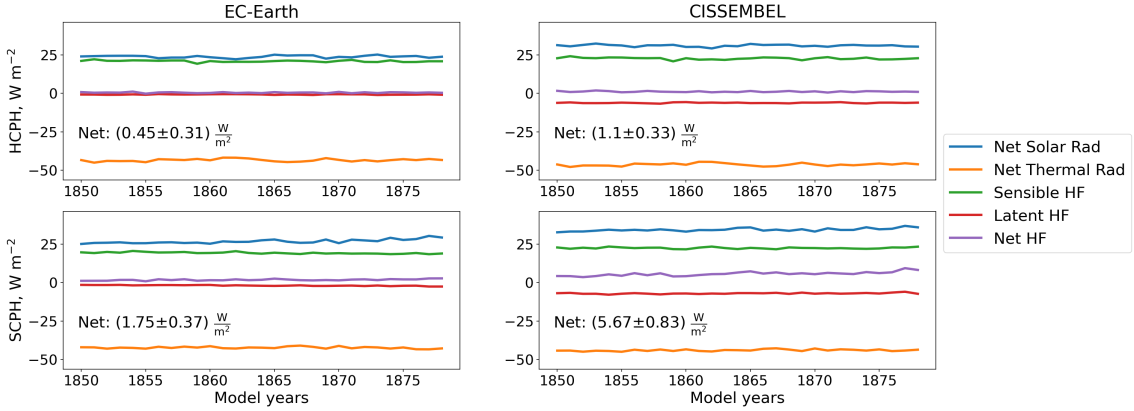

Figure 15: Net surface radiation, sensible heat and latent heat fluxes in EC-Earth 3 and CISSEMBEL. The net flux is calculated from these four to given an indication. However, additional terms apply in the surface energy balance calculations in both models. The text fields show the average 'net' heat flux. Uncertainties are calculated as the standard deviation of the linearly detrended timeseries.

CISSEMBEL receives the incoming **solar radiative flux** as climate forcing from EC-Earth 3. This means that the difference in net flux is due to albedo differences between the models. In the historical experiment, EC-Earth 3 shows an average net solar radiation flux of (23.8 ± 0.8) W m^{-2}, while in CISSEMBEL, it is (31.0 ± 0.7) W m^{-2}. In the scenario experiment, the net solar radiation flux is higher in both models (EC-Earth 3: (26.8 ± 0.8) W m^{-2}, CISSEMBEL: (34.3 ± 0.8) W m^{-2}) due to lower albedo values. These values reveal the necessary subtlety when analyzing albedo values. From the two left columns in table 3, one would expect a lower net solar radiation flux in CISSEMBEL-HCPH than in EC-Earth 3-SCPH. The two right columns show that it might be different but are still diluted by albedo values during times, when no or only little solar radiation reaches the surface. Therefore, the net surface solar radiation flux is a better estimate of the impact of an albedo scheme.

Another driver of higher melting rates in CISSEMBEL than in EC-Earth 3 is the higher **sensible heat flux** (SHF). In both HCPH and SCPH the average sensible heat flux hov-

ers around 22.5 W m^{-2} in CISSEMBEL while EC-Earth 3 shows slightly lower values, around 20 W m^{-2}. CISSEMBEL on average has a lower surface temperature, causing a higher sensible heat flux from the atmosphere to the surface.
The net **thermal radiative flux** is slightly more negative in CISSEMBEL, than in EC-Earth 3. The downward surface thermal radiative flux in CISSEMBEL is provided by EC-Earth 3. The main difference in calculation is that EC-Earth 3 uses a surface emissivity of 0.98 for snow while CISSEMBEL assumes 1.0. As a result, CISSEMBEL calculates a higher outgoing thermal radiative flux than EC-Earth 3, despite having an on average colder surface. An experiment with a surface emissivity of 0.98 in CISSEMBEL for SCPH yielded an average thermal radiative flux of (-40.3 ± 0.6) W m^{-2}, now reflecting the colder surface conditions.
The surface **latent heat flux** differs strongly between the two models, just as their way of calculation. This makes it difficult to assess what might cause the stark difference. Both methods rely on different parameterized vapor pressure calculations. CISSEMBEL uses these calculated vapor pressures directly, while EC-Earth 3 uses them indirectly as part of the humidity calculation. The difference plays an important role in balancing the large differences in net solar radiative flux.

Differences in the way of calculating the energy balance in both models as well as the presence of other terms, makes it difficult to quantitatively assess, how much of the difference in simulated melt, the difference in the here shown summed energy flux from these four components accounts for. If all components were considered, however, it is likely that the difference in surface energy flux between the two models would be larger than between the sums of the four components presented here.
In EC-Earth 3, the Q_{sn}^{INT}-term plays an important role in inhibiting melt when the skin temperature approaches the melting point, as described in section 3.2.1. CISSEMBEL, on the other hand, has no such mechanism but models refreezing of produced melt water actively, reducing the actually run-off fraction of produced melt.

From the description of the calculation of surface energy balance in the two models, it is apparent, that choice of parameters plays an important role in the resulting melt calculation. Albedo schemes and the values in different scenarios within them constitute one such choice. Another one concerns the layering in the models. In EC-Earth 3, for example, the snow layer thickness in the surface energy balance calculation (parameter D_{sn} in equation 6) is restricted to one meter, while in CISSEMBEL, the top-most layer is chosen to have a thickness of 0.33 meters.
In order to gauge the importance of some of these parameters for the resulting surface mass balance calculation, four different simulations were carried out for experiment HCPH with CISSEMBEL. Three simulations were run with modified values in Albedo Scheme Copenhagen: a melting albedo of 0.55 (MIN-0.55, instead of 0.6), a refreezing albedo of 0.6 (RFRZ-0.6, instead of 0.65) and a maximum albedo of 0.8 (MAX-0.8, instead of

0.85). One simulation was run with modified layering: the top layer thickness was set to 1.0 meters (THK-1.0, instead of 0.33 m).
The results of these modified simulations are summarized in table 5. The surface energy balance in the last row of the table now takes all CISSEMBEL surface energy balance components into account (thus also the terms G^B_{sn}, H_{pp}, H_{rain} in equation 15). It is therefore not equivalent to 'Sum HF' in table 4.

all in Gt yr^{-1}	MIN-0.55	RFRZ-0.6	MAX-0.8	THK-1.0	CPH
SMB	(289 ± 75)	(345 ± 68)	(332 ± 68)	(388 ± 67)	(348 ± 67)
Melt	(394 ± 75)	(321 ± 63)	(321 ± 63)	(245 ± 56)	(318 ± 61)
Refreeze	(113 ± 22)	(116 ± 20)	(116 ± 20)	(76 ± 16)	(115 ± 20)
Acc	(549 ± 52)	(550 ± 52)	(537 ± 52)	(556 ± 52)	(550 ± 52)
SEB (W m^{-2})	(2.21 ± 0.42)	(1.81 ± 0.36)	(1.80 ± 0.35)	(1.35 ± 0.34)	(1.79 ± 0.35)

Table 5: Average integrated surface mass balance, net melt, refreezing and accumulation (Acc) fluxes in Gt yr^{-1} from four CISSEMBEL experiments with modified albedo scheme and layering parameters: 0.55 minimum albedo, 0.6 refreezing albedo, 0.8 fresh snow/maximum albedo and a top layer thickness of 1.0 m. The CPH-acronym denotes the unmodified CISSEMBEL Albedo Scheme Copenhagen - setup.

The largest difference in the resulting surface mass balance to the unmodified setup is caused by dropping the melt-condition albedo from 0.6 to 0.55. The latter would also be a reasonable choice for melting conditions. In a paper by [Helsen et al., 2017], where multiple different albedo schemes are proposed and compared, several of the proposed schemes use values of 0.45 and 0.5 for these conditions. Although, in these schemes the albedo does not drop immediately upon melting like in Albedo Scheme Copenhagen. The modification hardly affects accumulation and refreezing rates but rather causes a strong increase of almost 24% in net melt. This is driven by an increase in the net solar radiative flux which is on average 0.5 W m^{-2} higher than in the unmodified setup.
Dropping the refreezing-condition albedo from 0.65 to 0.6 has little effect, only slightly decreasing melt and refreezing rates. The difference in the surface energy balance is due to to a slight increase in net solar radiative flux which is not completely balanced by the slight decreases in the net thermal radiative, sensible heat and latent heat fluxes.
Changing the maximum albedo, which comes into effect when enough accumulation is registered, has the strongest effect on the accumulation rate through increasing sublimation. The higher uptake of solar radiation by the surface in these conditions increases the surface temperature, especially over the ice sheet interior and thereby sublimation. While the surface energy flux is on average very similar to the one in the standard setup, individual fluxes differ strongly. A sharp increase in the net solar radiative flux of about 3.19 W m^{-2} is mostly balanced by decreases in the net thermal radiative (-0.78 W m^{-2}), sensible heat (-1.77 W m^{-2}) and latent heat (-0.62 W m^{-2}) fluxes all of which are linked to higher surface temperatures over the ice sheet interior.
Thickness 1 meter for the CISSEMBEL surface layer was chosen to mimic the choice in EC-Earth 3, although there the top layer can also be thinner than 1 meter. This model choice heavily impacts the net melt (-23%) and refreezing rate (-34%). The change im-

pacts several surface energy balance components. The largest negative impact is seen in the net solar radiative flux (-0.68 W m^{-2}) followed by the basal heat flux (-0.23 W m^{-2}) and net thermal radiative flux (-0.14 W m^{-2}). The latent heat (+0.42 W m^{-2}) and sensible heat (+0.17 W m^{-2}) fluxes on the other hand increase. Additionally, the layer thickness factors inversely into the surface energy balance, as can be seen in equation 16. The decrease in refreezing, caused by a significantly increased surface layer density, covers part of the decrease in net melt rate. The resulting surface mass balance is on average 40 Gt yr^{-1} higher than in the unmodified setup.

[Box, 2013] offers a surface mass balance reconstruction for the 1840-2010 time period and thus the 1850-1878 subset allows comparison with the two historical experiments in this project. With a method based on meteorological station records, ice cores and regional climate modeling, he estimates an average net melt rate of about 330 Gt yr^{-1}, an average accumulation rate of about 780 Gt yr^{-1} and an average surface mass balance rate of approximately 450 Gt yr^{-1}. While the CISSEMBEL simulated melt rate matches well, the average surface mass balance in CISSEMBEL is significantly lower due to a lower accumulation rate of (550 ± 52) Gt yr^{-1}. Through compentation of low melt and accumulation rates, the surface mass balance estimates from EC-Earth 3 as well as from CISSEMBEL when using the standard albedo scheme match better.
Using a coupled Global climate/ice sheet model, [Muntjewerf et al., 2020a] present a similar SMB rate estimate of around 450 Gt yr^{-1}. The same paper also extends until 2100. Under SSP5-8.5 greenhouse gas forcing, for the 2015 to 2043 period the study estimates an average SMB rate between 200-250 Gt yr^{-1}. None of the simulations presented here yield comparable estimates. The EC-Earth 3 simulation, using Albedo Schame Copenhagen, simulates the closest SMB with an estimate of (419 ± 99) Gt yr^{-1}.

5.2 1950-2014 GrIS SMB from Energy Balance Model and ERA5-Reanalysis Data

Surface mass balance rates were obtained from ERA5 reanalysis data for the 1950-2014 time period. The acronym ERA5 henceforth denotes surface mass balance rates that are calculated directly from ERA5 variables while CIS-ERA5 denotes SMB results that were simulated by CISSEMBEL, receiving ERA5 climate forcing. For the same time period, climate forcing data generated by EC-Earth 3 experiment 20ST (which uses the standard 0.8 albedo scheme) was used to model the surface mass balance with CISSEMBEL (CIS-20ST). CISSEMBEL data in this section was generated with Albedo Scheme Copenhagen and incoming climate forcing was not downscaled.

5.2.1 Results

Table 6 shows the integrated average values of the resulting ice sheet integrated surface mass balance, snow melt and accumulation fluxes.
The ERA5 and EC-Earth 3 forced CISSEMBEL runs deliver similar results. Accumulation

	ERA5	CIS-ERA5	20ST	CIS-20ST
SMB (Gt yr^{-1})	(643 ± 70)	(252 ± 112)	(538 ± 63)	(261 ± 99)
Melt (Gt yr^{-1})	(36 ± 11)	(477 ± 94)	(100 ± 22)	(458 ± 107)
Acc (Gt yr^{-1})	(666 ± 68)	(582 ± 75)	(639 ± 66)	(571 ± 68)

Table 6: Average integrated surface mass balance, net melt and accumulation (Acc) fluxes in Gt yr^{-1} from ERA5 data, an ERA5 forced CISSEMBEL experiment, EC-Earth 3 experiment 20ST and an EC-Earth 3 forced CISSEMBEL experiment.

rates are again smaller than ERA5 snowfall due to larger sublimation values. Net melt rates differ greatly between ERA5 data and CISSEMBEL output. This results in smaller average surface mass balance fluxes from CISSEMBEL.
Figure 16 shows a spatial comparison of time averaged ERA5 and ERA5 forced CISSEMBEL surface mass balance and net melt rates. The average ERA5 surface mass balance rate is positive over the whole ice sheet in the 1950-2014 period. CISSEMBEL generated surface mass balance rates are negative in the lower ablation zone along the perimeter of the ice sheet with the highest net melt rates occurring over the western and south-eastern ice sheet.

5.2.2 Analysis & Discussion

When comparing data from ERA5 and EC-Earth 3 experiment 20ST, a cold bias in the the latter has to be taken into account. The annual mean temperature over the entire Greenland land mass is on average (1.2 ± 1.1) K colder than in ERA5. This changes over time as EC-Earth 3 is colder in 37 out of 39 years between 1960 and 1989 but warmer in 13 out of the last 16 years between 1999 and 2014.
The evolution of this cold bias is also reflected in the net melt rates CISSEMBEL models and leads to the CIS-20st experiment showing a slightly lower average integrated net melt flux than CIS-ERA5. The bias also affects accumulation rates which show a similar evolution as the temperature. EC-Earth 3 simulates lower accumulation rates than ERA5 during the first part of the 1950-2014 time period but higher accumulation rates towards the end.
Comparing ERA5 snow melt rates to an estimate using the mass budget method by [Broeke et al., 2016] suggests, that they are likely underestimated in the dataset. The ERA5 estimate for snow melt at an average (37 ± 11) Gt yr^{-1} between 1961-2014 is significantly lower than the estimate by [Broeke et al., 2016] of around 500 Gt yr^{-1} for 1961-2015. The latter matches well with the net melt rate from CIS-ERA5 of (494 ± 95) Gt yr^{-1} during 1961-2014.

[Fettweis et al., 2020] performed an intercomparison of modelled 1980-2012 SMB over the Greenland ice sheet with a range of different models including positive degree day models, energy balance models, regional climate models and general circulation models. Over the same time period, CIS-ERA5 calculates an average SMB of (198 ± 110) Gt yr^{-1}. Energy balance models in the study were forced by ERA-interim reanalysis data and esti-

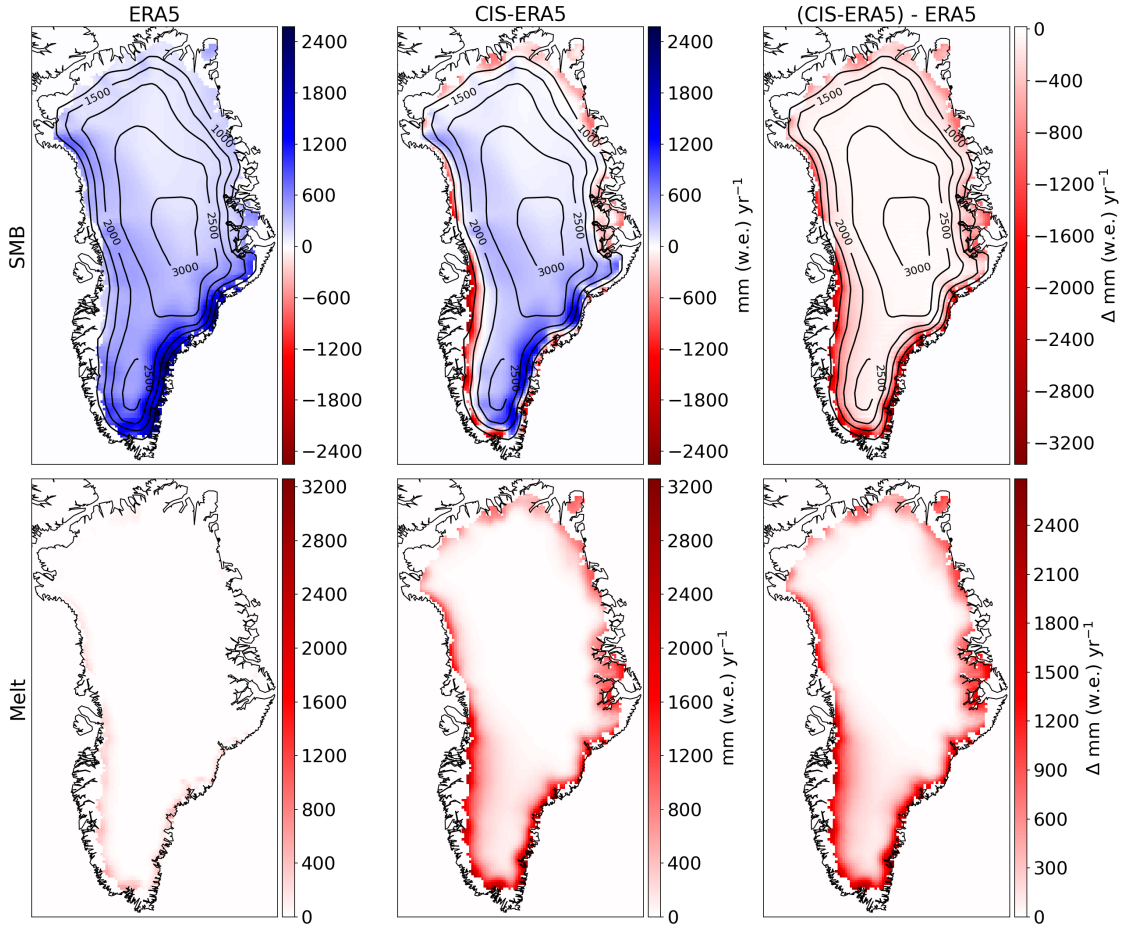

Figure 16: Average 1950-2014 SMB (top) and snow melt (bottom) rates as calculated directly from ERA5 data (left column) and by CISSEMBEL, forced with ERA5 data (CIS-ERA5, middle). The right column shows the difference as CISSEMBEL minus ERA5 data. CISSEMBEL is run with Albedo Scheme Copenhagen.

mate average SMB values ranging from (96 ± 179) Gt yr^{-1} (SNOWMODEL) to (387 ± 80) Gt yr^{-1} (BESSI). The ensemble mean of all models in the study is (338 ± 111) Gt yr^{-1}. The SMB trend is slightly weaker in CIS-ERA5 (-5.4 Gt yr^{-2}) than in the ensemble mean (-7.3 Gt yr^{-2}).

While the CIS-ERA5 modeled SMB falls outside of the study's ensemble mean standard deviation, the melt water runoff in CISSEMBEL of (386 ± 31) Gt yr^{-1} is comparable within the standard deviation ((331 ± 102) Gt yr^{-1}). It shows a weaker trend (5.3 vs. 8.0 Gt yr^{-2}) as well, however.

6 Ice Sheet Model Initialization for Coupled Experiments

This section details the results of PISM initialization experiments as well as the forcing fields used. The PISM initialization experiments as well as the EC-Earth 3 experiment for generating surface forcing were performed by Marianne Sloth Madsen. The experiment for generating the CISSEMBEL surface forcing was performed by the author.
The ice sheet states that were generated by these experiments and that are described here, are used as PISM ice sheet initial states in the coupled EC-Earth 3 - PISM experiments which are addressed in section 7. Since the PISM ice sheet in the two coupled experiments is forced in two different ways - once with surface forcing generated by EC-Earth 3, once with surface forcing generated by CISSEMBEL - initialization experiments under both ways of forcing were performed. The initialized ice sheet states are not in equilibrium with climate states simulated by the climate model.
Since a full initial state for the initialization experiments, which would include fields such as internal ice temperature was not available, the bootstrapping method is used. Provided fields of initial bedrock altitude and land ice thickness as well as surface forcing in the form of surface mass balance and below-firn temperature, PISM uses heuristics to solve for the ice temperatures and velocities to generate a full initial state. Based on this initial state, the simulation was then run for 250,000 years.
For initial bedrock altitude and land ice thickness, BedMachine v3 data, bilinearly remapped to the PISM grid, is used. [Morlighem et al., 2017]

6.1 Ice Sheet Surface Forcing Data

Monthly data was used to simulate a seasonal cycle. Figure 17 shows the monthly focing as SMB and below-firn temperature averaged over the GrIS obtained directly from EC-Earth3 and using CISSEMBEL. Figure 18 shows a spatial plot of the annual average of the monthly forcing fields in the two different forcing methods. Additionally, the last column shows the difference in the temperature and surface mass balance forcing between the two methods.
The **EC-Earth 3 surface forcing data** was generated by a pre-industrial control run of 106 years. The monthly surface mass balance forcing data is obtained as average by month over the whole period, while the below-firn temperature is obtained from a 30 year period, model years 77 to 106.
The surface mass balance is calculated from model variables according to equation 3. The HTESSEL temperature of soil layer 4 is used as the below-firn temperature. The data is first converted from the linear reduced to a regular Gaussian grid. Then, the surface mass balance is conservatively remapped to the PISM grid. For the surface temperature, bilinear remapping is used.

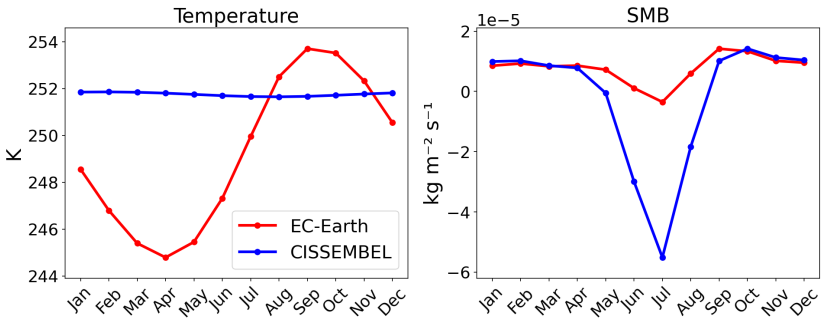

Figure 17: Timeseries of monthly surface forcing for PISM, averaged over points within the PISM retreat mask (mostly consistent with the mask shown in figure 9, the retreat mask has additional ice shelf points). Ice that advances beyond the retreat mask is discharged. The left graph shows the average below-firn temperature, the right the integrated SMB. The red lines show surface forcing from EC-Earth 3, the blue lines from CISSEMBEL.

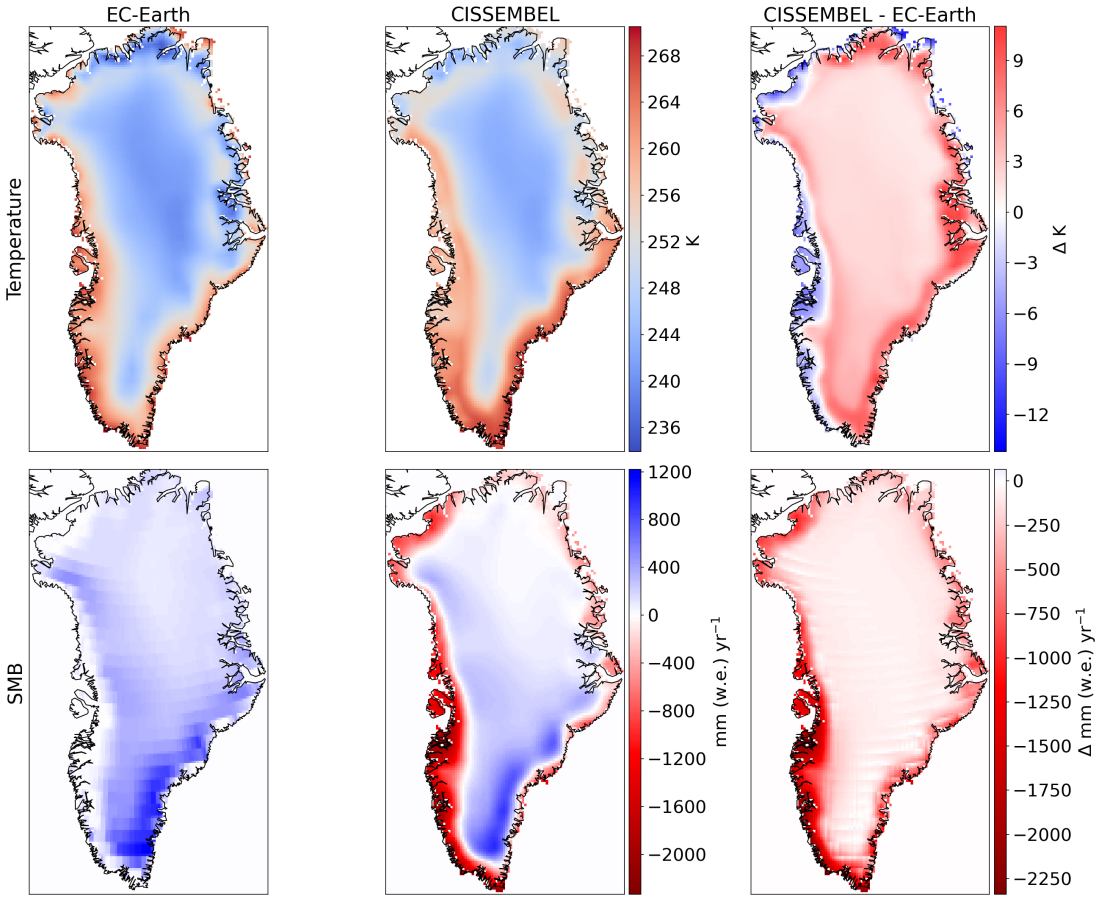

Figure 18: Spatial plot of temporal average of surface forcing for PISM. The left column shows EC-Earth 3 generated forcing data, the middle column CISSEMBEL generated forcing data. The right column shows the difference between the two, defined as CISSEMBEL minus EC-Earth 3 values.

The **CISSEMBEL surface forcing data** is obtained from a CISSEMBEL model run, forced with the full period pre-industrial EC-Earth 3 data from the same run, as the EC-Earth 3

surface forcing above. The climatic forcing for CISSEMBEL is first converted from the linear reduced to a regular Gaussian grid and then bilinearly remapped to the PISM grid. Monthly forcing fields are obtained in the same way as for the forcing from EC-Earth 3. Climatic forcing is not downscaled by CISSEMBEL.

6.2 Results

Figure 19 shows the temporal evolution of the ice sheet area and mass during the PISM run. Values are shown for model years 2,000 to 250,000.
The model experiences a strong drift during the first 2,000 years, especially under forcing from EC-Earth 3, which is positive over all of Greenland. At the end of the initialization experiment, the ice sheet under forcing from EC-Earth 3 covers a 28% larger area, under forcing from CISSEMBEL a 5.2% larger area than the observed present-day ice sheet ([Morlighem et al., 2017]). Compared to the present-day ice sheet, the resulting ice sheet mass 15% higher under EC-Earth 3-forcing and 8.5% lower under CISSEMBEL-forcing.

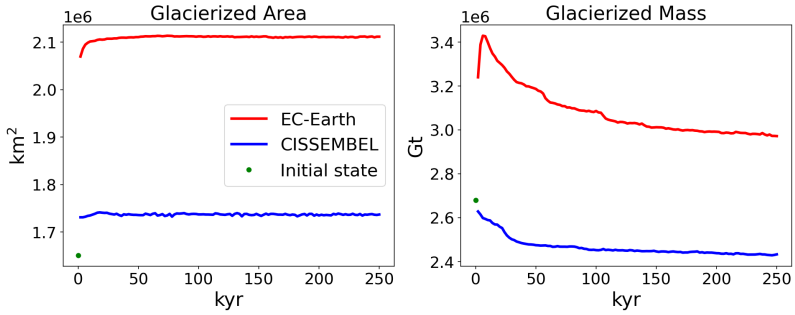

Figure 19: Temporal evolution of PISM glacierized area and glacierized ice mass for model years 2,000 to 250,000. The initial state values from the observed present-day ice sheet BedMachine version 3 data ([Morlighem et al., 2017]) are signified by the green dot. The BedMachine dataset's nominal date is 2007.

Figure 20 shows the ice thickness at the end of the run under both forcings as well as the CISSEMBEL- minus EC-Earth 3-forced difference.

6.3 Analysis & Discussion

Forcing data from EC-Earth 3 and CISSEMBEL were used since forcing from these two models is also used in the coupled experiments. The ice sheet mass shows a slightly decreasing trend in both initialization experiments. In order for the ice sheets to reach equilibrium with the modeled climate states, the experiments would have to be run longer. The below-firn temperature forcing from EC-Earth 3 shows a strong seasonal cycle, while it stays relatively constant in the forcing from CISSEMBEL. Soil layering is different in EC-Earth 3 and CISSEMBEL. In EC-Earth 3, the temperature of a soil layer with covers a depth of 1.0-2.89 meters is used. On top of the soil, a snow pack with a maximum depth of 1 meter (for energy balance calculations) can exist. In CISSEMBEL, on the other hand, the temperature of a soil layer that spans a depth of 10.33-19.33 meters is used. This

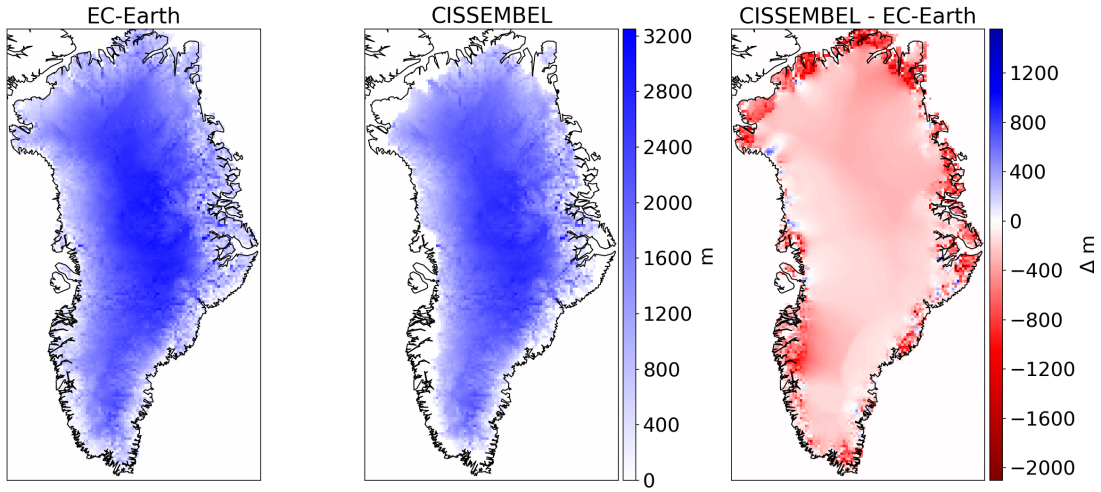

Figure 20: PISM ice thickness at end of initialization run. The left and middle column show the results of the EC-Earth 3- and CISSEMBEL-forced PISM runs, respectively. The right column shows the difference.

layer experiences less seasonal temperature variation than the more shallow layers. The average annual below-firn forcing temperature is lower over most of Greenland in the EC-Earth 3 forcing, with the exception of coastal areas where EC-Earth 3's atmospheric and surface component HTESSEL has only seasonal snow or no snow.

In many Greenland coastal areas, little to no snow is present in IFS during the summer months in the simulation. Therefore, EC-Earth 3 cannot simulate high enough melt rates to actually cause a negative surface mass balance in the lower ablation zones. In these areas EC-Earth 3 has a low, non-negative surface mass balance, as runoff removes most of the precipitation that is not evaporated. The result is a positive surface mass balance over the whole Greenland land area. The combined effect of accumulation under positive surface mass balance over the entire Greenland land mass and an advance of the ice sheet due to thickening over the interior induces an expansion of the ice sheet into areas, that are not glaciated by the present-day ice sheet.

The strong model drift during the first 100,000 years of the experiment is amplified by the fact, that the initialization experiment starts from a bootstrapped ice sheet and does not capture the true evolution of the ice sheet due to the applied surface forcing.

CISSEMBEL has an inexhaustible pack of, depending on the conditions, snow or ice everywhere and models melting rates consistent with the climatic forcing it receives over all of Greenland. This leads to a negative surface mass balance in lower altitude ablation zones, especially in south western Greenland. While the ice sheet thickens over the interior under positive surface mass balance forcing, advancing ice sheet areas in lower ablation zones are melted due to the local surface mass balance forcing. In some north eastern regions, where CISSEMBEL simulates less negative surface mass balance rates, the ice sheet's dynamical advance leads to an expansion beyond the extent of the present-day ice sheet (figure 21).

The resulting ice sheets are consistent with the applied surface forcing. The ice thickness plot shows, that the CISSEMBEL-forced ice sheet is lower over the ice sheet interior. Higher sublimation rates in CISSEMBEL cause a slightly less positive SMB there.
Comparison with the present day ice sheet shows that both ice sheets are significantly thinner over large parts.
The EC-Earth 3-forced ice sheet is thinner than the observed present-day ice sheet in mid to western Greenland. In eastern and northern Greenland, on the other hand, it is thicker by more than 1000 meters in many areas where the present-day ice sheet has no ice.
The outline of the CISSEMBEL-forced ice sheet matches well with the present-day ice sheet in the south-western ablation zone. This area is of high importance for the overall surface mass balance of Greenland as it is area that experiences the strongest negative surface mass balance forcing. Outside of areas in eastern and northern Greenland, where the CISSEMBEL-forced ice sheet has ice and the present-day ice sheet has none, the CISSEMBEL-forced ice sheet is thinner than the observed present-day ice sheet by on average (280 ± 180) meters.

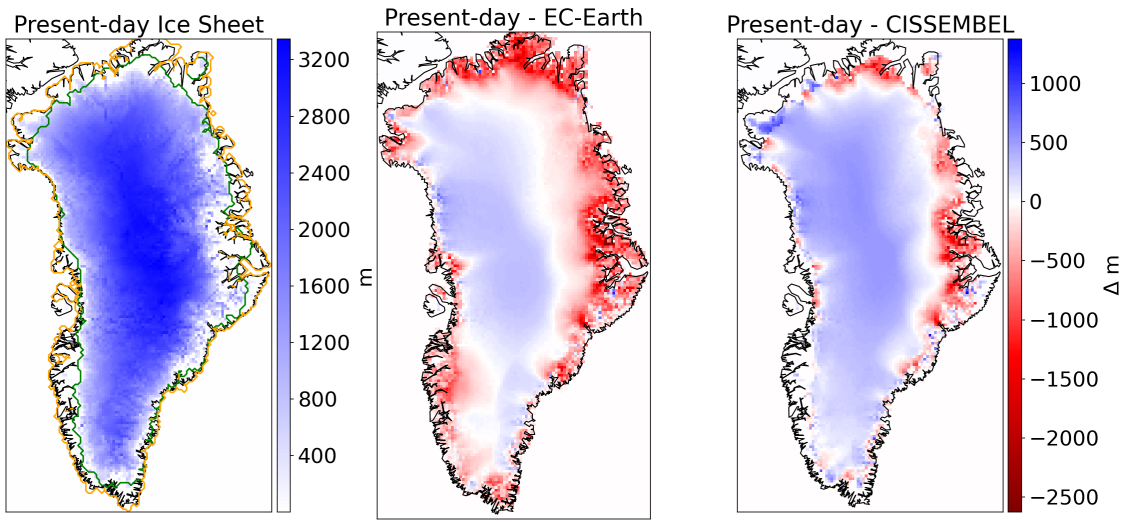

Figure 21: Ice thickness of observed present-day ice sheet from [Morlighem et al., 2017]. The green and orange lines in the left plot encircle areas, where the CISSEMBEL- and EC-Earth 3-forced ice sheets have an ice thickness greater than 10 meters. The middle shows the difference to the EC-Earth 3-forced ice sheet, the right column the difference to the CISSEMBEL-forced ice sheet.

Since the initialization experiments start from the present-day ice sheet and have a positive surface mass balance over the ice sheet interior, the reason for the progressive thinning lies with ice dynamics. The dynamical parameter with the biggest impact on the ice sheet geometry is the Shallow Ice Enhancement Factor $E_{SIA} = 3.0$. [Gevik, 2019] found that using lower enhancement factors leads to thicker ice sheets. Under CISSEMBEL forcing, a lower enhancement factor would likely lead to a closer fit between initialized and observed ice sheet over the interior. When decreasing the enhancement factor in

the experiment using forcing from EC-Earth 3, a better fit over the mid-western ice sheet interior would likely come at the cost of a further divergence in ice sheet mass between initialized and observed state.

7 Coupled Global Climate - Greenland Ice Sheet Experiments

Abrupt-4xCO_2 scenario experiments, where the atmospheric CO_2 concentration is set at 4 times pre-industrial values, were performed for three different setups: an uncoupled EC-Earth 3-Veg setup (ECE-STA, with Albedo Scheme Copenhagen, 49 years), the EC-Earth 3-Veg - PISM coupled setup (ECE-PISM) and the EC-Earth 3-Veg - CISSEMBEL - PISM coupled setup (ECE-CIS-PISM, both 80 years). These experiments are restarted from pre-industrial 1850 IFS, NEMO and LPJ-Guess initial states. Figure 22 shows the evolution of the global and Greenland mean temperatures under the high CO_2 forcing as temperature anomalies to the pre-industrial 1850-1879 global (experiment ECE-STA) and Greenland mean temperatures. High atmospheric CO_2 concentration causes an immediate spike in global mean temperature of about 1.4 K during the first year and the temperature anomaly continues to grow to an average of approximately 6.1 K above pre-industrial mean during years 31-49 of the ECE-STA experiment.

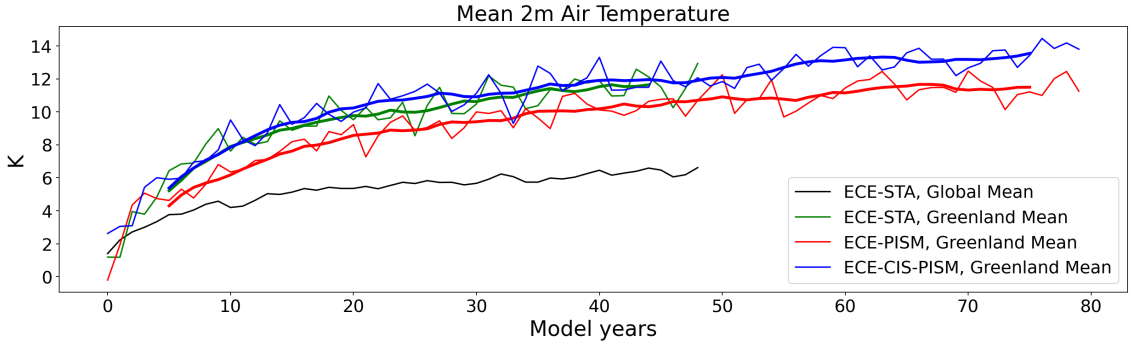

Figure 22: Global and Greenland mean temperature evolution in the EC-Earth 3 standard and coupled runs. Thick lines show the 10-year running average temperatures.

The performed experiments are first test runs of the coupled system. During this, several bugs were detected. While these bugs either were already fixed or are in the process of being fixed, they impacted the results in this section, especially the freshwater flux into the ocean (details in section 7.4). Hence, the results will focus on demonstrating effects on the temperature, SMB and SEB over Greenland as well as on the ice sheet.
First, the effect of topography and ice sheet extent on the temperature and runoff over Greenland is presented. Following, the surface mass balance forcing and resulting discharge fluxes from both coupled setups is addressed. Finally, the evolution of the ice sheet is examined.
CISSEMBEL uses albedo scheme Cph-mod, as described in section 3.3.2 and downscales received climate forcing to the ECE-CIS-PISM ice sheet topography.
Experiment ECE-STA was performed by Marianne Sloth Madsen, while the coupled experiments ECE-PISM and ECE-CIS-PISM were performed by the author.

7.1 Impact on the Climate System

The assessment of effects of the coupling on the climate system is based on comparison with the uncoupled EC-Earth 3 experiment which was run for 49 years.

Topography

In the uncoupled setup, IFS uses a fixed topography while in the coupled setup the topography is annually updated to reflect changes in the ice sheet geometry. Figure 23 shows a comparison of the topography in the coupled ECE-PISM and ECE-CIS-PISM experiments after 49 model years with their respective initial states as well as with the IFS standard topography.

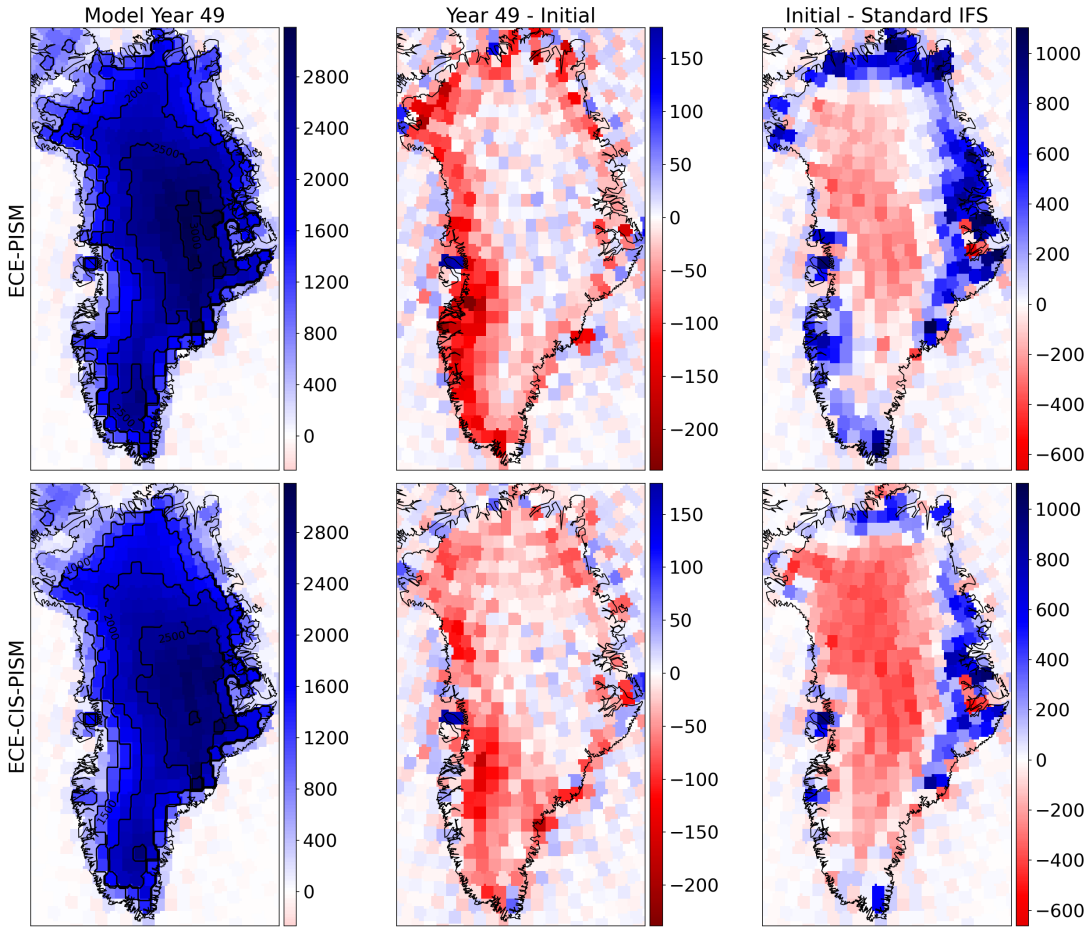

Figure 23: IFS topography over Greenland in different setups. The EC-Earth 3-PISM coupled system topographies in model year 49, the difference between model year 49 and the respective initial topographies as well as the difference between initial topography and the IFS standard topography are shown in the three columns. The top row shows these fields for the coupled setup using ice sheet surface forcing from EC-Earth 3, the bottom row for the coupled setup using forcing from CISSEMBEL. All fields were remapped from the linear reduced Gaussian IFS grid to the PISM grid using nearest neighbor interpolation.

After 49 model years, the topography in the ECE-PISM experiment is more than 100 me-

ters higher than the topography in ECE-CIS-PISM over most of Greenland as was the case in the initial states. The elevation decreased in both coupled setups with regards to their respective initial states. This is most visible in the ablation zones along the perimeter of the ice sheet. The standard IFS topography is more than 100 meters higher over most of the interior of Greenland than the ice sheet initial states in the coupled setup. However, it has lower elevations along multiple coastal regions, especially the eastern and northern coastal areas.

Temperature, Surface Mass Balance & Surface Energy Fluxes

A comparison of model years 20-49 temporal averages of pre-industrial temperature anomaly, surface mass balance and the sum of the net solar and thermal radiative fluxes, latent and sensible heat fluxes over Greenland is shown in figure 24. For readability, the acronym STLS-flux denotes this sum. The surface mass balance is calculated from the IFS model variables runoff, evaporation and total precipitation according to equation 3. Since this concerns the study of IFS quantities, none of the results in this subsection were generated with CISSEMBEL.

The temperature anomaly plots show a sharp increase in the 2 meter air temperature in all experiments. In the ECE-STA experiment, the temperature rises quite uniformly over all of Greenland. In glaciated regions (see figure 30) by an average of (10.0 ± 1.1) K. The spatial distribution of the temperature anomaly in the coupled experiments reflects the topography differences to the standard IFS topography. Stronger warming over the interior of the ice sheet is somewhat balanced in the average ice sheet temperature by weaker warming along higher altitude coastal areas. Compared to ECE-STA this, over glaciated areas, yields a lower average temperature anomaly in the ECE-PISM experiment of (9.6 ± 0.9) K and a higher average temperature anomaly of (10.9 ± 1.0) K in the ECE-CIS-PISM experiment.
The integrated ice sheet surface mass balance is significantly lower in the coupled than in the uncoupled experiments, fuelled by larger ice sheet areas in the coupled experiments which allow more wide spread snow melt. Total precipitation and evaporation values vary with the temperature differences between the experiments but cause only a small fraction of the differences in SMB between the experiments. The average Greenland integrated runoff values during the 30 year period are (1120 ± 120) Gt yr^{-1} in ECE-STA, (2900 ± 470) Gt yr^{-1} in ECE-PISM and (2310 ± 470) Gt yr^{-1} in ECE-CIS-PISM.
The differences in runoff correlate spatially with higher surface energy fluxes. Along the coastal regions, the STLS-flux is significantly higher in the coupled experiments than in the uncoupled experiment. The experiments have Greenland ice sheet averaged STLS-fluxes of (4.2 ± 0.7) W m^{-2} (ECE-STA), (12.1 ± 2.2) W m^{-2} (ECE-PISM) and (9.2 ± 2.2) W m^{-2} (ECE-CIS-PISM).

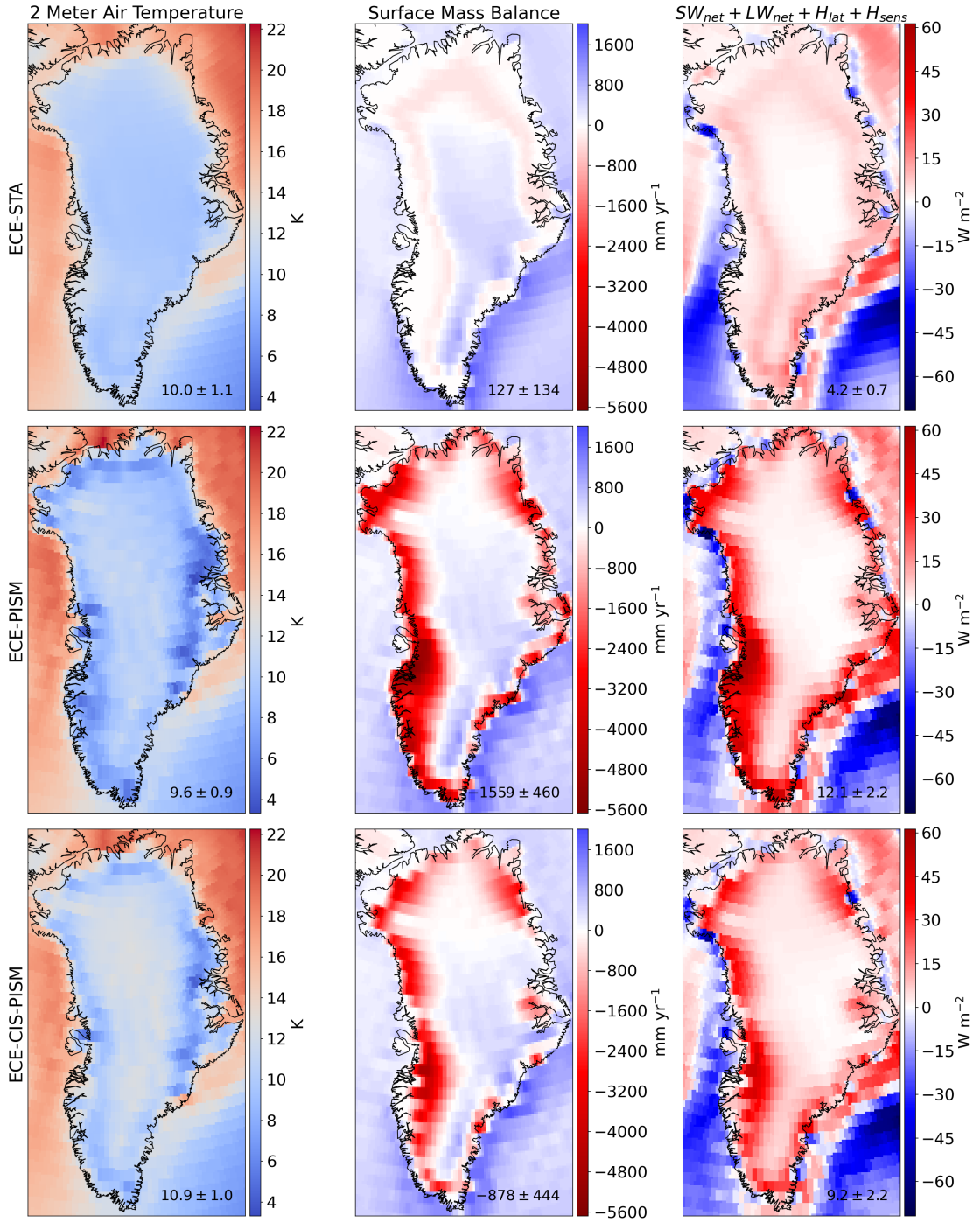

Figure 24: Model year 20-49 averages of pre-industrial temperature anomaly (left column), surface mass balance (middle) and the sum of the net solar and thermal radiative, latent and sensible heat fluxes (right). The top row shows these averages for the uncoupled EC-Earth 3 run, the middle row for the coupled setup where PISM is forced by EC-Earth 3 and the bottom row for the setup using PISM forcing from CISSEMBEL. The SMB is calculated according to equation 3. The numbers in the lower right corner show the average pre-industrial temperature anomaly (K), Greenland integrated average annual SMB (Gt yr^{-1}) and the average heat flux from the four components (W m^{-2}). These averages were calculated over glaciated areas.

7.2 Greenland Ice Sheet Mass Balance

From this point on, results focus on the ice sheet in PISM, rather than the climate. Thus, surface mass balance rates are the ones applied to the ice sheet and ice discharge and basal melt fluxes are produced by PISM.

The temporal evolution of the integrated Greenland ice sheet surface mass balance is shown in figure 25 along with the ice sheet averaged below-firn temperature. These fields were provided to PISM to force the ice sheet at the surface. Since the ice sheet in the EC-Earth 3-forced simulation has a significantly larger extent than the one in the CISSEMBEL-forced simulation (see section 6), the dashed line in the left graph shows the ECE-PISM SMB from EC-Earth 3, integrated over the area of the CISSEMBEL-forced PISM ice sheet for comparison.

The integrated ice sheet surface mass balance quickly drops below zero at the start of the stimulation in both experiments. Due to the larger ice sheet extent and ablation area, the ECE-PISM experiment shows lower integrated SMB forcing during model years 20 to 55 than the ECE-CIS-PISM experiment.

The EC-Earth 3 soil layer four temperature responds less quickly to warmer atmospheric conditions than the ice temperature below 10 m in CISSEMBEL, and still shows a warming trend at the end of the simulation. The ice temperature in CISSEMBEL reaches a plateau after about 30 model years.

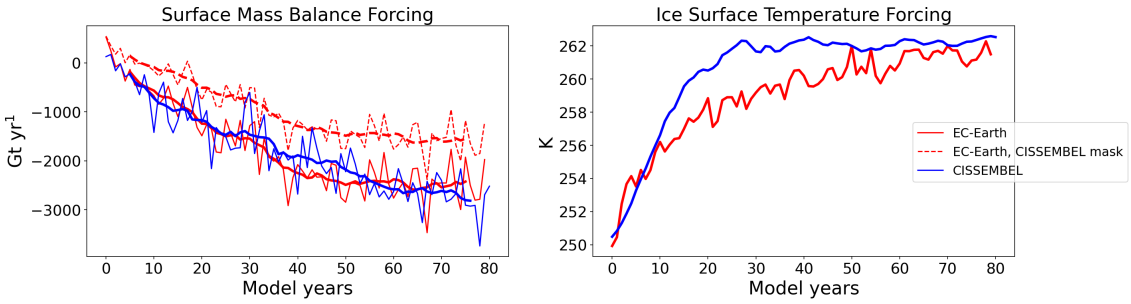

Figure 25: Surface mass balance and below-firn temperature, integrated over the native ice sheets as modeled by EC-Earth 3 (red) and CISSEMBEL (blue). In the surface mass balance graph (left), thin lines show annual values, while the thick lines show 10 year running averages. The dashed line indicates integrated EC-Earth 3 SMB forcing, over the area of the smaller ECE-CIS-PISM ice sheet.

Figure 26 shows 20-year averaged spatial distributions of surface mass balance forcing in PISM in the ECE-PISM and ECE-CIS-PISM experiments. The number in the lower right corner gives the surface mass balance, integrated over the native ice sheets, during these periods.

The forcing from EC-Earth 3 in ECE-PISM maintains a positive surface mass balance over the high elevation interior of the ice sheet throughout the experiment. The area of positive SMB forcing from CISSEMBEL in ECE-CIS-PISM is smaller in comparison and reduced to a small region in the south east of the ice sheet during the last 20 years. This is reflected in the 20-year averaged ablation area fraction of the ice sheets, which are

shown in table 7.

	Year 1-20	Year 31-50	Year 61-80
ECE-PISM	$(40.1 \pm 6.7)\%$	$(73.1 \pm 6.8)\%$	$(77.1 \pm 7.4)\%$
ECE-CIS-PISM	$(49.3 \pm 13.7)\%$	$(84.7 \pm 12.0)\%$	$(95.1 \pm 4.7)\%$

Table 7: 20-year averaged ablation area fractions of the native ice sheets in the two coupled experiments. Uncertainties are calculated as the standard deviation of the linearly detrended timeseries and thus reflect interannual variability.

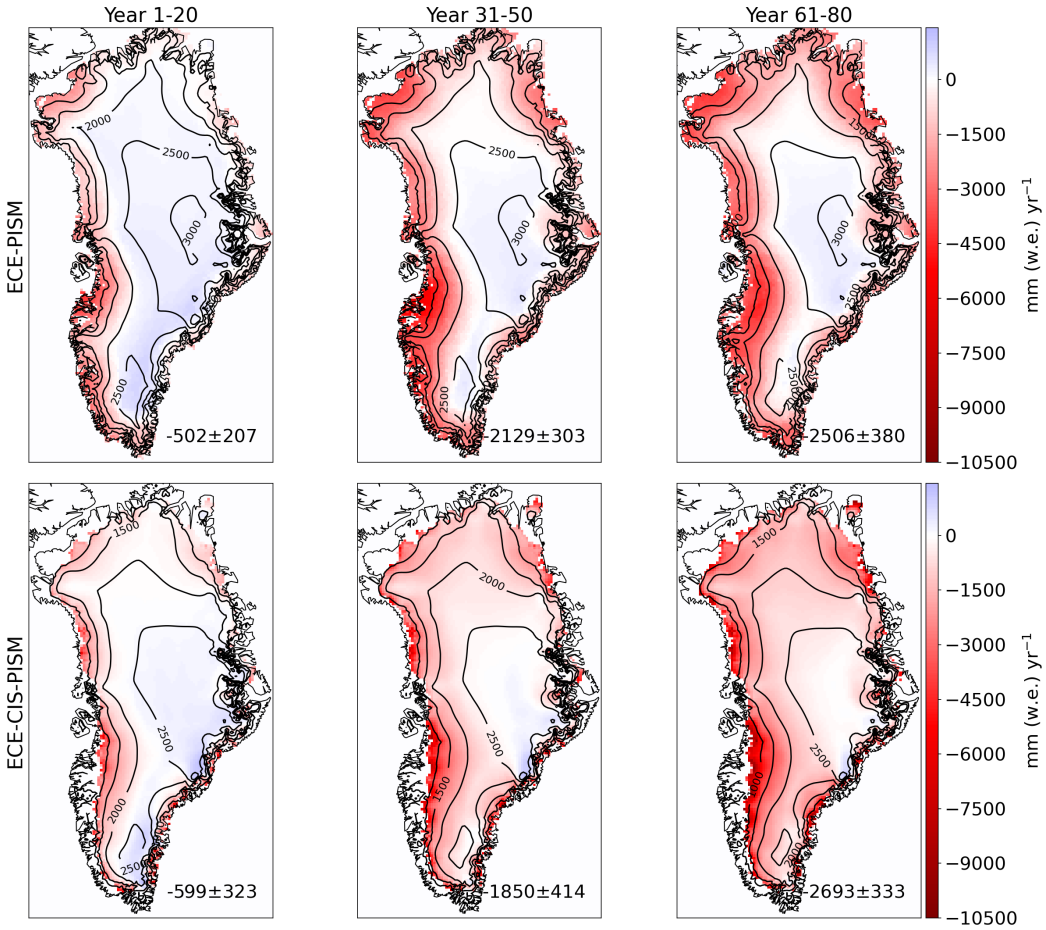

Figure 26: Surface mass balance forcing from EC-Earth 3 (top) and CISSEMBEL (bottom) over the GrIS, averaged over the given 20 year periods. The values in the lower right corners show the ice sheet integrated SMB in Gt yr^{-1}. Uncertainties are the standard deviation of the linearly detrended timeseries.

By combining the Greenland ice sheet SMB-forcing with ice discharge and basal melt fluxes from PISM, the total ice sheet mass balance is calculated. These values can be seen in figure 27. The ECE-PISM experiment shows a significantly higher discharge flux. The discharge flux as well as the basal melt flux decrease with time in both experiments. The resulting ice sheet mass balance is negative for the entirety of the two experiments.

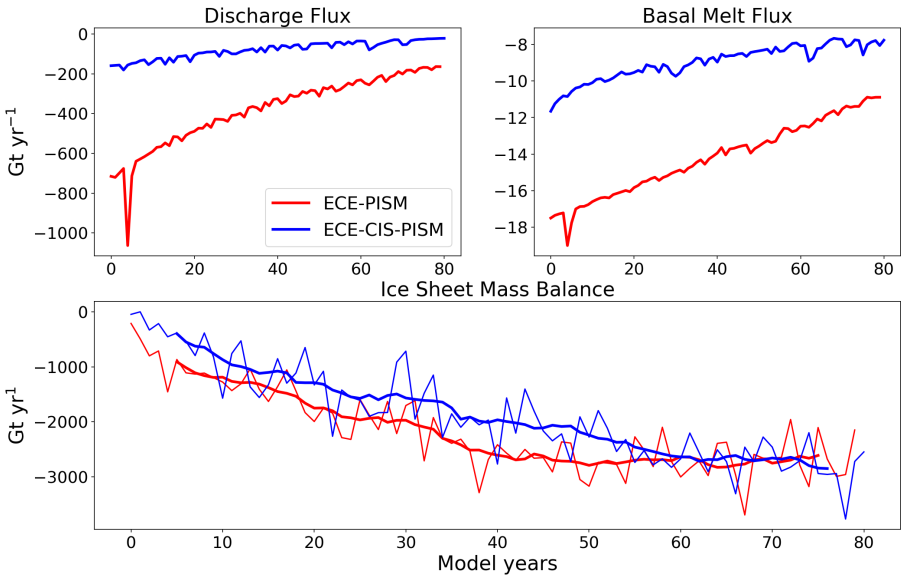

Figure 27

7.3 Greenland Ice Sheet Evolution

Figure 28 shows the temporal evolution of the ice sheet glaciated area and mass as well as the sea level rise potential in PISM.

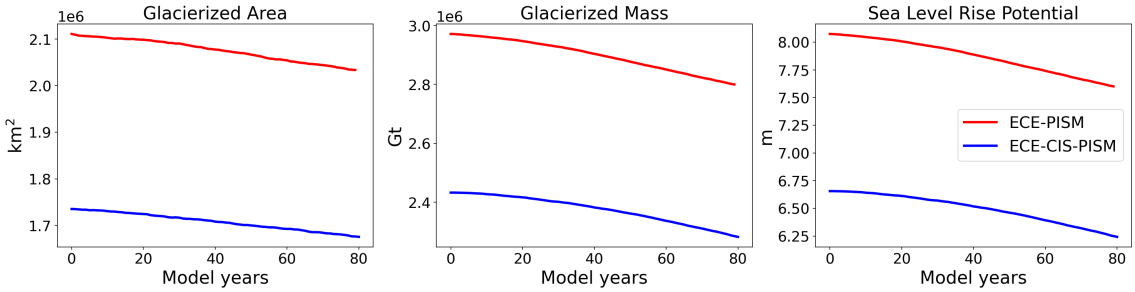

Figure 28: Temporal evolution of PISM glacierized area (left, km^2), glacierized ice mass (middle, Gt) and sea level rise potential (right, m) for 80 model years.

In the ECE-PISM experiment, the ice sheet area decreases by about 3.7% and the ice sheet mass by about 5.7%. During the 80 years of experiment, this equates to a cumulative sea level rise contribution of about 473 mm or 5.91 mm per year. Over the entire experiment, this rate is accelerating but somewhat stabilizes during the last 20 years. Over this time period, the average sea level rise contribution of the Greenland ice sheet is about 7.0 mm per year.

The numbers for the ice sheet in the ECE-CIS-PISM experiment are similar, as its area decreases by about 3.4% and its mass by about 6.1%. In this experiment, the ice sheet causes a sea level rise of about 406 mm, which are 5.07 mm per year. This number accelerates more quickly in the ECE-CIS-PISM experiment as during the last 20 years, it adds about 7.1 mm per year to the global mean sea level.

The spatial plots of ice thickness change between the last model year and the respective initial states in both experiments, shown in figure 29, are consistent with the SMB-forcing. In ECE-PISM, the ice sheet increases in thickness over a small region in the ice sheet interior. A larger region shows thickness values remaining close to the initial state. In the ECE-CIS-PISM experiment, this region is much smaller, as the CISSEMBEL produces negative surface mass balance rates over the interior of the ice sheet. The highest values of thickness decrease are registered in the lower ablation zone, especially in western Greenland and are on the order of one to several hundreds of meters. A small number of detached points along the coast in both experiments (2 in ECE-PISM, 11 in ECE-CIS-PISM) show a thickness decrease of more than 500 meters. The scale was limited to improve the plot.

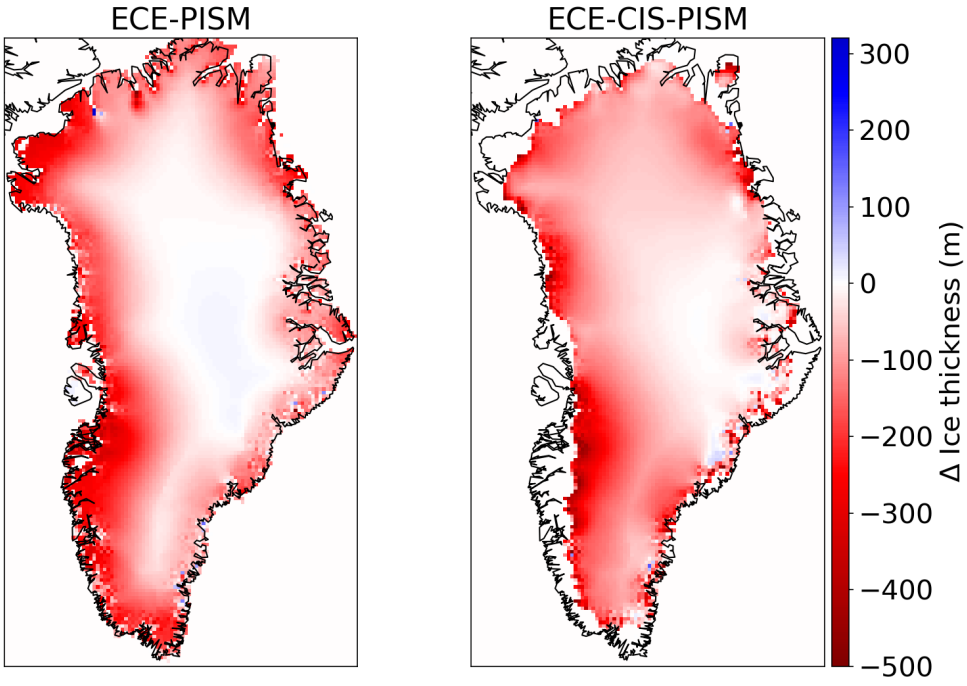

Figure 29: Differences in ice thickness between model year 80 and the respective initial states. The EC-Earth 3 SMB-forced result is shown on the left side, the CISSEMBEL-forced one on the right.

7.4 Analysis & Discussion

Limitations

As stated in the introduction to this section, the performed experiments were the first test runs of the coupled system and bugs in the setup, which affect results, were revealed. Calving fluxes both from Greenland and other glaciated regions are affected. The PISM ice discharge and basal melt fluxes were remapped to the Runoff-Mapper grid using a faulty PISM mask which lead to part of these fluxes not being routed properly to the ocean.

This strongly affected ECE-PISM where during the first 50 years of the experiment, PISM simulated an average discharge flux of 492 Gt per year of which only an average of 19 Gt per year were properly sent to the ocean. In the ECE-CIS-PISM experiment, PISM simulated an average discharge flux of 112 Gt per year of which on average 66 Gt were sent to the ocean. For reference, the calving mechanism in the uncoupled ECE-STA experiment simulated an average discharge flux of (307 ± 22) Gt yr^{-1}.
Due to an error in the Runoff-Mapper, only discharge fluxes from the Greenland and Ellesmere Island basin were sent to the ocean. Runoff fluxes were properly accounted for, for all regions. This error predominantly affects the ocean around the Antarctic ice sheet, where a missing influx of cold freshwater lead to an increase of several degrees in the surface ocean temperature around Antarctica, when compared to the uncoupled ECE-STA experiment.

Impact on the Climate System

The 2 meter air temperature fields in figure 24 show the consequences of a different topography in IFS. The ECE-STA experiment uses the same standard topography as the pre-industrial experiment that produced the reference field. The result is a near uniform temperature increase over Greenland due to the high greenhouse gas forcing.
Topography changes also cause a change in precipitation distribution over Greenland. Patterns in the precipitation anomaly between the uncoupled experiments and the coupled one are similar for ECE-PISM and ECE-CIS-PISM. IFS simulates higher precipitation rates in both ECE-PISM and ECE-CIS-PISM in south eastern and western coastal areas that have a higher elevation than the standard IFS topography. It is likely, that the steeper topography in these regions causes humid air to rise faster and cause local precipitation, rather than moving further inland and precipitating over a larger area. Over the ice sheet interior, precipitation rates are very similar in all experiments but highest in ECE-CIS-PISM and lowest in ECE-PISM. Extended areas of decreased precipitation with respect to ECE-STA are found in the coupled experiments along the western coast, where the topography in the coupled experiments is lower than the standard IFS topography.
The average annual Greenland integrated precipitation in ECE-PISM is slightly lower than in the uncoupled experiment and slightly higher in ECE-CIS-PISM.

all in Gt yr^{-1}	ECE-STA	ECE-PISM	ECE-CIS-PISM
Precipitation	(1478 ± 121)	(1341 ± 109)	(1484 ± 125)
Evaporation	(189 ± 13)	(68 ± 5)	(116 ± 6)
Runoff	(1120 ± 113)	(2898 ± 282)	(2305 ± 322)
SMB	(169 ± 133)	(-1625 ± 292)	(-937 ± 315)

Table 8: Model year 20-49 average annual Greenland integrated surface mass balance components in ECE-STA, ECE-PISM and ECE-CIS-PISM. Uncertainties given as standard deviation of linearly detrended timeseries.

While total precipitation over Greenland is mainly affected by changes in the topography, the surface related evaporation and runoff quantities are strongly impacted by use of the ice sheet extent and the resulting wider spread of ice sheet surface conditions. In figure 30 shades of blue show the snow depth in IFS, while red areas show areas in the coupled experiments where ice sheet conditions are prescribed in IFS by the PISM ice sheet extent while IFS has no snow.
In low elevation areas, which are largely snow-free in all experiments, evaporation rates in ECE-STA are higher than in the coupled experiments where ice sheet conditions prevail. The Greenland integrated evaporation values for the three experiments thus reflect the extent of ice sheet surface conditions.
The same is true for the integrated Greenland runoff values. A much smaller snow-covered area in ECE-STA consequently allows much less snow melt over Greenland. Over snow-covered areas in IFS, where all three experiments simulate melt, differences in snow melt reflect differences in the topography. Lower, warmer regions in the coupled experiments, such as the Greenland interior, yield higher snow melt rates. Higher elevation regions, predominantly in north-eastern Greenland, yield lower melting rates.
While it is clear that areas of lower elevation experience more melt in the coupled experiments, it is difficult to detect whether the elevation - SMB feedback mechanism also causes accelerating melt in the coupled experiments. This signal is overlaps with the warming signal over Greenland due to the high CO_2 concentration. Longer experiments would have to be run where the climate state reaches equilibrium with high CO_2 forcing in order to cleanly observe the impact of the elevation - SMB feedback.
In south western Greenland, snow exists consistently above 2000 m a.s.l. The ECE-PISM and ECE-STA topographies rise faster in that region than the ECE-CIS-PISM topography, resulting in a larger snow covered area there. The distribution of snow in IFS shows the necessity of the ice sheet mask for realistically modeling melt over the whole ice sheet region. Fast retreat of the snow pack in IFS due to its relatively low maximum depth of 10 meters is a further problem, that was already seen in section 5.1. In ECE-PISM, the area over Greenland where the average annual snow depth in IFS exceeds 1 meter decreases by 31% between model year 20 and 49. In ECE-CIS-PISM by 34% and in ECE-STA by 32%.

The activated surface scheme impacts the surface energy balance in the respective regions. Table 9 shows 30-year (model years 20-49) averages of SEB components over glaciated areas. Uncertainties are given as the standard deviation of the linearly detrended timeseries.
During the 30 year period, for which spatial averages are shown in figure 24, the annual mean Greenland STLS-flux in ECE-STA stays relatively constant, while it persistently increases in the coupled experiments.

The annual mean net solar radiative flux over glaciated areas shows an increasing trend

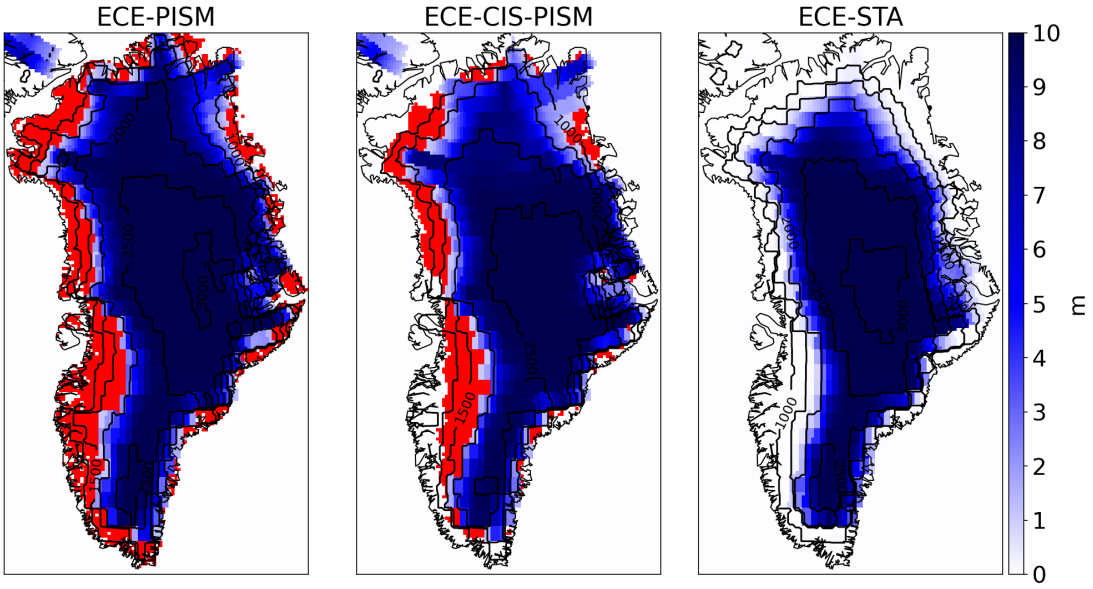

Figure 30: The model year 20-49 average snow depth in IFS is shown in blue shades. Snow-free areas in IFS, where the adjusted surface scheme reflecting the presence of an ice sheet is activated in the coupled system, are red. IFS has a maximum snow depth of 10 meters, excess snow is directly routed to the ocean as calving in the uncoupled experiment.

all in W m^{-2}	ECE-STA	ECE-PISM	ECE-CIS-PISM
Net solar RF	(28.9 ± 1.8)	(37.2 ± 1.5)	(33.2 ± 1.7)
Net thermal RF	(-40.1 ± 1.1)	(-38.3 ± 0.8)	(-37.1 ± 0.8)
Sensible HF	(17.0 ± 0.6)	(15.3 ± 0.5)	(15.7 ± 0.4)
Latent HF	(-1.6 ± 0.3)	(-2.1 ± 0.2)	(-1.6 ± 0.2)
Sum HF	(4.2 ± 0.3)	(12.1 ± 1.3)	(10.2 ± 1.4)

Table 9: Model year 20-49 average surface energy balance components in ECE-STA, ECE-PISM and ECE-CIS-PISM. Uncertainties given as standard deviation of linearly detrended timeseries.

in all experiments. With rising temperatures, more frequent melt events activate the melt-albedo feedback. This is the case especially for low elevation ablation areas which are larger in the coupled experiments, thus yielding higher ice sheet averaged net solar radiative fluxes.

Net thermal radiative fluxes in all three experiments increase with time. The continued increase in downward radiative flux dominates over an increase in outgoing thermal radiation due to rising skin temperatures. ECE-CIS-PISM receives the highest downward thermal radiation fluxes followed by ECE-PISM, both of which have a lower altitudes over most of the ice sheet than ECE-STA.

The sensible heat flux is lowest in ECE-PISM since it has the largest ablation area, where the skin temperature is higher than over the ice sheet interior.

Sublimation over the GrIS increases in all experiments, leading to stronger latent heat fluxes over time.

Greenland Ice Sheet Mass Balance

Surface mass balance rates in ECE-PISM and ECE-CIS-PISM are difficult to compare since not only the extent of the ice sheet but also the topography and albedo schemes differ.
Results in section 5 suggest, that applying CISSEMBEL to the ECE-PISM ice sheet would lead to more negative surface mass balance rates than the ones calculated by EC-Earth 3. Furthermore, the different albedo scheme, Cph-mod with a value of 0.55 under melting conditions, contributes to higher melt rates.
A comparison of CISSEMBEL calculated surface mass balance fluxes with the SMB calculated by EC-Earth 3 in ECE-CIS-PISM shows, that for the same 30 year period as in the section on impact on the climate, CISSEMBEL simulates an average ice sheet integrated surface mass balance of (-1698 ± 430) Gt yr^{-1}, which is almost twice as negative as the SMB calculated in EC-Earth 3 ((-878 ± 444) Gt yr^{-1}). This fuelled by higher melt and sublimation rates.
As mentioned in the results section, initial state ice sheets that have ice sheet geometry closer to the present day ice sheet and thus higher elevations over large areas, would lead to less negative surface mass balance forcing.

Ice discharge is significantly stronger in ECE-PISM due to the larger ice sheet extent. As such, the ice sheet has more marine terminating points than the smaller ECE-CIS-PISM ice sheet. The timeseries of ice discharge and basal melt show a spike, which appears in year 5 and continues, albeit weakened, in year 6. This spike is caused by unusually high values in one grid cell in northern Greenland, which is consistent with the position of the Ryder outlet glacier. In model years 5 and 6, it discharges 353 and 84 Gt of ice respectively, while producing basal mass fluxes of 1.8 and 0.3 Gt. These values exceed the Ryder glacier's average discharge (15 Gt yr^{-1}) and basal melt (0.03 Gt yr^{-1}) fluxes significantly. This behavior is likely caused by an instability in the initialized ice sheet.
As the negative ice sheet surface mass balance forcing at the perimeter of the ice sheet gets stronger and the ice sheet thins, the amount of discharge per point as well as the number of ice discharge points decreases. This describes the negative SMB - ice discharge feedback.
[Muntjewerf et al., 2020b] is a study performed with the Community Earth System Model version 2.1 (CESM2.1) which includes an interactive Greenland ice sheet, modeled by the Community Ice Sheet Model 2.1 (CISM2.1) componet model. It will be referenced on multiple occasions going forward. A short description of the model can be found in the introduction to the thesis. The paper details results of an idealized 350 year simulation, where atmospheric CO_2 concentration rises by 1% each year until reaching four times the pre-industrial atmospheric CO_2 concentration by year 140. After year 140, the CO_2 concentration is kept constant at 4xCO_2 level.
[Muntjewerf et al., 2020b] simulate discharge fluxes similar to the ECE-PISM experiment of around 700 Gt yr^{-1} during the initial period of their run, when the ice sheet covers an

area of more than 1.95×10^6 km^2. This extent lies between the extent of the ECE-PISM and ECE-CIS-PISM ice sheets. Under rising greenhouse gas forcing, the study models a similar behavior of significantly decreasing discharge fluxes.

In a recent study, [Karlsson et al., 2021] estimate that the current basal melt water production of the Greenland ice sheet is $(21.4 + 4.4/ - 4.0)$ Gt yr^{-1}. While the initial basal melt flux of the ECE-PISM ice sheet of 17.5 Gt yr^{-1} narrowly falls within the given margin, the basal mass flux trend is one of continuous decrease in both experiments. This is in contrast to [Karlsson et al., 2021], who expect the basal mass flux to increase in a warming Arctic.
In PISM, basal melt over grounded ice is the dominant contribution to the total basal melt flux. PISM calculates the basal melt rate from energy conservation across the ice-bedrock layer. PISM points that correspond to outlet glaciers show the largest basal melt fluxes. These points also have the highest basal ice velocities, implying that a large part of the energy for basal melting stems from frictional heating. Points that show the strongest decrease in basal melt rate are also the ones showing the strongest decrease in basal velocity. Thinning outlet glaciers under negative surface mass balance forcing are the likely reason for decreasing basal melt fluxes.
The model by [Muntjewerf et al., 2020b] calculates decreasing basal melt fluxes under high greenhouse gas concentration and therefore increasingly negative surface mass balance forcing at the perimeter of the ice sheet.

Total mass balance rates in ECE-PISM and ECE-CIS-PISM appear to stabilize towards the end of the experiments at (-2720 ± 390) Gt yr^{-1} and (-2730 ± 360) Gt yr^{-1}, respectively. These are calculated as averages over the last 20 years, model years 60-80, of the respective experiments. [Muntjewerf et al., 2020b] simulate a total GrIS mass balance between -2400 and -2500 Gt yr^{-1} over the last 20 years of their experiment, model years 330-350, agreeing within one standard deviation with the simulated total mass balances in this project. The pre-industrial temperature anomaly over the GrIS during those years of around 11 K is comparable to the Greenland temperature anomalies in ECE-PISM (~ 10 K) and ECE-CIS-PISM (~ 12 K). However, the length of the here presented simulations would have to be extended in order to see whether the total mass balance actually stabilizes and at which values.

Greenland Ice Sheet Evolution

The sea level rise contributions in the two experiments are consistent with the total mass balance and comparable to [Muntjewerf et al., 2020b]. The impact of the increased freshwater flux on ocean temperature, salinity and circulation is unfortunately not available due to the problems in the model described in the section on ”Limitations”.
A similar cumulative contribution to global mean sea rise in [Muntjewerf et al., 2020b] is

reached between model years 200 and 250. During the experiment, significant weakening of the North Atlantic Meridional Overturning Circulation (NAMOC) is observed along with a complete halt of deep convection in the Labrador Sea, Irminger Sea, Iceland Basin and Barents Sea. Multiple overlapping climate signals, such as surface warming, enhanced Arctic precipitation, additional freshwater fluxes from melting of sea ice and enhanced GrIS runoff make it difficult to attribute modeled changes in the ocean state to the increased freshwater flux from the GrIS. The NAMOC, for example, shows significant weakening well before an enhanced GrIS runoff signal is modeled in their experiment.

The modeled thinning of the Greenland ice sheet in the ECE-PISM and ECE-CIS-PISM experiments is consistent with the applied surface mass balance forcing.

8 Conclusion

In this thesis, a new coupling interface for a coupled global climate - ice sheet model system was developed based on EC-Earth 3-Veg and PISM v1.2. Two coupling approaches featuring different ways of forcing the ice sheet in PISM were implemented. One using surface forcing from EC-Earth 3 directly and another calculating surface forcing with CISSEMBEL, a downscaled energy balance model.

Differences in the modeling of surface mass balance in the uncoupled, stand-alone EC-Earth 3 and CISSEMBEL were studied. Two different albedo schemes were tested: one with a static 0.8 albedo over glaciated areas and another, more sophisticated scheme which allows albedo-melt feedback. The latter was found to induce more melt both in EC-Earth 3 and in CISSEMBEL. Especially when using the sophisticated albedo scheme, CISSEMBEL was found to produce significantly higher snow melt rates and thus lower surface mass balance rates. Melt rates for the 1850-1878 period in CISSEMBEL match well with a surface mass balance reconstruction study by [Box, 2013], although lower accumulation values yield a lower surface mass balance by CISSEMBEL. For the 2015-2043 period, CISSEMBEL models significantly higher melt rates than EC-Earth 3 and other modeling studies, when using an albedo scheme that allows albedo-melt feedback. CISSEMBEL does, however, have an explicit calculation of refreezing. The dependence of melt rates and the total surface mass balance on model parameter choices was estimated, showing the importance for choosing sensitive parameters carefully.

Before the main coupled experiments, PISM ice sheet initialization results were described. Two initialization experiments were run by Marianne Sloth Madsen for 250,000 years each, under pre-industrial surface forcing from EC-Earth 3 and CISSEMBEL (latter generated by the author). EC-Earth 3 surface forcing lead to the initialized ice sheet covering almost the entire Greenland land mass and being significantly larger in extent and mass than the observed present-day ice sheet. Under CISSEMBEL surface forcing, the resulting ice sheet extent is closer to, yet still slightly larger than the extent of the observed present-day ice sheet. The extent in the important south-western ablation zone matches the observed present-day ice sheet well, however. Both initialized ice sheets are flatter over the Greenland interior. These ice sheet states are used as PISM initial states in the coupled experiments and their respective geometries have implications for the surface mass balance in these experiments.

Coupled abrupt-4xCO_2 scenario experiments were performed which illustrate the importance of coupling EC-Earth 3 to an interactive Greenland ice sheet in order to improve its representation in the global climate model under warm conditions. The modeled surface mass and energy balance along with fresh water fluxes into the ocean show significant

differences between an uncoupled EC-Earth 3 and the coupled experiments. Snow was found to retreat quickly in an uncoupled EC-Earth 3 simulation which leads to a failure to accurately capture high runoff rates in lower altitude ablation zones under high greenhouse gas forcing. The coupled setup improves on this, prescribing ice sheet conditions in the global climate model in all areas that are covered by the GrIS in PISM.

In the coupled experiments, the Greenland ice sheet loses significant mass under high greenhouse gas forcing. GrIS integrated SMB forcing applied to the ice sheets cause mass loss at similar rates. This indicates that surface mass balance rates are more negative over the smaller CISSEMBEL-forced ice sheet. While SMB rates from EC-Earth 3 and CISSEMBEL are comparable at the perimeter of the smaller ice sheet, the fact that the ablation zone reaches much further into the ice sheet interior heavily contributes to this. This is likely due to CISSEMBEL modeling more melt under comparable conditions, as could be seen in section 5 but lower altitudes over the whole CISSEMBEL-forced ice sheet (see figure 20) and a modified albedo scheme play a role as well. The larger EC-Earth 3 forced ice sheet loses more mass via ice discharge and basal melting.

8.1 Outlook

The current state of the coupled model system offers several opportunities for improvement.
First of all, the current issues in the Runoff-Mapper have to be resolved. An updated version addressing the issues of properly remapping the PISM ice discharge and taking calving contributions from basins outside of Greenland into account is currently being tested.

The impact of topography and ice sheet extent on surface mass balance and ice discharge, and thus freshwater influx into the ocean, in the coupled experiments highlights the importance of a realistic ice sheet initial state. More work has to be done on fine-tuning the atmospheric forcing in the initialization of the PISM ice sheet in order to improve the initial state.

The configuration of PISM itself in the coupled system also offers room for improvement. As initially planned, PISM will be run with 5 km x 5 km horizontal resolution in future experiments. Performance considerations will decide the upgrade of the PISM hydrology from the currently used simple scheme, which does not conserve mass, to a mass conserving routing scheme.

The interaction of the ice sheet with the ocean is currently represented by a constant frontal melt rate. Variability of ocean forcing with ocean temperatures around Greenland would likely add value to the system. The planned integration of a coupled Antarctic ice sheet into the system would especially benefit from a more sophisticated approach.

Finally, the downscaled energy balance model CISSEMBEL offers great promise for improving surface mass balance calculations in the coupled system. Running CISSEMBEL synchronously with EC-Earth 3 as the surface scheme over glaciated regions would allow a mass conserving coupled setup involving CISSEMBEL and help improve surface mass balance modeling in narrow ablation zones through downscaling climate forcing in CISSEMBEL to the higher resolution PISM topography.

Statement

Some results presented in this work were generated with or contain modified Copernicus Climate Change Service information 2020. Neither the European Commission nor ECMWF is responsible for any use that may be made of the Copernicus information or data it contains.
Development of PISM is supported by NSF grants PLR-1603799 and PLR-1644277 and NASA grant NNX17AG65G.

A Tables

Model	Resolution	Timestep	IFS	NEMO	LPJ
IFS - HTESSEL	T255L91	2700 s	-	2700 s	86400 s
NEMO - LIM	ORCA1°L75	2700 s	2700 s	-	-
LPJ-GUESS	T255	86400 s	86400 s	-	-

Table 10: EC-Earth component configurations and coupling timesteps. Connections '-' are self-referential or imply no coupling between models.

Constant	Value	Description
ρ_{ice}	920 kg m^{-3}	ice density
$(\rho C)_{ice}$	2.05×10^6 J m^{-3} K^{-1}	volumetric heat capacity of ice
L_f	3.30×10^5 J kg^{-1}	latent heat of fusion
L_e	2.501×10^6 J kg^{-1}	latent heat of evaporation
L_s	2.8345×10^6 J kg^{-1}	latent heat of sublimation
ε	0.98	surface longwave emissivity

Table 11: Constants in IFS and HTESSEL. (jump to HTESSEL SEB)

Constant	Value	Description
ρ_{ice}	917 kg m^{-3}	ice density
$C_{p,snow}$	2000 J kg K^{-1}	specific heat capacity of snow
$C_{p,water}$	4186 J kg K^{-1}	specific heat capacity of water
L_f	3.36×10^5 J kg^{-1}	latent heat of fusion
L_s	2.834×10^6 J kg^{-1}	latent heat of sublimation
Γ_T	-6.5×10^{-3} K m^{-1}	temperature lapse rate
Γ_{LW}	$-\frac{75}{2600}$ W m^{-2} m^{-1}	longwave radiation lapse rate
ε	1.0	surface longwave emissivity

Table 12: Constants in CISSEMBEL. (jump to CISSEMBEL SEB)

Constant	Value	Description
E_{SIA}	3.0	SIA enhancement factor
E_{SSA}	1.0	SSA enhancement factor
q	0.25	exponent in "pseudo-plastic" power law
c_0	0	till cohesion
$N_{till,min}$	$0.02P_0$	minimum effective pore water pressure
Γ_{bf}	-5.4×10^{-3} K m^{-1}	below-firn temperature lapse rate
$\theta_{calving}$	125.0 m	thickness calving threshold

Table 13: Constants in PISM. (jump to PISM)

References

[Adolph et al., 2017] Adolph, A. C., Albert, M. R., Lazarcik, J., Dibb, J. E., Amante, J. M., and Price, A. (2017). Dominance of grain size impacts on seasonal snow albedo at open sites in new hampshire. *Journal of Geophysical Research: Atmospheres*, 122(1):121–139.

[Amundson et al., 2010] Amundson, J. M., Fahnestock, M., Truffer, M., Brown, J., Lüthi, M. P., and Motyka, R. (2010). Ice mélange dynamics and implications for terminus stability, jakobshavn isbræ, greenland. *Journal of Geophysical Research: Earth Surface*, 115(F1).

[Balsamo et al., 2009] Balsamo, G., Beljaars, A., Scipal, K., Viterbo, P., van den Hurk, B., Hirschi, M., and Betts, A. K. (2009). A revised hydrology for the ecmwf model: Verification from field site to terrestrial water storage and impact in the integrated forecast system. *Journal of hydrometeorology*, 10(3):623–643.

[Box et al., 2012] Box, J., Fettweis, X., Stroeve, J., Tedesco, M., Hall, D., and Steffen, K. (2012). Greenland ice sheet albedo feedback: thermodynamics and atmospheric drivers. *The Cryosphere*, 6(4):821–839.

[Box, 2013] Box, J. E. (2013). Greenland ice sheet mass balance reconstruction. part ii: Surface mass balance (1840–2010). *Journal of Climate*, 26(18):6974–6989.

[Box and Colgan, 2013] Box, J. E. and Colgan, W. (2013). Greenland ice sheet mass balance reconstruction. part iii: Marine ice loss and total mass balance (1840–2010). *Journal of Climate*, 26(18):6990–7002.

[Broeke et al., 2016] Broeke, M. R., Enderlin, E. M., Howat, I. M., Kuipers Munneke, P., Noël, B. P., Berg, W. J. v. d., Meijgaard, E. v., and Wouters, B. (2016). On the recent contribution of the greenland ice sheet to sea level change. *The Cryosphere*, 10(5):1933–1946.

[Buck, 1981] Buck, A. L. (1981). New equations for computing vapor pressure and enhancement factor. *Journal of Applied Meteorology and Climatology*, 20(12):1527–1532.

[Bueler and Brown, 2009] Bueler, E. and Brown, J. (2009). Shallow shelf approximation as a “sliding law” in a thermomechanically coupled ice sheet model. *Journal of Geophysical Research: Earth Surface*, 114(F3).

[Dahl-Jensen et al., 2009] Dahl-Jensen, D., Bamber, J., Boggild, C., Buch, E., Christensen, J., Dethloff, K., Fahnestock, M., Marshall, S., Rosing, M., Steffen, K., et al. (2009). The greenland ice sheet in a changing climate.

[Devilliers et al., 2021] Devilliers, M., Swingedouw, D., Mignot, J., Deshayes, J., Garric, G., and Ayache, M. (2021). A realistic greenland ice sheet and surrounding glaciers and ice caps melting in a coupled climate model. *Climate Dynamics*, pages 1–23.

[Döscher et al., 2021] Döscher, R., Acosta, M., Alessandri, A., Anthoni, P., Arneth, A., Arsouze, T., Bergmann, T., Bernadello, R., Bousetta, S., Caron, L.-P., et al. (2021). The ec-earth3 earth system model for the climate model intercomparison project 6. *Geoscientific Model Development Discussions*, pages 1–90.

[EC-Earth-Consortium, 2021] EC-Earth-Consortium (2021). The ec-earth consortium. `http://www.ec-earth.org/community/consortium/`. Accessed: 27.06.2021.

[ECMWF, 2010] ECMWF (2010). *IFS Documentation CY36R1 - Part IV: Physical Processes*. Number 4 in IFS Documentation. ECMWF.

[Enderlin et al., 2014] Enderlin, E. M., Howat, I. M., Jeong, S., Noh, M.-J., Van Angelen, J. H., and Van Den Broeke, M. R. (2014). An improved mass budget for the greenland ice sheet. *Geophysical Research Letters*, 41(3):866–872.

[Fausto et al., 2009] Fausto, R. S., Ahlstrøm, A. P., Johnsen, S. J., Langen, P. L., Steffen, K., et al. (2009). Improving surface boundary conditions with focus on coupling snow densification and meltwater retention in large-scale ice-sheet models of greenland. *Journal of Glaciology*, 55(193):869–878.

[Fettweis et al., 2020] Fettweis, X., Hofer, S., Krebs-Kanzow, U., Amory, C., Aoki, T., Berends, C. J., Born, A., Box, J. E., Delhasse, A., Fujita, K., et al. (2020). Grsmbmip: intercomparison of the modelled 1980–2012 surface mass balance over the greenland ice sheet. *The Cryosphere*, 14(11):3935–3958.

[Fyke et al., 2018] Fyke, J., Sergienko, O., Löfverström, M., Price, S., and Lenaerts, J. T. (2018). An overview of interactions and feedbacks between ice sheets and the earth system. *Reviews of Geophysics*, 56(2):361–408.

[Gevik, 2019] Gevik, S. (2019). Greenland ice sheet modelling: A study of calving parametrisations. *Master's Thesis*.

[Goelzer et al., 2020] Goelzer, H., Nowicki, S., Payne, A., Larour, E., Seroussi, H., Lipscomb, W. H., Gregory, J., Abe-Ouchi, A., Shepherd, A., Simon, E., et al. (2020). The future sea-level contribution of the greenland ice sheet: a multi-model ensemble study of ismip6. *The Cryosphere*, 14(9):3071–3096.

[Hanna et al., 2016] Hanna, E., Cropper, T. E., Hall, R. J., and Cappelen, J. (2016). Greenland blocking index 1851–2015: a regional climate change signal. *International Journal of Climatology*, 36(15):4847–4861.

[Helsen et al., 2012] Helsen, M., Van De Wal, R., Van Den Broeke, M., Van De Berg, W., and Oerlemans, J. (2012). Coupling of climate models and ice sheet models by surface mass balance gradients: application to the greenland ice sheet. *The Cryosphere*, 6(2):255–272.

[Helsen et al., 2017] Helsen, M. M., Van De Wal, R. S., Reerink, T. J., Bintanja, R., Madsen, M. S., Yang, S., Li, Q., and Zhang, Q. (2017). On the importance of the albedo parameterization for the mass balance of the greenland ice sheet in ec-earth. *The Cryosphere*, 11(4):1949–1965.

[IPCC, 2021] IPCC (2021). Climate change 2021: The physical science basis. contribution of working group i to the sixth assessment report of the intergovernmental panel on climate change. *[Masson-Delmotte, V., P. Zhai, A. Pirani, S. L. Connors, C. Péan, S. Berger, N. Caud, Y. Chen, L. Goldfarb, M. I. Gomis, M. Huang, K. Leitzell, E. Lonnoy, J. B. R. Matthews, T. K. Maycock, T. Waterfield, O. Yelekçi, R. Yu and B. Zhou (eds.)]*.

[Jackson et al., 2014] Jackson, R. H., Straneo, F., and Sutherland, D. A. (2014). Externally forced fluctuations in ocean temperature at greenland glaciers in non-summer months. *Nature Geoscience*, 7(7):503–508.

[Karlsson et al., 2021] Karlsson, N. B., Solgaard, A. M., Mankoff, K. D., Gillet-Chaulet, F., MacGregor, J. A., Box, J. E., Citterio, M., Colgan, W. T., Larsen, S. H., Kjeldsen, K. K., et al. (2021). A first constraint on basal melt-water production of the greenland ice sheet. *Nature Communications*, 12(1):1–10.

[Konzelmann and Ohmura, 1995] Konzelmann, T. and Ohmura, A. (1995). Radiative fluxes and their impact on the energy balance of the greenland ice sheet. *Journal of Glaciology*, 41(139):490–502.

[Kwiatkowski et al., 2019] Kwiatkowski, L., Naar, J., Bopp, L., Aumont, O., Defrance, D., and Couespel, D. (2019). Decline in atlantic primary production accelerated by greenland ice sheet melt. *Geophysical Research Letters*, 46(20):11347–11357.

[Langen et al., 2015] Langen, P., Mottram, R., Christensen, J., Boberg, F., Rodehacke, C., Stendel, M., Van As, D., Ahlstrøm, A., Mortensen, J., Rysgaard, S., et al. (2015). Quantifying energy and mass fluxes controlling godthåbsfjord freshwater input in a 5-km simulation (1991–2012). *Journal of Climate*, 28(9):3694–3713.

[Langen et al., 2017] Langen, P. L., Fausto, R. S., Vandecrux, B., Mottram, R. H., and Box, J. E. (2017). Liquid water flow and retention on the greenland ice sheet in the regional climate model hirham5: Local and large-scale impacts. *Frontiers in Earth Science*, 4:110.

[Lenaerts et al., 2015] Lenaerts, J. T., Le Bars, D., Van Kampenhout, L., Vizcaino, M., Enderlin, E. M., and Van Den Broeke, M. R. (2015). Representing greenland ice sheet freshwater fluxes in climate models. *Geophysical Research Letters*, 42(15):6373–6381.

[Madec et al., 2017] Madec, G., Bourdallé-Badie, R., Bouttier, P.-A., Bricaud, C., Bruciaferri, D., Calvert, D., Chanut, J., Clementi, E., Coward, A., Delrosso, D., et al. (2017). Nemo ocean engine.

[Madsen et al., 2021a] Madsen, M., Yang, S., Aðalgeirsdóttir, G., Svendsen, S. H., Rodehacke, C. B., and M., R. I. (2021a). The role of an interactive greenland ice sheet in the coupled ice sheet-climate model ec-earth-pism. *Danish Meteorological Institute, Copenhagen, Denmark*. submitted.

[Madsen et al., 2021b] Madsen, M. S., Rodehacke, C., Lindpointner, L., Olesen, M., and Yang, S. (2021b). Dmi report 21-17 including a dynamic greenland ice sheet in the ec-earth global climate model.

[Mikolajewicz et al., 2007] Mikolajewicz, U., Vizcaino, M., Jungclaus, J., and Schurgers, G. (2007). Effect of ice sheet interactions in anthropogenic climate change simulations. *Geophysical Research Letters*, 34(18).

[Morlighem et al., 2017] Morlighem, M., Williams, C. N., Rignot, E., An, L., Arndt, J. E., Bamber, J. L., Catania, G., Chauché, N., Dowdeswell, J. A., Dorschel, B., et al. (2017). Bedmachine v3: Complete bed topography and ocean bathymetry mapping of greenland from multibeam echo sounding combined with mass conservation. *Geophysical research letters*, 44(21):11–051.

[Muntjewerf et al., 2020a] Muntjewerf, L., Petrini, M., Vizcaino, M., da Silva, C. E., Sellevold, R., Scherrenberg, M. D., Thayer-Calder, K., Bradley, S. L., Lenaerts, J. T., Lipscomb, W. H., et al. (2020a). Greenland ice sheet contribution to 21st century sea level rise as simulated by the coupled cesm2. 1-cism2. 1. *Geophysical Research Letters*, 47(9).

[Muntjewerf et al., 2021] Muntjewerf, L., Sacks, W. J., Lofverstrom, M., Fyke, J., Lipscomb, W. H., Ernani da Silva, C., Vizcaino, M., Thayer-Calder, K., Lenaerts, J. T., and Sellevold, R. (2021). Description and demonstration of the coupled community earth system model v2–community ice sheet model v2 (cesm2-cism2). *Journal of Advances in Modeling Earth Systems*, 13(6):e2020MS002356.

[Muntjewerf et al., 2020b] Muntjewerf, L., Sellevold, R., Vizcaino, M., Ernani da Silva, C., Petrini, M., Thayer-Calder, K., Scherrenberg, M. D., Bradley, S. L., Katsman, C. A., Fyke, J., et al. (2020b). Accelerated greenland ice sheet mass loss under high greenhouse gas forcing as simulated by the coupled cesm2. 1-cism2. 1. *Journal of Advances in Modeling Earth Systems*, 12(10):e2019MS002031.

[Muñoz Sabater, 2019] Muñoz Sabater, J. (2019). Era5-land monthly averaged data from 1981 to present. *Copernicus Climate Change Service (C3S) Climate Data Store (CDS)*. Accessed on 12. 07. 2021.

[Oerlemans, 1981] Oerlemans, J. (1981). Some basic experiments with a vertically-integrated ice sheet model. *Tellus*, 33(1):1–11.

[Pachauri et al., 2014] Pachauri, R. K., Allen, M. R., Barros, V. R., Broome, J., Cramer, W., Christ, R., Church, J. A., Clarke, L., Dahe, Q., Dasgupta, P., et al. (2014). *Climate change 2014: synthesis report. Contribution of Working Groups I, II and III to the fifth assessment report of the Intergovernmental Panel on Climate Change*. IPCC.

[Painter et al., 2009] Painter, T. H., Rittger, K., McKenzie, C., Slaughter, P., Davis, R. E., and Dozier, J. (2009). Retrieval of subpixel snow covered area, grain size, and albedo from modis. *Remote Sensing of Environment*, 113(4):868–879.

[PISM-Authors, 2020] PISM-Authors, T. (2020). Pism, a parallel ice sheet model. Accessed: 23.07.2021.

[Ridley et al., 2005] Ridley, J. K., Huybrechts, P., Gregory, J. u., and Lowe, J. (2005). Elimination of the greenland ice sheet in a high co2 climate. *Journal of Climate*, 18(17):3409–3427.

[Rignot et al., 2008] Rignot, E., Box, J., Burgess, E., and Hanna, E. (2008). Mass balance of the greenland ice sheet from 1958 to 2007. *Geophysical Research Letters*, 35(20).

[Rignot and Mouginot, 2012] Rignot, E. and Mouginot, J. (2012). Ice flow in greenland for the international polar year 2008–2009. *Geophysical Research Letters*, 39(11).

[Rodehacke, 2020] Rodehacke, C. (2020). Cissembel documentation. `https://gitlab.dmi.dk/cr/CISSEMBLE`. Accessed: 19.07.2021.

[Rousset et al., 2015] Rousset, C., Vancoppenolle, M., Madec, G., Fichefet, T., Flavoni, S., Barthélemy, A., Benshila, R., Chanut, J., Lévy, C., Masson, S., et al. (2015). The louvain-la-neuve sea ice model lim3.6: global and regional capabilities. *Geoscientific Model Development*, 8(10):2991–3005.

[Schuenemann et al., 2009] Schuenemann, K. C., Cassano, J. J., and Finnis, J. (2009). Synoptic forcing of precipitation over greenland: Climatology for 1961–99. *Journal of Hydrometeorology*, 10(1):60–78.

[Schwierz and Davies, 2002] Schwierz, C. B. and Davies, H. C. (2002). 5.2 cyclone tracks in the vicinity of greenland–aspects of an interaction process.

[Smith et al., 2001] Smith, B., Prentice, I. C., and Sykes, M. T. (2001). Representation of vegetation dynamics in the modelling of terrestrial ecosystems: comparing two contrasting approaches within european climate space. *Global ecology and biogeography*, pages 621–637.

[Svendsen et al., 2015] Svendsen, S., Madsen, M., Yang, S., Rodehacke, C., and Adalgeirsdottir, G. (2015). An introduction to the coupled ec-earth-pism model system. *Danish Meteorological Institute, Copenhagen, Denmark*.

[Valcke et al., 2015] Valcke, S., Craig, T., and Coquart, L. (2015). *OASIS3-MCT User Guide, OASIS3-MCT 3.0*.

[Van den Broeke et al., 2011] Van den Broeke, M., Smeets, C., and Van de Wal, R. (2011). The seasonal cycle and interannual variability of surface energy balance and melt in the ablation zone of the west greenland ice sheet. *The Cryosphere*, 5(2):377–390.

[Vancoppenolle et al., 2009] Vancoppenolle, M., Fichefet, T., Goosse, H., Bouillon, S., Madec, G., and Maqueda, M. A. M. (2009). Simulating the mass balance and salinity of arctic and antarctic sea ice. 1. model description and validation. *Ocean Modelling*, 27(1–2):33 – 53.

[Vizcaíno et al., 2013] Vizcaíno, M., Lipscomb, W. H., Sacks, W. J., van Angelen, J. H., Wouters, B., and van den Broeke, M. R. (2013). Greenland surface mass balance as simulated by the community earth system model. part i: Model evaluation and 1850–2005 results. *Journal of climate*, 26(20):7793–7812.

[Vizcaino et al., 2015] Vizcaino, M., Mikolajewicz, U., Ziemen, F., Rodehacke, C. B., Greve, R., and Van Den Broeke, M. R. (2015). Coupled simulations of greenland ice sheet and climate change up to ad 2300. *Geophysical Research Letters*, 42(10):3927–3935.

[Wehrlé et al., 2021] Wehrlé, A., Box, J. E., Niwano, M., Anesio, A. M., and Fausto, R. S. (2021). Greenland bare-ice albedo from promice automatic weather station measurements and sentinel-3 satellite observations. *GEUS Bulletin*, 47.

[Winkelmann et al., 2011] Winkelmann, R., Martin, M. A., Haseloff, M., Albrecht, T., Bueler, E., Khroulev, C., and Levermann, A. (2011). The potsdam parallel ice sheet model (pism-pik)–part 1: Model description. *The Cryosphere*, 5(3):715–726.